



CoCo2

Prototype system for a
Copernicus CO₂ service

Assessment of plume model performance

Erik Koene & Dominik Brunner



Co-ordinated by
 ECMWF



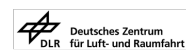


CoCO2

Prototype system for a
Copernicus CO₂ service

D4.2 ASSESSMENT OF PLUME MODEL PERFORMANCE

| | |
|-----------------------------------|--|
| Dissemination Level: | Public |
| Author(s): | Erik Koene & Dominik Brunner (Empa) |
| Date: | 19/01/2023 |
| Version: | 0.3 |
| Contractual Delivery Date: | 31/12/2022 |
| Work Package/ Task: | WP4/ T4.2 |
| Document Owner: | Empa |
| Contributors: | Empa/WUR/TNO/LSCE/DWD |
| Status: | Final |





CoCO2: Prototype system for a Copernicus CO₂ service

Coordination and Support Action (CSA)
H2020-IBA-SPACE-CHE2-2019 Copernicus evolution –
Research activities in support of a European operational
monitoring support capacity for fossil CO₂ emissions

Project Coordinator: Dr Richard Engelen (ECMWF)
Project Start Date: 01/01/2021
Project Duration: 36 months

Published by the CoCO2 Consortium

Contact:
ECMWF, Shinfield Park, Reading, RG2 9AX,
richard.engelen@ecmwf.int



The CoCO2 project has received funding from the European Union's Horizon 2020 research and innovation programme under grant agreement No 958927.



Table of Contents

| | | |
|-------|---|----|
| 1 | Executive Summary..... | 10 |
| 2 | Introduction..... | 10 |
| 2.1 | Background..... | 10 |
| 2.2 | Scope of this deliverable..... | 11 |
| 2.2.1 | Objectives of this deliverables..... | 11 |
| 2.2.2 | Work performed in this deliverable..... | 11 |
| 2.2.3 | Deviations and counter measures..... | 11 |
| 3 | Modelling methods..... | 11 |
| 3.1 | Model set-up..... | 11 |
| 3.1.1 | COSMO-GHG..... | 11 |
| 3.1.2 | ICON-ART..... | 12 |
| 3.1.3 | LOTOS-EUROS..... | 12 |
| 3.1.4 | MicroHH..... | 13 |
| 3.1.5 | WRF-CHEM..... | 14 |
| 3.2 | Output format and storage..... | 14 |
| 3.3 | Postprocessing..... | 15 |
| 3.3.1 | Column computation..... | 15 |
| 3.3.2 | Synthetic CO ₂ M observation..... | 15 |
| 3.3.3 | NO _x to NO ₂ conversion..... | 16 |
| 3.3.4 | Analyse NO _x /CO ₂ ratio downstream of the plume..... | 16 |
| 3.3.5 | Analysis of the plume width downstream..... | 17 |
| 3.3.6 | Curtain plots for in-situ data..... | 18 |
| 4 | Case studies..... | 18 |
| 4.1 | Point sources..... | 19 |
| 4.1.1 | Bełchatów (2018-06-06 – 2018-06-07)..... | 19 |
| 4.1.2 | Jämschwalde (2018-05-22 – 2018-05-23)..... | 32 |
| 4.1.3 | Lipetsk (2019-06-12 – 2019-06-13)..... | 43 |
| 4.1.4 | Matimba (2020-07-24 – 2020-07-25)..... | 47 |
| 4.2 | Cities..... | 51 |
| 4.2.1 | Berlin (2018-07-18 – 2018-07-26)..... | 51 |
| 4.2.2 | Paris (2018-08-01 – 2018-08-08)..... | 57 |
| 4.2.3 | Randstad (2018-06-16 – 2018-06-23 & 2018-12-16 – 2018-12-23)..... | 64 |
| 5 | Conclusion..... | 69 |
| 6 | Recommendations..... | 70 |
| 7 | References..... | 71 |
| 8 | Modelling protocols..... | 77 |

Figures

| | |
|--|----|
| Figure 1. Example of obtaining plume cross-sections for column images. (a) Column image of NO ₂ simulated with COSMO-GHG. (b) Estimation of a 'plume centre line' for this source. (c) Example of fitted plume coordinate system, with x_p the distance along the plume in meters. (d) Extracted NO ₂ plume pixels, sorted in bins of a fixed distance along the plume. (e) The associated 'across plume distance' for each of the selected pixels in meters relative to the plume centre. (f) An example plot of the NO ₂ plume cross-section at a distance of roughly 15 km downstream along the plume (the blue dots, unequally spaced in the across plume direction, are the data; the red dotted line is a Gaussian curve fitted to the data). | 17 |
| Figure 2. Map of the seven cases considered in this study (indicated by their abbreviations or case IDs), including the source location (indicated by a coloured dot) and the "large" model extent (indicated by the bounding box). | 19 |
| Figure 3. Total column images as generated by four modelling systems of the Bełchatów powerplant plume, on June 7 th , 2018, for the "middle" emissions profile M. The location of the powerplant is indicated by the red dot. | 21 |
| Figure 4. Total column images as generated by four modelling systems of the Bełchatów powerplant plume, on June 7 th , 2018, for the "surface" emissions profile L. The location of the powerplant is indicated by the red dot. This emission profile case was not modelled in MicroHH. | 21 |
| Figure 5. Zoom on the total column images as generated by four modelling systems of the Bełchatów powerplant plume, on June 7 th , 2018, for the "middle" emissions profile M. The location of the powerplant is indicated by the red dot. | 22 |
| Figure 6. COSMO-GHG comparison against DLR-Cessna for Bełchatów, 7 June 2018. | 23 |
| Figure 7. ICON-ART comparison against DLR-Cessna for Bełchatów, 7 June 2018. | 24 |
| Figure 8. LOTOS-EUROS comparison against DLR-Cessna for Bełchatów, 7 June 2018. | 25 |
| Figure 9. MicroHH comparison against DLR-Cessna for Bełchatów, 7 June 2018. | 26 |
| Figure 10. Time series of CO ₂ column enhancements simulated and observed by MAMAP along the FUB-Cessna flight at Bełchatów on 7 June 2018. The plumes observed around 12:20 and 13:45 UTC, which are not reproduced by any of the models, were measured upwind of the power plant. These plumes are caused by retrieval issues over water surfaces rather by real CO ₂ enhancements. | 27 |
| Figure 11. Observations of CO ₂ column enhancements simulated and observed by CHARM-F along the HALO flight at Bełchatów on 7 June 2018. | 28 |
| Figure 12. Comparison for TROPOMI columns with the total simulated NO ₂ . For COSMO-GHG, the NO ₂ column was created based on an NO _x tracer (NOX_PP_M + NOX_ANTH + NOX_BG) converted into an NO ₂ tracer. For LOTOS-EUROS and MicroHH, the NO ₂ column was modelled including full chemistry (NO2_PP_M + NO2_BG for MicroHH, and additionally NO2_PP_ANTH + NO2_BIO for LOTOS-EUROS). | 28 |
| Figure 13. Zoom on the comparison for TROPOMI columns with the total simulated NO ₂ , see Figure 12. | 29 |
| Figure 14. Comparison of downstream NO ₂ and NO _x decay for Bełchatów for the three models that submitted nitrogen oxide tracers. The ratios are normalized to 1. The effective wind speed is the wind speed weighted with the vertical distribution of NO ₂ or NO _x around the source position. | 30 |
| Figure 15. The downwind evolution of the plume width for the Bełchatów power plant, following a Gaussian plume fit to the CO2_PP_M tracer. The black line shows one standard deviation of the fitted plume width. | 31 |
| Figure 16. Synthetic CO2M observation of the total CO ₂ column around Bełchatów. | 32 |

| | |
|--|----|
| Figure 17. Total column images as generated by four modelling systems of the Jänschwalde powerplant plume, on May 23 rd , 2018, for the "middle" emissions profile M. The location of the powerplant is indicated by the red dot. | 33 |
| Figure 18. Total column images as generated by four modelling systems of the Jänschwalde powerplant plume, on May 23 rd , 2018, for the "surface" emissions profile L. The location of the powerplant is indicated by the red dot. This emission profile case was not modelled in MicroHH. | 34 |
| Figure 19. Zoom on the total column images as generated by four modelling systems of the Jänschwalde powerplant plume, on May 23 rd , 2018, for the "middle" emissions profile M. The location of the powerplant is indicated by the red dot. | 34 |
| Figure 20. COSMO-GHG comparison against FUB-Cessna for Jänschwalde, 23 May 2018 | 35 |
| Figure 21. ICON-ART comparison against FUB-Cessna for Jänschwalde, 23 May 2018..... | 36 |
| Figure 22. LOTOS-EUROS comparison against FUB-Cessna for Jänschwalde, 23 May 2018 | 36 |
| Figure 23. MicroHH comparison against FUB-Cessna for Jänschwalde, 23 May 2018. | 37 |
| Figure 24. Plot of the potential temperature for the different models around Jänschwalde... | 38 |
| Figure 25. Time series of CO ₂ column enhancements simulated and observed by MAMAP along the FUB-Cessna flight at Jänschwalde on 23 May 2018. | 39 |
| Figure 26. Observations of CO ₂ column enhancements simulated and observed by CHARM-F along the HALO flight at Jänschwalde on 23 May 2018..... | 39 |
| Figure 27. Comparison for TROPOMI columns with the total simulated NO ₂ . For COSMO-GHG, the NO ₂ column was created based on an NO _x tracer (NO _x _PP_M + NO _x _ANTH + NO _x _BG) converted into an NO ₂ tracer. For LOTOS-EUROS and MicroHH, the NO ₂ column was modelled including full chemistry (NO ₂ _PP_M + NO ₂ _BG for MicroHH, and additionally NO ₂ _PP_ANTH + NO ₂ _BIO for LOTOS-EUROS)..... | 40 |
| Figure 28. Zoom on the comparison for TROPOMI columns with the total simulated NO ₂ , see Figure 27. | 40 |
| Figure 29. Comparison of downstream NO ₂ and NO _x decay for Jänschwalde for the three models that submitted nitrogen oxide tracers. The ratios are normalized to 1. The effective wind speed is the wind speed weighted with the vertical distribution of NO ₂ or NO _x around the source position..... | 41 |
| Figure 30. The downwind evolution of the plume width for the Jänschwalde power plant, following a Gaussian plume fit to the CO ₂ _PP_M tracer. The black line shows one standard deviation of the fitted plume width. | 42 |
| Figure 31. Synthetic CO ₂ M observation of the total CO ₂ column around Jänschwalde..... | 42 |
| Figure 32. Total column images as generated by two modelling systems of the Lipetsk steel plant, on June 13 th , 2019, for the "middle" emissions profile M in the large (L) and small (S) domains. The location of the steel plant is indicated by the red dot. | 44 |
| Figure 33. Comparison for TROPOMI columns with the total simulated CO. For MicroHH that is CO_PP_M + CO_BG, in COSMO-GHG additionally the other anthropogenic CO sources are included. | 44 |
| Figure 34. Zoom on the comparison for TROPOMI columns with the total simulated CO, see Figure 33. | 45 |
| Figure 35. Comparison of downstream NO ₂ and NO _x decay for Lipetsk. The ratios are normalized to 1. The effective wind speed is the wind speed weighted with the vertical distribution of NO ₂ or NO _x around the source position | 45 |
| Figure 36. The downwind evolution of the plume width for the Lipetsk steel plant, following a Gaussian plume fit to the CO ₂ _PP_M tracer. The black line shows one standard deviation of the fitted plume width. | 46 |
| Figure 37. Synthetic CO ₂ M observation of the total CO ₂ column around Lipetsk. | 46 |
| Figure 38. Total column images as generated by two modelling systems of the Matimba power plant, on July 25 th , 2020, for the "middle" emissions profile M in the large (L) and small (S) domains. The location of the power plant is indicated by the red dot..... | 48 |

| | |
|---|----|
| Figure 39. Comparison for TROPOMI columns with the total simulated NO ₂ . For COSMO-GHG, the NO ₂ column was created based on an NO _x tracer (NOX_PP_M + NOX_ANTH + NOX_BG) converted into an NO ₂ tracer. For MicroHH, the NO ₂ column was modelled including full chemistry (NO2_PP_M + NO2_BG). | 49 |
| Figure 40. Zoom on the comparison for TROPOMI columns with the total simulated NO ₂ , see Figure 39. | 49 |
| Figure 41. Comparison of downstream NO ₂ and NO _x decay for Matimba. The ratios are normalized to 1. The effective wind speed is the wind speed weighted with the vertical distribution of NO ₂ or NO _x around the source position. | 50 |
| Figure 42. The downwind evolution of the plume width for the Matimba power plant, following a Gaussian plume fit to the CO2_PP_M tracer. The black line shows one standard deviation of the fitted plume width | 50 |
| Figure 43. Synthetic CO2M observation of the total CO ₂ column around Matimba. | 51 |
| Figure 44. Total column images as generated by two modelling systems of the Berlin urban area, on July 20 and July 24, 2018. An approximate location centred within Berlin is indicated by the red dot. | 52 |
| Figure 45. COSMO-GHG comparison against DLR-Cessna for Berlin, 20 July 2018. | 53 |
| Figure 46. LOTOS-EUROS comparison against DLR-Cessna for Berlin, 20 July 2018. | 53 |
| Figure 47. COSMO-GHG comparison against DLR-Cessna for Berlin, 24 July 2018. | 54 |
| Figure 48. LOTOS-EUROS comparison against DLR-Cessna for Berlin, 24 July 2018. | 54 |
| Figure 49. Comparison for TROPOMI columns with the total simulated NO ₂ . For COSMO-GHG, the NO ₂ column was created based on an NO _x tracer (NOX_PP_M + NOX_ANTH + NOX_BG) converted into an NO ₂ tracer. For LOTOS-EUROS, the NO ₂ column was modelled including full chemistry (NO2_CITY + NO2_ANTH + NO2_BG + NO2_BIO). | 55 |
| Figure 50. Comparison of downstream NO ₂ and NO _x decay for the Berlin plume. The ratios are normalized to 1. The effective wind speed is the wind speed weighted with the vertical distribution of NO ₂ or NO _x around the source position. | 56 |
| Figure 51. The downwind evolution of the plume width for the Berlin plume, following a Gaussian plume fit to the CO2_CITY tracer. The black line shows one standard deviation of the fitted plume width | 56 |
| Figure 52. Synthetic CO2M observation of the total CO ₂ column around Berlin. | 57 |
| Figure 53. Total column images as generated by two modelling systems of the Paris urban area, on August 1 and August 5, 2018. An approximate location centred within Paris is indicated by the red dot. | 58 |
| Figure 54. COSMO-GHG comparison against the Jussieu station for Paris, 01-08 August 2018. | 59 |
| Figure 55. WRF-CHEM comparison against the Jussieu station for Paris, 01-08 August 2018. | 59 |
| Figure 56. Comparison between the Paris CO ₂ observations and simulations, shown both as a time-series and as a cross-plot. The observations are drawn in blue while the simulations are drawn in orange. | 61 |
| Figure 57. Comparison for TROPOMI columns with the total simulated NO ₂ . For COSMO-GHG, this NO ₂ column was created based on an NO _x tracer (NOX_PP_M + NOX_ANTH + NOX_BG) converted into an NO ₂ tracer. | 62 |
| Figure 58. The downwind evolution of the plume width for the Paris plume, following a Gaussian plume fit to the CO_CITY tracer. The black line shows one standard deviation of the fitted plume width. | 63 |
| Figure 59. Synthetic CO2M observation of the total CO ₂ column around Paris. | 63 |
| Figure 60. Total column images as generated by LOTOS-EUROS for the Randstad urban area with the CO2_RS tracer, on 18 th and 22 nd of June (S) and 18 th and 22 nd of December (W). An approximate location centred within the Randstad area is indicated by the red dot. | 64 |
| Figure 61. Comparison between the Cabauw CO ₂ observations and simulations, shown both as a time-series and as a cross-plot. The observations are drawn in blue while the | |

| | |
|--|----|
| simulations are drawn in orange. The left panels shows the summer (S) days, while the right columns show the winter (W) days. | 65 |
| Figure 62. Comparison between Randstad NO ₂ observations and simulations in the summer time, shown both as a time-series and as a cross-plot. The observations are drawn in blue while the simulations are drawn in orange. Identifying station IDs are given in the title for each subplot. | 66 |
| Figure 63. Comparison between Randstad NO ₂ observations and simulations in the winter time, shown both as a time-series and as a cross-plot. The observations are drawn in blue while the simulations are drawn in orange. Identifying station IDs are given in the title for each subplot. | 67 |
| Figure 64. Density plot of the R ² (higher is better) and RMSE (lower is better) scores, for the fit between NO ₂ observations and simulated values, for the summer and winter dataset of the Randstad region. | 67 |
| Figure 65. Comparison for TROPOMI columns with the total simulated NO ₂ . For LOTOS-EUROS, the NO ₂ column was modelled including full chemistry (NO ₂ _RS + NO ₂ _ANTH + NO ₂ _BG + NO ₂ _BIO). | 68 |
| Figure 66. Synthetic CO ₂ M observation of the total CO ₂ column around the Randstad area. | 68 |
| Figure 67. Example of online plume rise (top) versus a fixed emission profile (bottom) for a simplified 1D model around Jänschwalde, produced in MicroHH. The average vertically simulated profiles (right panels) differ considerably as a result. | 70 |

Tables

| | |
|---|----|
| Table 1. List of case studies considered in this study. | 18 |
| Table 2. Submitted tracers by the different models for the Bełchatów case. | 19 |
| Table 3. Submitted tracers by the different models for the Jänschwalde case. | 32 |
| Table 4. Submitted tracers by the different models for the Lipetsk case. | 43 |
| Table 5. Submitted tracers by the different models for the Matimba case. | 47 |
| Table 6. Submitted tracers by the different models for the Berlin case. | 51 |
| Table 7. Submitted tracers by the different models for the Paris case. | 57 |
| Table 8. CRDS measurement stations around Paris. | 58 |
| Table 9. Submitted tracers by one model for the Randstad case. | 64 |

1 Executive Summary

This deliverable is the result of an assessment of five high-resolution transport models (COSMO-GHG, ICON-ART, LOTOS-EUROS, MicroHH, WRF-CHEM) to simulate the plume from three large coal-fired power stations, a steel plant, and three (conglomerate) city plumes. The simulated results are compared against observations (in-situ airplane observations for two power plant cases and one city case are available; in-situ ICOS and other high-precision CO₂ measurements are available for two city cases; 43 NO₂ measuring stations are available for a city case; TROPOMI images are available for all cases), as well as amongst each other.

Over all, the transport models as run in their high-resolution setups (≤ 2 km horizontally) are capable of reproducing the in-situ observations moderately to extremely well. This partially answers a previously open research question regarding the “skill” of transport models to realistically reproduce individual plumes. The higher the model resolution, the better the fit with in-situ observations. The LES model of MicroHH (which ran at a high resolution of ~ 50 m horizontally) led to the most spatially resolved and narrowest plumes, and the best fit with the observations were obtained with this LES model. On the other end, when using a numerical weather prediction model at a low resolution (ICON-ART at ~ 2 km to 6 km horizontally), less spatially resolved and wider plumes were obtained, yielding a poorer fit to observations. The other models, ran at intermediate resolutions, generally produced plumes that fell in-between these two ends. Furthermore, full or simplified NO_x chemistry models used in LOTOS-EUROS and MicroHH could to some extent be approximated with a simple decaying NO_x tracer that was post-processed into NO₂ densities in a later step (when looking at NO_x:CO₂ and NO₂:CO₂ ratios in cross sectional slices along the plume, where NO_x=NO+NO₂). However, the degree of accuracy of these various chemistry models, and their dependency on model resolution, still requires further research.

The produced data were furthermore used to generate synthetic CO₂M satellite images, by computing total columns and binning these to the CO₂M resolution of about 2×2 km² pixels. This dataset (a “library of plumes”) is made available in a standardised NetCDF format, which may be obtained online (Koene & Brunner, 2022). After remapping to the CO₂M pixels, differences between the different model resolutions remained apparent (e.g., the MicroHH results remained more confined and of higher amplitude over the background and simulated noise floor), but generally it seems that all high-resolution setups (≤ 2 km horizontal resolution) produce roughly similar CO₂M images.

2 Introduction

2.1 Background

The future CO₂M satellites will be able to image plumes of strong (conglomerate) CO₂ point sources with a horizontal resolution of 2×2 km². In order to use this information in atmospheric inverse modelling systems, the underlying atmospheric models must be able to resolve these plumes and reproduce their basic properties. Currently, large uncertainties exist regarding the ability of atmospheric transport models to describe individual observed plumes, and the sensitivity to different model settings such as resolution, boundary layer and advection schemes, and the sensitivity to the representation of the source such as its temporal variability and injection height in the case of stack emissions. The aim of Task 4.1 is to investigate whether current high-resolution transport models can reproduce the basic properties of plumes originating from strong (clusters of) point sources.

2.2 Scope of this deliverable

2.2.1 Objectives of this deliverables

The objective of this deliverable is two-fold:

1. Assessing if current atmospheric transport models can reproduce plumes realistically, by comparing simulated tracer fields against observational data. The simulated fields are furthermore compared amongst the participating models, to investigate the variance amongst the models.
2. Generating synthetic CO₂M satellite observations from the model output. This dataset will be published, and may be used for investigations of plume detection and quantification methods (e.g., those explored in CoCO₂ WP4.2) or localized inversion techniques (e.g., those explored in CoCO₂ WP4.3).

2.2.2 Work performed in this deliverable

Seventeen simulations (4 for the Belchatów Power Station, 4 for the Jänschwalde Power Station, 2 for the Lipetsk Steel Plant, 2 for the Matimba Power Station, 2 for the Berlin urban area, 2 for the Paris urban area, 1 for the Randstad urban area) were performed, using five different modelling systems. The results were collected in a standardized format and compared against each other as well as against observations.

2.2.3 Deviations and counter measures

N/A.

3 Modelling methods

A description of the participating models can be found in deliverable CoCO₂ D4.1 (Krol & van Stratum, 2021). This section documents the model-specific set-ups used, and how the model output was generated and post-processed in a standardized way.

3.1 Model set-up

3.1.1 COSMO-GHG

COSMO-GHG (Jähn et al., 2020) was run for the Belchatów, Jänschwalde and Matimba power plant cases, the Lipetsk steel plant case, and the Berlin and Paris urban cases, at a horizontal modelling resolution of 0.01° on a rotated grid centred around the source of interest (i.e., a horizontal resolution of about 1.1 km), and on 60 vertical levels ranging from the surface to 23 km altitude. The output was horizontally remapped onto the target latitude-longitude output grids using bilinear interpolation. A biospheric model for vegetation uptake and respiration of CO₂ was achieved through the Vegetation Photosynthesis and Respiration Model (VPRM; Mahadevan et al., 2008), with a vegetation fraction cover map from the CORINE Land Cover (CLC) dataset for the year 2018 (EEA & JRC, n.d.) and the VPRM parameters from Gerbig (2021). A mistake was detected in the VPRM implementation within COSMO-GHG (concerning both the vegetation fractions and radiation parameter used to drive the model), due to which only the Berlin and Paris cases have a biogenic CO₂ tracer correctly modelled by the VPRM module, while the biogenic tracer for the other cases is not correctly modelled. A decaying NO_x(=NO+NO₂) tracer was implemented with a 4-hour exponential decay time (or “lifetime”) (i.e., following the ordinary differential equation $\dot{\rho} = -\frac{\rho}{4[\text{hrs}]}$ for a concentration ρ), instead of having a separate NO and NO₂ tracer. In section 3.3.3 it is described how the NO_x tracer is converted into an NO₂ tracer.

Simulations were driven with initial and boundary conditions from CAMS data for CO₂, CO (at 0.1° horizontal resolution) and NO_x (at 0.5° horizontal resolution). COSMO-7 fields (the operational analyses of MeteoSwiss) were used for initial and boundary conditions for the meteorology for cases within the EU, while the European Centre for Medium-Range Weather Forecasts (ECMWF) Integrated Forecast System (IFS) fields were used for cases outside of it. Meteorological nudging towards weather observations was performed for the regions within Europe.

3.1.2 ICON-ART

The *Icosahedral Nonhydrostatic* (ICON) model (Zängl et al., 2015) was run with its *Aerosols and Reactive Trace gases* (ART) transport scheme (Schröter et al., 2018) to simulate the CO₂ plumes of the Jänschwalde and Bełchatów and power plants as passive tracers. As explained in Zängl (2013): “to allow for mass-consistent tracer transport, the air mass fluxes are aggregated over the small timesteps in the dynamical core and then passed to the transport scheme. Tracer transport is performed with a flux-form semi-Lagrangian scheme following Miura (2007) with options for second-order and third-order accuracy for horizontal transport. The second-order variant is also used in the dynamical core”. Further citing Zängl: “For vertical transport, a piecewise parabolic reconstruction of the sub-grid tracer distribution provides third-order accuracy, and an option for summation of partial fluxes allows vertical CFL numbers much larger than 1. For horizontal and vertical transport, monotonous and positive definite limiters are available. Further information on the horizontal transport scheme, and a set of idealized validation tests, can be found in Lauritzen et al. (2014).”

Only passive tracer transport (i.e., no ART chemistry) was applied for CO₂ tracers in the limited area model (LAM) simulations, spanning for the Jänschwalde case two resolutions of 6.5 km and 2.2 km, respectively, with 60 and 65 vertical levels, respectively, and choosing the domain over Europe (60 levels) and Germany (65 levels), respectively. In this report, only the 2.2 km case will be discussed. The model top height for Europe is 23 km while it is 22 km for Germany. As not the full vertical output is of interest, only the lowest 24 levels had been provided, which cover from the ground to at least 5 km height. For the Bełchatów case, only one resolution of 6.5 km, with 60 vertical levels, in the domain over Europe was run.

Meteorological initial conditions and boundary conditions (every hour) were taken from the operational ICON-EU model analysis fields of DWD (which are generated operationally). A free LAM forecast was run for 48 hours (ICON binary used: icon-master-a0fa90499).

Plume vertical emission profiles were interpolated (mass-conserving) onto the ICON vertical layers. In the Jänschwalde case, no other emissions than the power plant plumes were used. No initial or boundary conditions for background fields had been used. In the Bełchatów case, besides the power plant plume, the TNO anthropogenic area and point source emissions were also simulated. Initial and boundary conditions from CAMS global GHG reanalysis (EGG4) were used for modelling the background field.

The resulting CO₂ concentration fields on the original ICON grids (ICON EU with 6.5 km resolution) were interpolated onto the (finer) target lon-lat grids with cdo command remapdis, employing the weighted distances of 3 next neighbour grid points (because of the triangular grid). Naturally, the (coarser) triangular modelling cells are still visible in the (finer) target resolution, which is desirable as any resolution refinement would be an artefact.

3.1.3 LOTOS-EUROS

The atmospheric chemical transport model LOTOS-EUROS v2.2 (Manders et al., 2017) was used to simulate the Berlin and Randstad urban areas, and the Bełchatów and Jänschwalde power plants. The model includes the full chemistry scheme to investigate the chemical processes in the plumes related to NMVOC, OH and NO_x. In addition, the concentrations were

labelled (Kranenburg et al., 2013). This way, the source category of the emissions (power plant, anthropogenic, biogenic, boundary and initial conditions) is traced back while non-linear effects in the chemistry are still correctly represented. The biogenic tracer includes the vegetation respiration (source of CO₂) only, while the vegetation uptake (sink of CO₂) is implemented by subtracting from all labelled concentrations the same percentage as the percentage of CO₂ uptake to the total CO₂ concentration. Simulations were driven with initial and boundary conditions from the CAMS global (greenhouse gas) reanalysis. The output was interpolated onto the target latitude-longitude output grids using bilinear interpolation.

The model for the power plant simulations (Bełchatów and Jänschwalde) was set up with 14 vertical levels ranging from the surface to about 10 km altitude, and a horizontal modelling resolution of 0.01° (about 1.1 km). The simulations are driven by the meteorology fields as provided by Empa using COSMO-GHG. Therefore, both LOTOS-EUROS and COSMO-GHG simulations use the same meteorological conditions for the power plant runs. The vegetation uptake and respiration of CO₂ is based on the same models as also applied in the CAMS global greenhouse gas reanalysis.

For the urban runs (Berlin and Randstad) the model was set up with 26 vertical levels ranging from the surface to about 11 km altitude. For these runs, the horizontal modelling resolution was set to 0.02° (about 2 km). The simulations are driven by COSMO-2km meteorology fields. The biogenic model for vegetation uptake and respiration of CO₂ was achieved with VPRM as in COSMO-GHG, with the VPRM parameters from Gerbig (2021).

3.1.4 MicroHH

The MicroHH (van Heerwaarden et al., 2017) large-eddy simulations (LESs) were run on a domain of 51.2 km × 51.2 km × 4 km for the Jänschwalde, Bełchatów, and Lipetsk cases, and a 128 km × 128 km × 4 km domain for the Matimba case. All cases were simulated on a 50 m × 50 m × 25 m resolution, except for the Matimba case, which used a 100 m horizontal resolution. As this spatial resolution is much finer than the target grid, the 3D output was interpolated onto the target latitude/longitude grid.

All simulations were performed using an interactive land-surface (HTESSEL, without CO₂ interactions; Balsamo et al., 2009) and radiation (RTE-RRTMGP; Pincus et al., 2019) model. The chemistry scheme used for the chemical reactive species is a condensed version of the chemical scheme implemented in IFS (Huijnen et al., 2016) and focusses on correct calculations of the equilibrium between NO_x and ozone (photo-stationary state) and the NO_x lifetime. Photolysis rates are calculated for clear sky conditions with the TUV module (Madronich & Flocke, 1999). The Rosenbrock solver of the kinetic rate equations is generated automatically by the Kinetic Pre Processor (KPP; Damian et al., 2002; Sandu et al., 2022).

The LES simulations were initialised and driven by ERA5 (meteorology) and CAMS (scalars and reactive gasses), with a coupling as described by e.g. Neggers et al. (2012). In this setup, the atmosphere and soil are initialised from ERA5 and CAMS. Furthermore, the LESs are coupled to the large-scale weather through a set of large-scale forcings acting on the LES domain. These forcings contain the advective tendencies of heat, moisture, and momentum, the large-scale subsidence velocity, and the geostrophic wind components. These terms are applied in LES as time- and height-varying, but spatially constant, external forcings. To limit the required domain size, the simulations used periodic lateral boundary conditions (BCs) for temperature, humidity, and momentum. Only the scalars and reactive gasses used a Dirichlet lateral BC (CAMS) on the inflow boundaries, and a Neumann lateral BC on the outflow boundaries. The land-surface properties were obtained from the 2018 CORINE dataset (EEA & JRC, n.d.).

3.1.5 WRF-CHEM

The WRF-Chem V3.9.1 model was used to simulate atmospheric CO₂ concentrations for the Paris urban case. The model consists of one-way interactive triple-nested domains at horizontal resolutions of 25 km, 5 km and 1 km, covering Europe, Northern France and the Paris metropolitan area respectively (Lian et al., 2019). All domains use a Lambert conformal projection. The output was horizontally remapped onto the target latitude-longitude output grids using bilinear interpolation. The model was run with 44 terrain-following (Eta) vertical levels, of which 25 layers are within the lowest 1.5 km and the top layer is at about 20 km altitude.

Biogenic CO₂ fluxes are simulated with VPRM (as in COSMO-GHG), forced by meteorological fields simulated by WRF, and online-coupled to the atmospheric transport. The vegetation indices (enhanced vegetation index and land surface water index) were derived from the 8-day MODIS Surface Reflectance Product (MOD09A1) and four parameters for each vegetation category (PAR0, λ , α , β) were optimized against eddy covariance flux measurements over Europe collected during the Integrated EU project “CarboEurope-IP” (<http://www.carboeurope.org/>). The land cover data used by VPRM are derived from the 1-km global Synergetic Land Cover Product (SYNMAP, Jung et al., 2006), reclassified into 8 different vegetation classes (Ahmadov et al., 2007).

The meteorological initial and lateral boundary conditions were retrieved from the global ECMWF Reanalysis v5 (ERA5), available at 0.75° × 0.75° spatial resolution and 6 h temporal resolution. We nudged the 3D fields of temperature and wind to the ERA5 reanalysis in layers above the atmospheric boundary layer (ABL) of the outer two domains using the grid nudging option in WRF. We also assimilated surface weather station data (ds461.0) and upper-air meteorological fields (ds351.0) (National Centers For Environmental Prediction/National Weather Service/NOAA/U.S. Department Of Commerce, 2004; Satellite Services Division/Office Of Satellite Data Processing And Distribution/NESDIS/NOAA/U.S. Department Of Commerce & National Centers For Environmental Prediction/National Weather Service/NOAA/U.S. Department Of Commerce, 2004) using a nudging technique. Initial and lateral boundary conditions for CO₂ concentration fields were taken from the 3-hourly fields of the CAMS global CO₂ atmospheric inversion product (version v18r1) with a horizontal resolution of 3.75°×1.90° (longitude × latitude) and 39 vertical levels between the surface and the tropopause.

3.2 Output format and storage

A standardized CF-compliant NetCDF4 format was decided upon early in the process (described in CoCO₂ D4.1, Krol & van Stratum, 2021), with hourly output tracers (e.g., “CO₂_PP_M” to designate the “middle” CO₂ release profile for the power plant) at pre-defined latitude-longitude positions, at the model output's native vertical resolution.

Detailed modelling instructions (e.g., exact placement of the stacks, emission rates for all species, vertical and temporal profiles, etc.) have been provided in the modelling protocols for each of the cases, which will be provided as an appendix to this report. These protocols also define the exact set and meaning of tracers applicable for each of the case studies; these protocols are given as an appendix to this report. However, in short:

- For the three power plant cases and the steel plant case, output was requested on both a “small” and a “large” grid – with a finer horizontal resolution on the “small” domain and a coarser resolution on the “large” domain. For the city cases, only one output domain extent was prescribed.
- For the four point source cases, different vertical profiles were given: a surface release (“CO₂_PP_L”), a middle release corresponding to the expected emission height (“CO₂_PP_M”), and a high release (“CO₂_PP_H”). For all other sources, including those used in the three city cases (“CO₂_CITY” for Paris and Berlin, and “CO₂_RS”

for the Randstad case), the default TNO emission heights were used (see Table 3 in CoCO₂ deliverable D2.1, Denier van der Gon & CoCO₂ WP2 team, 2021).

- Other anthropogenic sources in or around the domain were output in a "CO₂_ANTH" tracer; a tracer for the background concentrations (i.e., transported initial and boundary conditions) was designated as "CO₂_BG"; a tracer for biogenic sources and sinks of CO₂ was stored as "CO₂_BIO".

If additional species were modelled (e.g., CO, or NO₂), an analogous naming scheme was used (e.g., "CO_PP_M", or "NO₂_PP_M").

Results were collected on the Integrated Carbon Observation System Carbon Portal (ICOS-CP) fileshare (<https://fileshare.icos-cp.eu/apps/files/>), where all the subsequent processing was performed using the ICOS-CP Jupyterhub (<https://jupyter.icos-cp.eu/>).

3.3 Postprocessing

3.3.1 Column computation

To compute CO₂ columns (as well as NO₂ or CO columns) from the simulated datasets, we follow the calculation

$$\left\{ \begin{array}{l} M_{dry-air, \frac{kg}{m^2}, i} = -\frac{P_{i+\frac{1}{2}} - P_{i-\frac{1}{2}}}{g} (1 - Q), \\ M_{dry-air, \frac{mol}{m^2}, i} = M_{dry-air, \frac{kg}{m^2}, i} \cdot \frac{1000}{m_{dry-air}}, \\ CO_{2, \frac{mol}{m^2}, i} = M_{dry-air, \frac{mol}{m^2}, i} \cdot CO_{2, \frac{mol}{mol}, i}, \\ CO_{2, \frac{mol}{m^2}} = \sum_i CO_{2, \frac{mol}{m^2}, i}, \\ XCO_{2, ppm} = \frac{CO_{2, \frac{mol}{m^2}}}{\sum_i M_{dry-air, \frac{mol}{m^2}, i}}, \end{array} \right.$$

where $g = 9.81 \text{ m/s}^2$ is the gravitational acceleration for the earth, $m_{dry-air} = 28.97 \text{ gram/mol}$ is the molecular weight of dry air, $P_i \text{ [Pa]}$ is the pressure in cell i , Q_i is the humidity fraction of cell i , and index i gives the discrete vertical index of each cell in increasing order. N.B.: $P_{i\pm\frac{1}{2}}$, the pressure at vertical half-levels in-between two cells, is one of the fields generated by the participating models. $CO_{2, \frac{mol}{mol}, i}$ (or analogous for other atmospheric gases) is the volume mixing ratio as generated by the participating models. Hence, all quantities in the above computations could be taken directly from the model output fields.

3.3.2 Synthetic CO₂M observation

To compute total column XCO₂, it is important to have access to the full column up to the top of the atmosphere. As CO₂ has a considerable volume mixing ratio up to the mesosphere (beyond the altitude of any of the participating models), it was important to add the missing mass of CO₂ and dry air above the simulated data before computing the total column. Therefore, we extended all XCO₂ fields by interpolating the additional weight of the CO₂ and the dry air in the layers above the model output from the CAMS atmospheric composition fields at 3-hourly and 0.1° horizontal resolution (at 137 vertical levels, (ECMWF, n.d.) but only using those levels at and above the maximum simulation altitude). CAMS experiment ID 'gznv' is used for the Bełchatów, Lipetsk, Berlin and Paris cases, 'ggpe' for Jänschwalde, and 'h9sp' for Matimba; Q. Errera et al., 2021).

To create a synthetic CO₂M observation, XCO₂ fields were computed following the computation described in the previous section(s). A local grid with pixels of 2×2 km² was defined around the emission source of interest. The computed XCO₂ field was remapped onto this grid using a ‘conservative remapping’ procedure from CDO (where the fraction of a source cell overlapping with target cells defines the weight given to convert the source values into the target values; Schulzweida, 2022). Finally, Gaussian noise of magnitude 0.7 ppm was added onto the remapped XCO₂ fields, which is the ‘medium’ noise case for a vegetation-type albedo and solar zenith angle of 50° for CO₂M, as described in Kuhlmann et al. (2019).

3.3.3 NO_x to NO₂ conversion

To convert from NO_x mole fractions to NO₂ mole fractions for the COSMO-GHG model, we first convert the NO_x concentrations from volume mixing ratios into densities following

$$C_{\frac{kg}{m^3}} = C_{\frac{mol}{mol}}(1 - Q) \frac{P}{R_{NO_2} T},$$

where C is the concentration in units given by the subscripts, $R_{NO_2} = 180.730$ [J/(kg K)] is the specific gas constant for NO₂ (i.e., the universal gas constant divided by the molar mass of NO₂), and T is the temperature of air. Then we follow Düring et al. (2011), who give an empirical relation to convert NO_x densities to NO₂ densities as

$$NO_{2, \frac{\mu g}{m^3}} = \frac{29 \cdot NO_{x, \frac{\mu g}{m^3}}}{(NO_{x, \frac{\mu g}{m^3}} + 35)} + 0.217 \cdot NO_{x, \frac{\mu g}{m^3}}.$$

We can convert back to a NO₂ volume mixing ratio by inverting the equation above. Then we can compute a total column of NO₂ following the equations given in section 3.3.1.

3.3.4 Analyse NO_x/CO₂ ratio downstream of the plume

To analyse the downstream chemistry of NO_x (e.g., the NO₂/CO₂ ratio, to determine the depletion of the reactive NO compounds compared to the inert CO₂ emissions in the downstream direction), we first compute columns of CO_{2, \frac{mol}{m^2}}} and NO_{2, \frac{mol}{m^2}}} following the procedure described above. Then, we apply a plume detection procedure from the Python package ‘ddeg’ (data-driven emission quantification, Kuhlmann et al., 2019, 2020, 2021; EMPA, n.d.). Following the plume detection, a 2nd order polynomial is fitted from the source location, downwind along the detected plume pixels to describe a local plume coordinate system (i.e., with one coordinate x following the “along plume” direction, and a perpendicular coordinate y following the “across plume” direction). At intervals of every 3 km in the

downstream direction of the plume and roughly 30 km across the plume, we select all the available pixels and bin these values. An example is given in Figure 1.

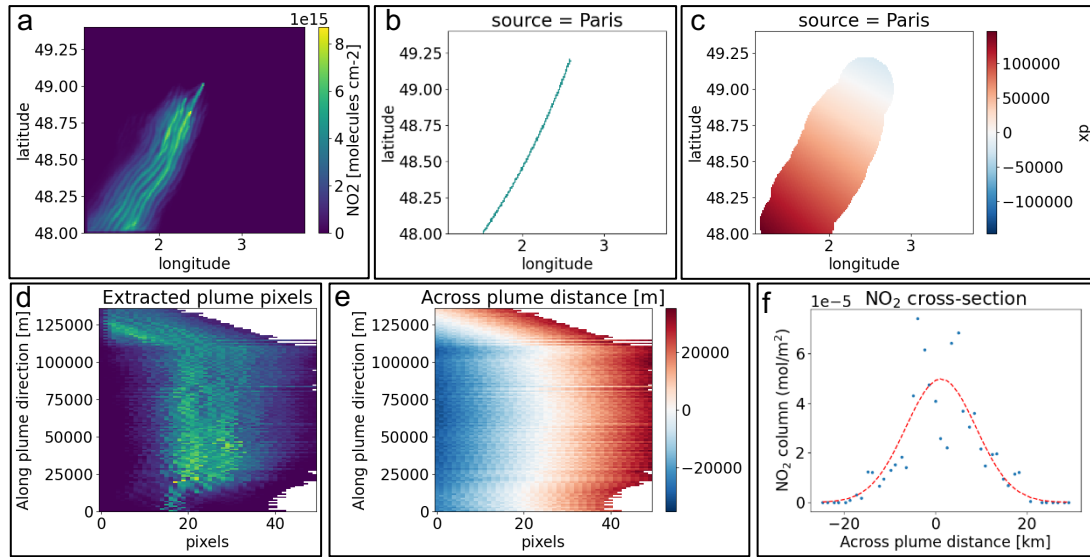


Figure 1. Example of obtaining plume cross-sections for column images. (a) Column image of NO₂ simulated with COSMO-GHG. (b) Estimation of a 'plume centre line' for this source. (c) Example of fitted plume coordinate system, with x_p the distance along the plume in meters. (d) Extracted NO₂ plume pixels, sorted in bins of a fixed distance along the plume. (e) The associated 'across plume distance' for each of the selected pixels in meters relative to the plume centre. (f) An example plot of the NO₂ plume cross-section at a distance of roughly 15 km downstream along the plume (the blue dots, unequally spaced in the across plume direction, are the data; the red dotted line is a Gaussian curve fitted to the data).

By this process of obtaining plume cross-sections, we can then approximate the ratio between NO₂ and CO₂ column line densities as

$$\frac{\text{NO}_2}{\text{CO}_2}(x) = \frac{\int \text{NO}_2(x, y) dy}{\int \text{CO}_2(x, y) dy} \approx \frac{\sum_y \text{NO}_{2, \frac{\text{mol}}{\text{m}^2}}(x, y)}{\sum_y \text{CO}_{2, \frac{\text{mol}}{\text{m}^2}}(x, y)}.$$

3.3.5 Analysis of the plume width downstream

Following the process of obtaining plume cross-sections as described above, we can attempt to fit a Gaussian profile to each across-track (y) in the downstream (x) direction,

$$\text{NO}_2(x) \approx \frac{L}{\sqrt{2\pi}\sigma(x)} e^{-\frac{(y-y_0)^2}{2\sigma^2(x)}},$$

using the Scientific Python (scipy) curvefit tool (Virtanen et al., 2020). The parameter y_0 allows us to account for an offset between the fitted plume coordinate system and the actual centre of mass of the plume for any given downstream 3 km polygon section, and parameter L expresses the integral under the plume cross-section, though this parameter is not used in this study. An example of such a fit can be seen in Figure 1. The fitted standard deviation $1\sigma(x)$ can be plotted in the downstream direction, to give an approximate measure of the plume width in the downstream direction. By additionally showing the standard deviation of the fitted width (also estimated by the scipy curvefit tool) we can visualize the uncertainty of our estimate.

3.3.6 Curtain plots for in-situ data

In cases where in-situ data is available (e.g., from aircraft measurements), curtain plots are shown which plot the observation time (on the horizontal axis) against a vertical cross-section of the atmospheric concentrations at the time-varying observation locations. These plots are generated by using the 3D location (longitude, latitude, altitude) for each time-step of the measuring station, and then interpolating the corresponding vertical profile of the atmosphere (in time and space) for that time-step using bilinear interpolation in the Python package xarray (Hoyer & Hamman, 2017). After the curtain is computed, it is simple to furthermore extract via vertical interpolation the simulated value at the same altitude as the observation station, to plot a comparison between the measured in-situ observations and the simulated observations.

4 Case studies

As described in CoCO₂ D4.1 (Krol & van Stratum, 2021), seven test cases were selected that are relevant for emission verification. A short description of the case studies is given in Table 1. The various case studies are displayed in the map of Figure 2. Detailed modelling instructions (e.g., exact placement of the stacks, emission rates for all species, vertical and temporal profiles, etc.) have been provided in the modelling protocols for each of the cases, which will be provided as an appendix to this report.

Table 1. List of case studies considered in this study.

| Case ID | Description | Time period | Available observations | Modelled with |
|------------|-----------------------------------|-----------------|---|---|
| BEL | Power plant Bełchatów, Poland | 6-7 June 2018 | In-situ observations (CO ₂) and remotely sensed observations (XCO ₂) from three aircraft; TROPOMI NO ₂ . | COSMO-GHG, ICON-ART, LOTOS-EUROS, MicroHH |
| JAE | Power plant Jänschwalde, Germany | 22-23 May 2018 | In-situ observations (CO ₂) and remotely sensed observations (XCO ₂) from two aircraft; TROPOMI NO ₂ . | COSMO-GHG, ICON-ART, LOTOS-EUROS, MicroHH |
| LIP | Steel plant Lipetsk, Russia | 12-13 June 2019 | TROPOMI CO. | COSMO-GHG, MicroHH |
| MAT | Power plant Matimba, South Africa | 24-25 July 2020 | TROPOMI NO ₂ . | COSMO-GHG, MicroHH |
| BER | Berlin urban area, Germany | 18-27 July 2018 | In-situ observations (CO ₂) from one aircraft; TROPOMI NO ₂ . | COSMO-GHG, LOTOS-EUROS |
| PAR | Paris Urban Area, France | 1-8 August 2018 | Seven high-precision stationary CO ₂ measuring stations; TROPOMI NO ₂ . | COSMO-GHG, WRF-CHEM |

| | | | | |
|-----------|----------------------------|--|---|-------------|
| NL | Randstad area, Netherlands | 16-23 June 2018, and 16-23 December 2018 | One high-precision stationary CO ₂ measuring station; forty-three stationary NO ₂ measuring stations; TROPOMI NO ₂ . | LOTOS-EUROS |
|-----------|----------------------------|--|---|-------------|

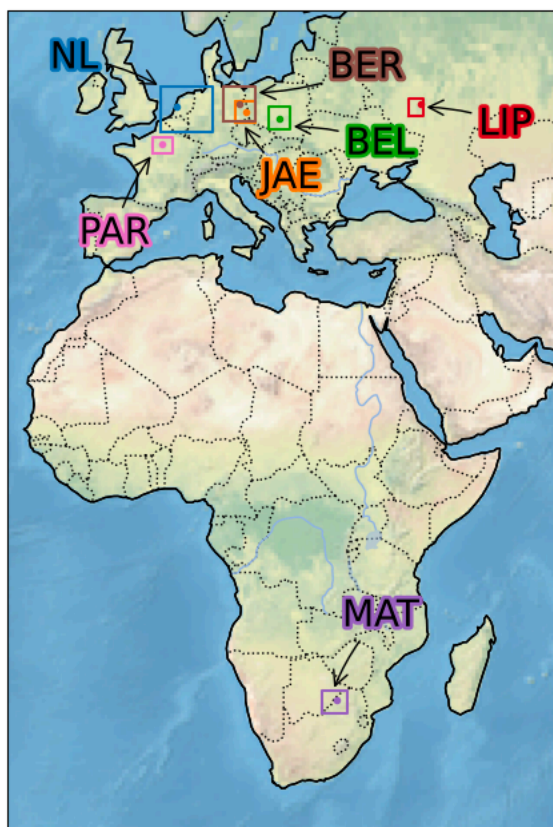


Figure 2. Map of the seven cases considered in this study (indicated by their abbreviations or case IDs), including the source location (indicated by a coloured dot) and the “large” model extent (indicated by the bounding box).

In the following sections, we will describe the simulation intercomparison and comparison against observations for each individual case study. As the analysis was carried out in a standardized form, the first case study will be described in greater detail than the cases that follow it.

4.1 Point sources

4.1.1 Bełchatów (2018-06-06 – 2018-06-07)

The Bełchatów Power Station is a coal-fired power station near Bełchatów, in central Poland. It is the largest thermal power station in Europe. Four models (COSMO-GHG, ICON-ART, LOTOS-EUROS, and MicroHH) simulated its plume. The LOTOS-EUROS model used the meteorology from COSMO-GHG. The submitted tracers can be found in Table 2.

Table 2. Submitted tracers by the different models for the Bełchatów case.

| Model | Submitted tracers |
|------------------|--|
| COSMO-GHG | CO2_PP_M, CO2_PP_L, CO2_PP_H, CO2_ANTH, CO2_BG, CO2_BIO, CO_PP_M, CO_ANTH, CO_BG, NOX_PP_M, NOX_ANTH, NOX_BG |

| | |
|--------------------|--|
| ICON-ART | CO2_PP_M, CO2_PP_L, CO2_PP_H, CO2_ANTH, CO2_BG |
| LOTOS-EUROS | CO2_PP_M, CO2_PP_L, CO2_PP_H, CO2_ANTH, CO2_BG, CO2_BIO, CO_PP_M, CO_PP_L, CO_PP_H, CO_ANTH, CO_BG, CO_BIO, NO_PP_M, NO_PP_L, NO_PP_H, NO_ANTH, NO_BG, NO_BIO, NO2_PP_M, NO2_PP_L, NO2_PP_H, NO2_ANTH, NO2_BG, NO2_BIO, OH, TNMVOC_PP_M, TNMVOC_PP_L, TNMVOC_H, TNMVOC_ANTH, TNMVOC_BG, TNMVOC_BIO, TPM10_PP_M, TPM10_PP_L, TPM10_PP_H, TPM10_ANTH, TPM10_BG, TPM10_BIO, TPM25_PP_M, TPM25_PP_L, TPM25_PP_H, TPM25_ANTH, TPM25_BG, TPM25_BIO |
| MicroHH | CO2_PP_M, CO2_BG, CO_PP_M, CO_BG, NO_PP_M, NO_BG, NO2_PP_M, NO2_BG, O3_PP_M, O3_BG, C3H6_PP_M, C3H6_BG, OH_PP_M, OH_BG |

4.1.1.1 Overview column images

We first show an overview plot of the plumes modelled with the middle emission profile ("M") in Figure 3. The plumes have been converted to total columns of CO₂ to allow a simple comparison. The plume is generally transported in the same direction in all models.

The results from COSMO-GHG and LOTOS-EUROS follow a relatively similar evolution over time, which is not surprising as the latter used the same meteorology as the former. Unlike the singular plume in COSMO-GHG, however, the plume simulated by LOTOS-EUROS clearly follows a bimodal cross-section in the form of two 'line-like' features in this column view. This effect also persists for the surface emission profile ("L"), shown in Figure 4. The reason for this is likely the coarse vertical resolution of the LOTOS-EUROS model (14 layers instead of 60 layers for COSMO-GHG), which is not able to capture the gradual- and altitude-varying wind direction. Furthermore, we can see that there is considerable small-scale turbulence developing from 12:00 onwards with relatively wide turbulent structures in both models. A notable effect can be observed around 16:00, where the COSMO-GHG plume mixes into the free troposphere, where the wind direction was nearly opposite to that in the ABL.

The ICON-ART simulations clearly contain triangular footprints corresponding to the used modelling grid (with a resolution of roughly 6 km). Correspondingly, the turbulence as simulated with ICON-ART is of a coarser length scale than what is visible for the other models, and shows up as more of a general downstream diffusion; but, e.g., at 20:00 it can still be observed that large-scale turbulence is simulated within the model.

On the other hand, MicroHH (which was only run for a small section due to computational limitations for their high-resolution simulation) shows a narrower plume than what is seen for the other models. Also, the turbulent structures appear to have a smaller length scale than what is visible in the other models.

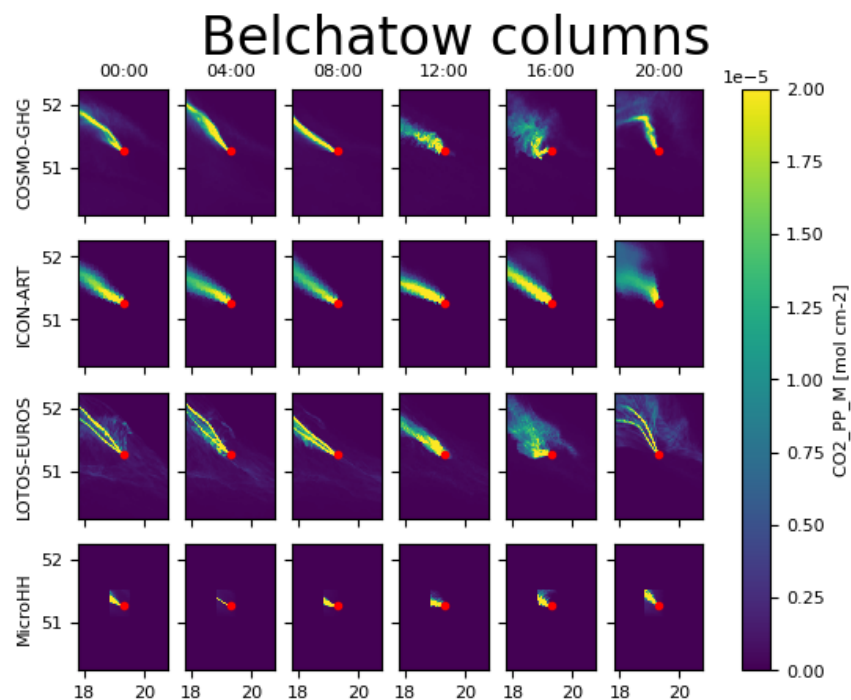


Figure 3. Total column images as generated by four modelling systems of the Belchatów powerplant plume, on June 7th, 2018, for the "middle" emissions profile M. The location of the powerplant is indicated by the red dot.

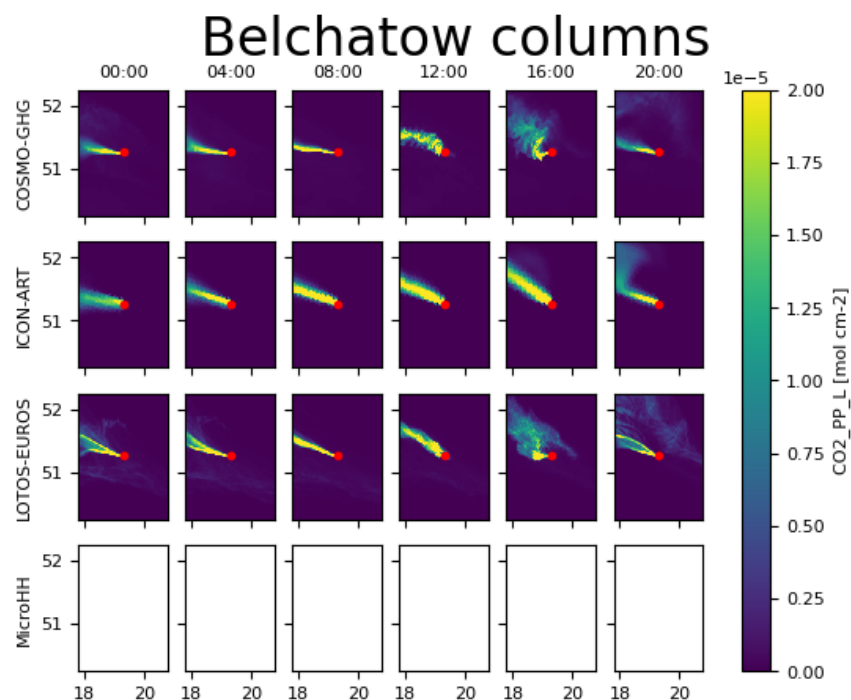


Figure 4. Total column images as generated by four modelling systems of the Belchatów powerplant plume, on June 7th, 2018, for the "surface" emissions profile L. The location of the powerplant is indicated by the red dot. This emission profile case was not modelled in MicroHH.

Zooming in on an area surrounding the powerplant, as done in Figure 5, we can see the finer-scale structures of wind shear and turbulence, e.g., as visible in the feather-like or density fingering features of the MicroHH results. The plume at 04:00 in the MicroHH model is considerably narrower than the plumes observed in the other models. One reason for this can

be that a 'point source' can still be only as narrow as the modelling grid allows. Coarser models thus emit the power plant emissions already in a wide plume, while the emissions in MicroHH can start very confined. If flow is furthermore primarily laminar as is typical at night time, the plume will not open up considerably. Onset of turbulence becomes visible at 08:00 for the MicroHH LES model, and the plume is slightly wider in this early morning setting compared to the other models which still show a more compact and laminar flow at this time. As becomes clear during the daytime, MicroHH resolves a lot more finer-scale turbulence than what can be seen for the other models.

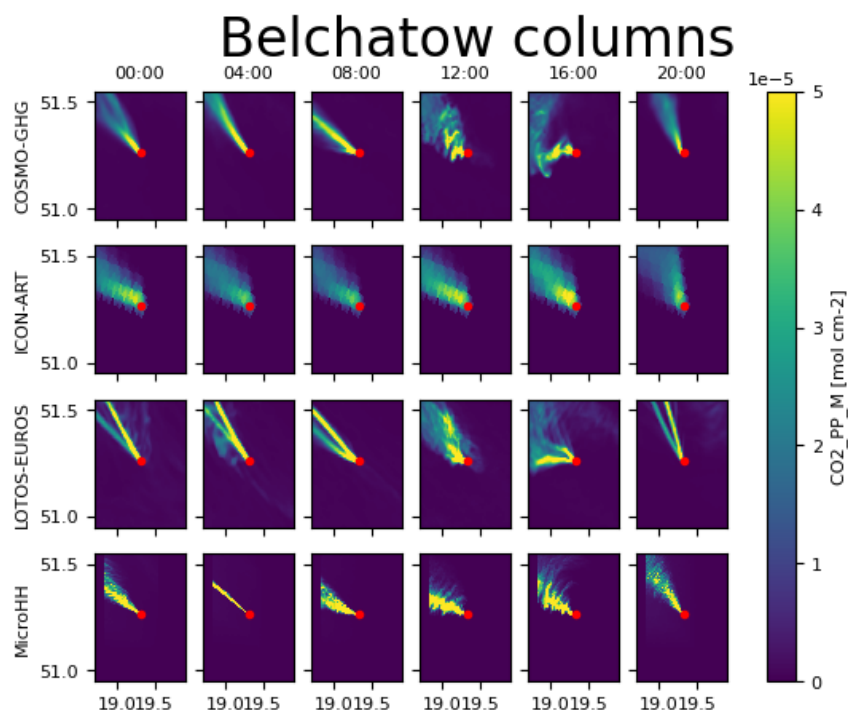


Figure 5. Zoom on the total column images as generated by four modelling systems of the Belchatów powerplant plume, on June 7th, 2018, for the "middle" emissions profile M. The location of the powerplant is indicated by the red dot.

4.1.1.2 Comparison against in-situ CO₂ observations

In-situ CO₂ measurements were made in the Cessna aircraft from DLR, equipped with a Picarro G1301-m instrument, in the context of the Carbon Dioxide and Methane (CoMet) mission (see Fiehn, Kostinek, et al. (2020) for further details; and Fiehn, Kostinek, Julian, et al. (2020) for the associated data). Twelve transects through the Belchatów plume were flown at multiple levels, at three increasing distances from the source, primarily within the ABL. The CO₂ measurements along these transects provide detailed insights into the horizontal and vertical extent of the plume. The simulations (that is, the CO₂_PP_M+CO₂_ANTH+CO₂_BG+CO₂_BIO tracers, where available) were interpolated to the corresponding flight locations at given times, to allow a comparison of the in-situ observations with the modelled fields, as well as providing curtain plots.

The results for COSMO-GHG can be found in Figure 6, where the simulation results are offset by -14 ppm to match the observations. It is clearly visible that the DLR-Cessna observations show large CO₂ concentrations at high altitudes above about 1800 m. These enhancements are likely due to the higher background CO₂ above the ABL, which is typical for summertime when biospheric uptake by photosynthesis reduces CO₂ within the continental ABL (Sweeney et al., 2015). These elevated values are not reproduced in any of the participating models. It is clearly visible in the curtain plot that the plume essentially extends from the surface to the top of the ABL in all transects, suggesting rapid vertical mixing in an unstable, convective ABL. There is considerable wind shear present, visible in the 'diagonal' shape of the plume in the

curtain plots. Time series of CO₂ along the DLR-Cessna flight were averaged over 5 s intervals along the flight track, which corresponds to a distance of about 350 m per sample. The observations reveal sharp peaks of more than 40 ppm in the first transects, and gradually wider and lower peaks in the later transects. These peaks are moderately well reproduced in the simulation, although the plumes modelled within COSMO-GHG are generally a bit too wide compared to the observations. As is clearly visible in the column plot in Figure 6, this was a turbulent plume at the moment of aircraft overpass, with eddies of large length scales. Hence, while the results for the transects at the first two distances with the plume (~13:00 until ~14:00) are relatively well modelled, the results at the further distances are not well-reproduced by COSMO-GHG in the region where the plume is highly turbulent (and thus contains a level of randomness). Hence, the lessening fit at further offsets is not unexpected.

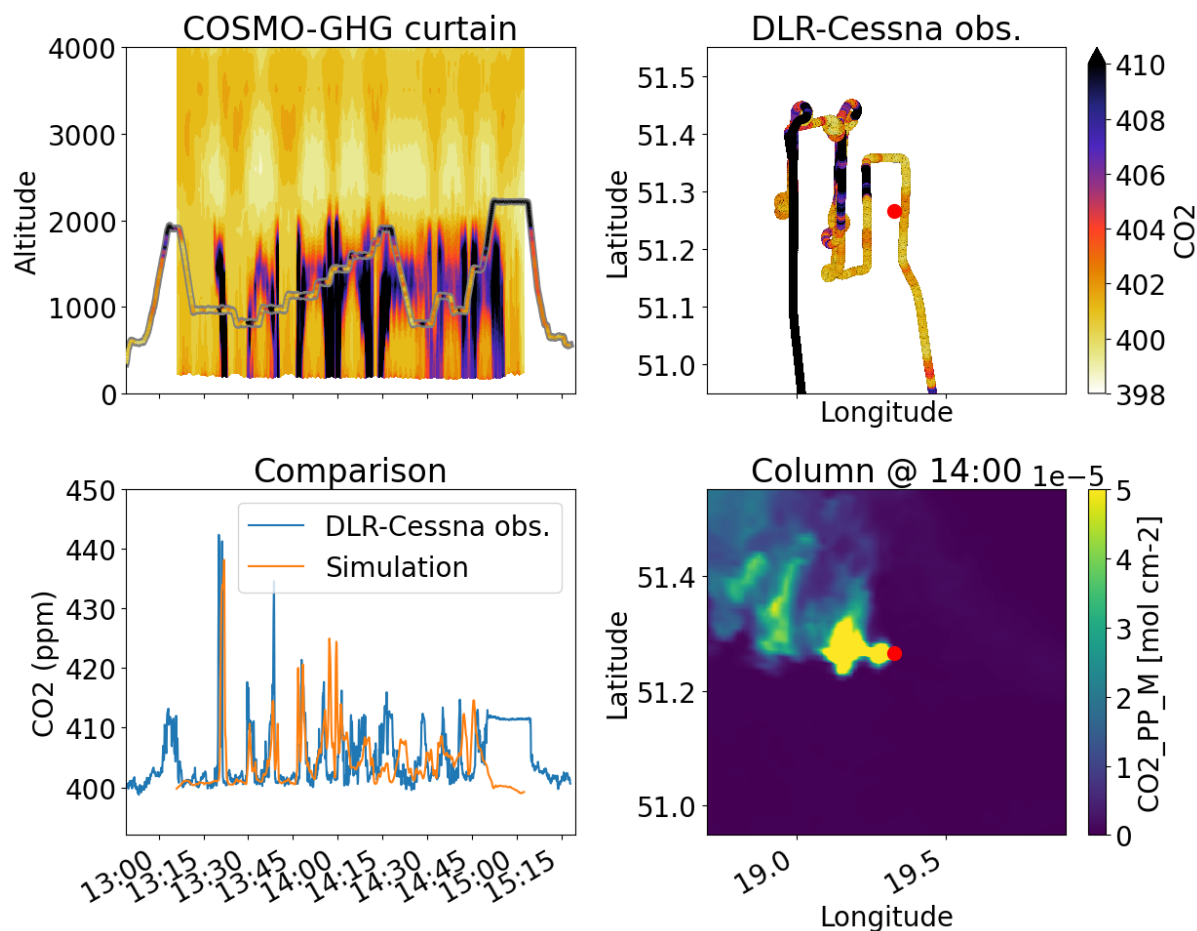


Figure 6. COSMO-GHG comparison against DLR-Cessna for Belchatów, 7 June 2018.

The results for ICON-ART can be found in Figure 7, where the simulation results are offset by -12 ppm to match the observations. As for the COSMO-GHG result, the transects close to the plume (~13:00 until ~14:00) are well-reproduced within the model, although it is clear that there is a significant imprint of the 6 km horizontal modelling resolution, meaning that the simulated plumes are considerably wider than the observed plumes. Unlike the COSMO-GHG result, there is no clear sign of wind shear, as the plumes extend rather straight within the curtain plot all the way from the surface to the ABL.

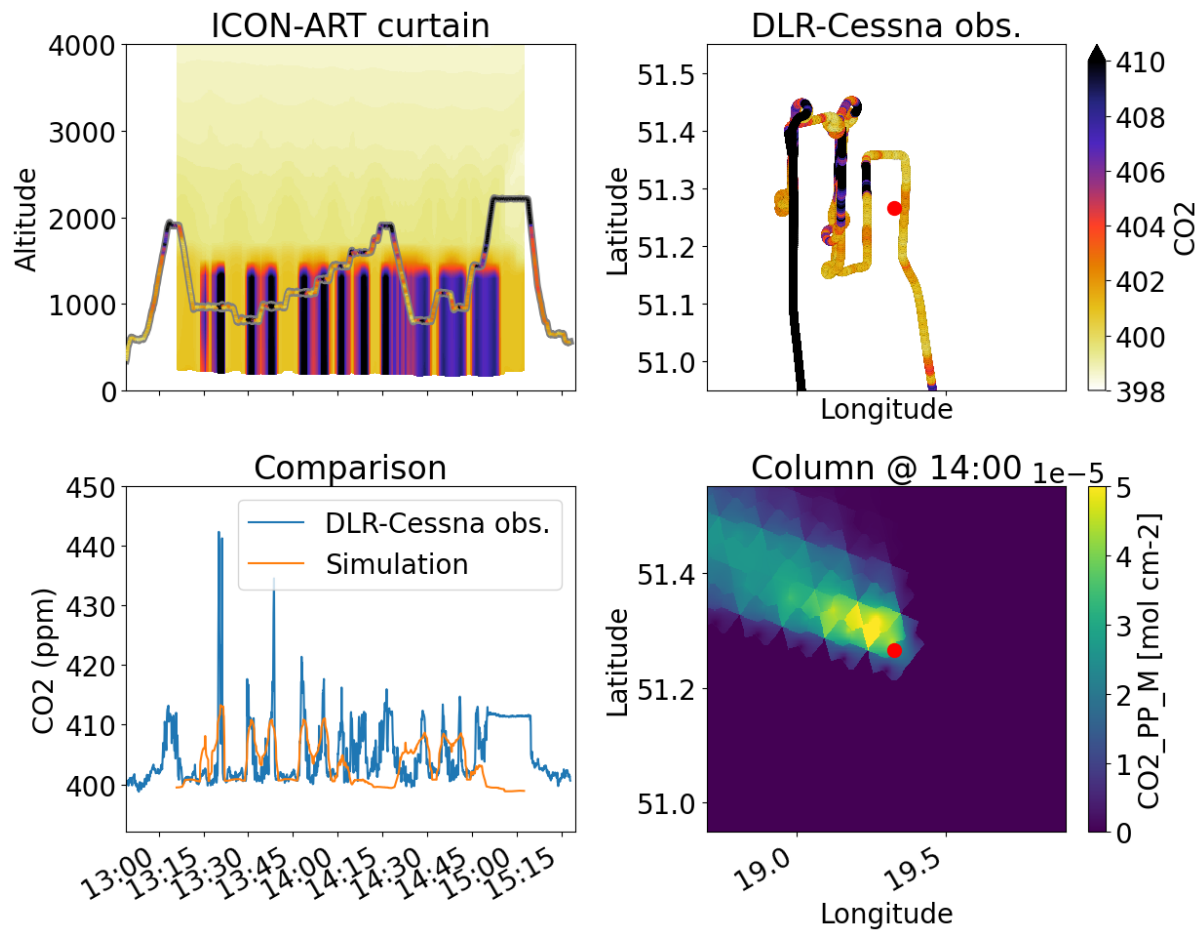


Figure 7. ICON-ART comparison against DLR-Cessna for Bełchatów, 7 June 2018.

The results for LOTOS-EUROS can be found in Figure 8, where the simulation results are offset by -8 ppm to match the observations. As in the case of COSMO-GHG and ICON-ART before, the transects close to the plume (~13:00 until ~14:00) are well reproduced, and also the final transects at the furthest distance from the plume are well reproduced (within the ABL). The model simulated slightly too wide plumes (and, correspondingly, slightly too low amplitudes compared to the transects), but matches their location remarkably well for such a turbulent state of the atmosphere. Like in the case of COSMO-GHG, there is considerable wind-shear visible in the curtain plots.

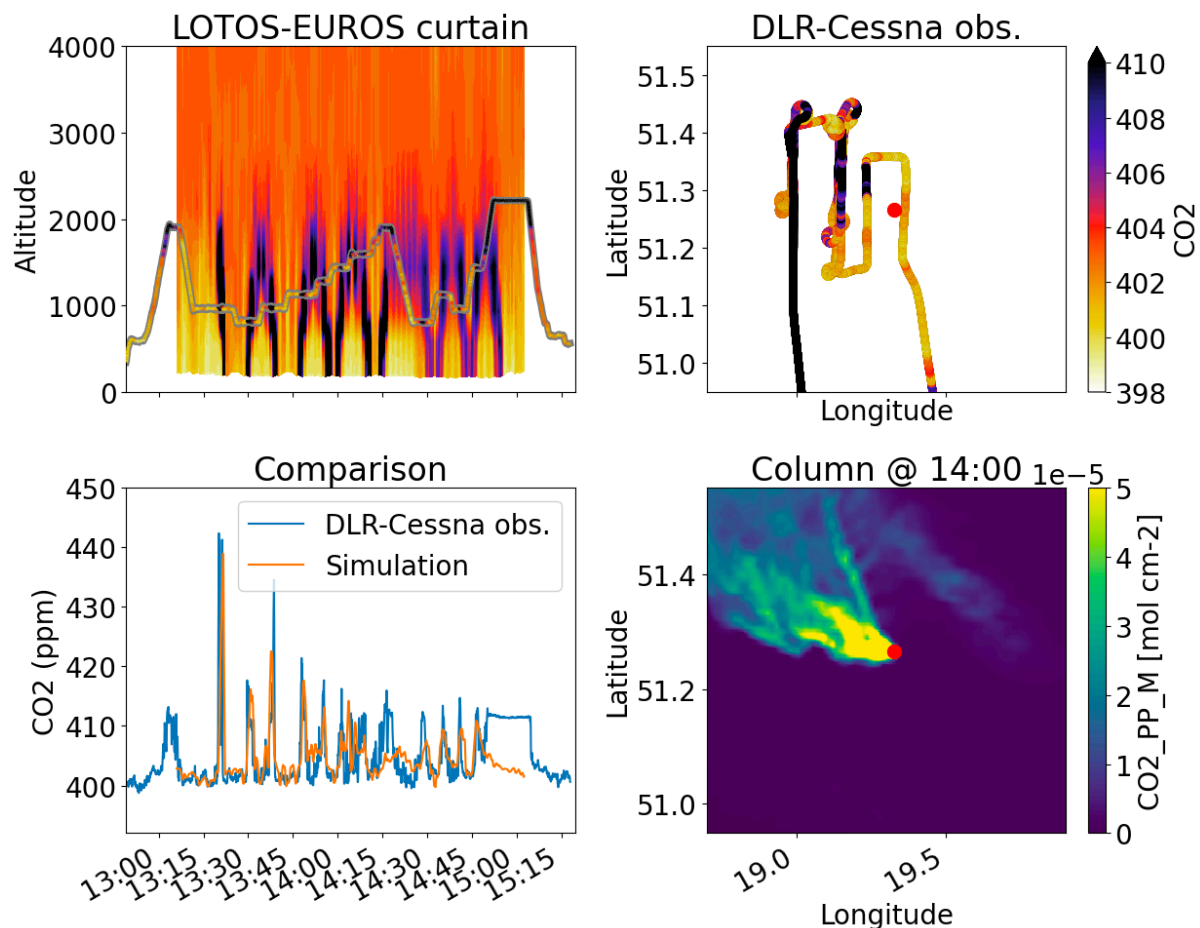


Figure 8. LOTOS-EUROS comparison against DLR-Cessna for Bełchatów, 7 June 2018.

The results for MicroHH can be found in Figure 9, where the simulation results are offset by -9 ppm to match the observations, and the vertical dimension of the simulation is offset by +192 m, corresponding to the mean surface elevation along the flight track. With MicroHH, the locations of all plume enhancements are well reproduced for all transects within the ABL. Also, the amplitudes of the CO₂ enhancements are well reproduced, albeit slightly overestimated in places. It appears that the plumes are slightly narrower than what is measured. Compared to the other models, we see in the column image that the fanning out of the plume takes place through eddies of a much smaller length-scale than those seen in COSMO-GHG or LOTOS-EUROS. There is also very little wind shear visible in the curtain plot, compared to COSMO-GHG and LOTOS-EUROS.

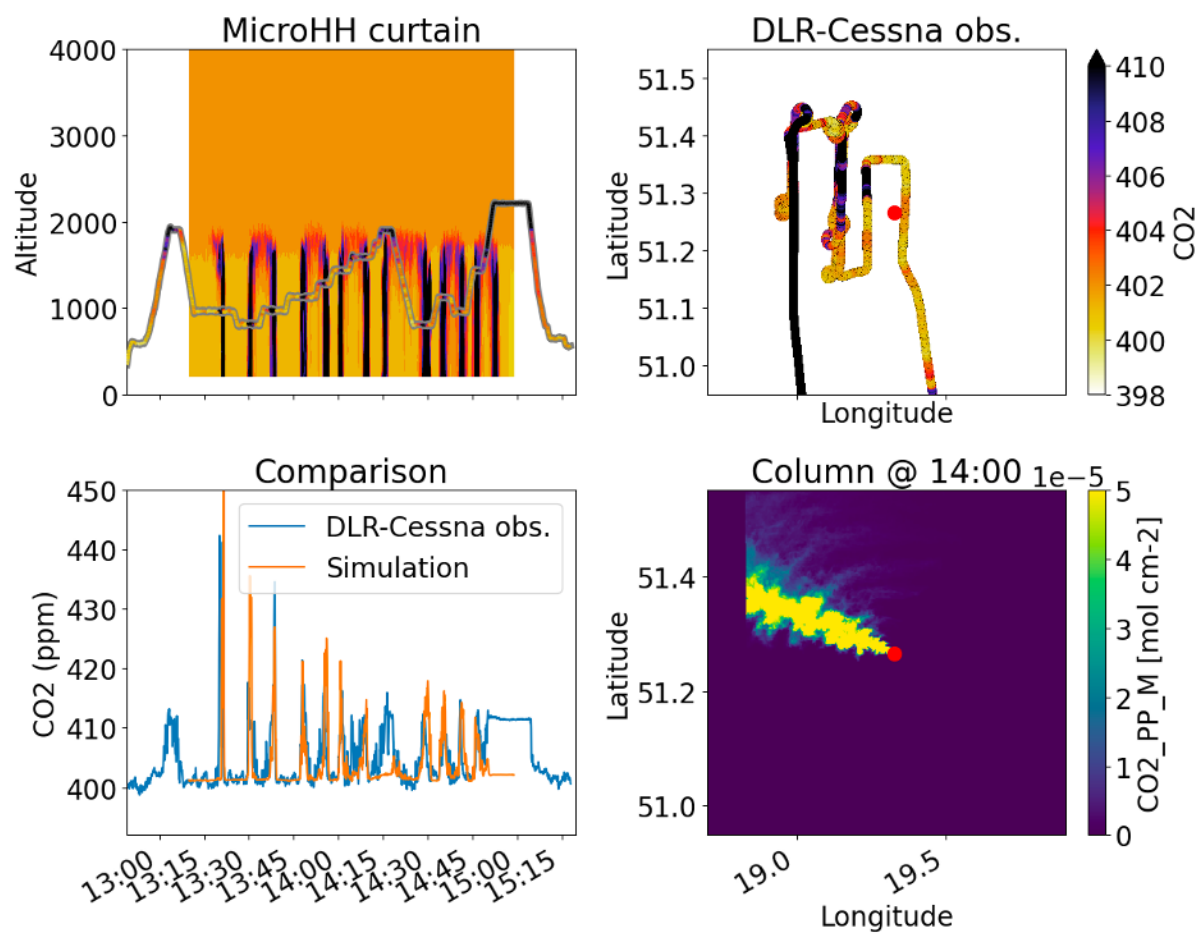


Figure 9. MicroHH comparison against DLR-Cessna for Belchatów, 7 June 2018.

4.1.1.3 Comparison against remotely sensed XCO₂ columns

In a point-by-point comparison between the observations and models (as done in the previous subsection), there is a considerable stochastic component that is very sensitive to the vertical transport, mixing and turbulence in the ABL. In comparison, models might be more successful in reproducing vertical columns, as these are much less sensitive to the aforementioned processes. Such columns were recorded along flight transects of the FUB-Cessna with the MAMAP instrument (Krautwurst et al., 2021) and along flight transects of the DLR-HALO with the CHARM-F instrument (Wolff et al., 2021). We refer to the cited references for more details about this data. Both aircraft flew above the ABL for their observations.

Results for the FUB-Cessna are shown in Figure 10. In contrast to in-situ CO₂ where COSMO-GHG stopped reproducing the observations after 14:00, we now see that COSMO-GHG matches the observed total columns at Belchatów with the MAMAP instrument quite well, while the total columns in ICON-ART are not well-matched in amplitude and generally too broad. This can be explained from the difference in modelling resolution, as with the in-situ CO₂ comparisons. LOTOS-EUROS simulates plume columns that are similar in shape compared to COSMO-GHG. MicroHH simulates the location of the plumes well, but overestimates the size of the peak amplitudes considerably for the first set of transects (~12:45), but peak amplitudes match the observations much better for the later transects (~13:10 and onwards).

Belchatow column measurements

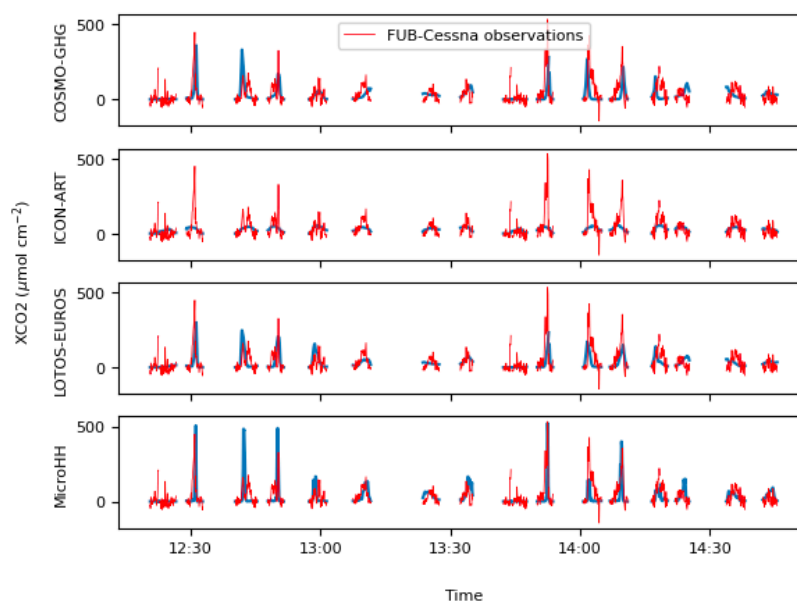


Figure 10. Time series of CO₂ column enhancements simulated and observed by MAMAP along the FUB-Cessna flight at Belchatow on 7 June 2018. The plumes observed around 12:20 and 13:45 UTC, which are not reproduced by any of the models, were measured upwind of the power plant. These plumes are caused by retrieval issues over water surfaces rather by real CO₂ enhancements.

Results for the DLR-HALO are shown in Figure 11. The results from the CHARM-F Lidar are at only 3-4 km distance from the source and rather noisy, although the plume transects are clearly visible. COSMO-GHG and LOTOS-EUROS generally get the correct width of the plume compared to the observations, but only fit the peak amplitude well for the transect around 13:15. The results from ICON-ART are generally too wide and too low in amplitude. Conversely, the MicroHH result gets plume widths that appear too narrow compared to the observations, though it does get the appropriate amplitude for one transect around 13:22, and prior to that simulates one largely underestimated and one largely overestimated transect.

Belchatow column measurements

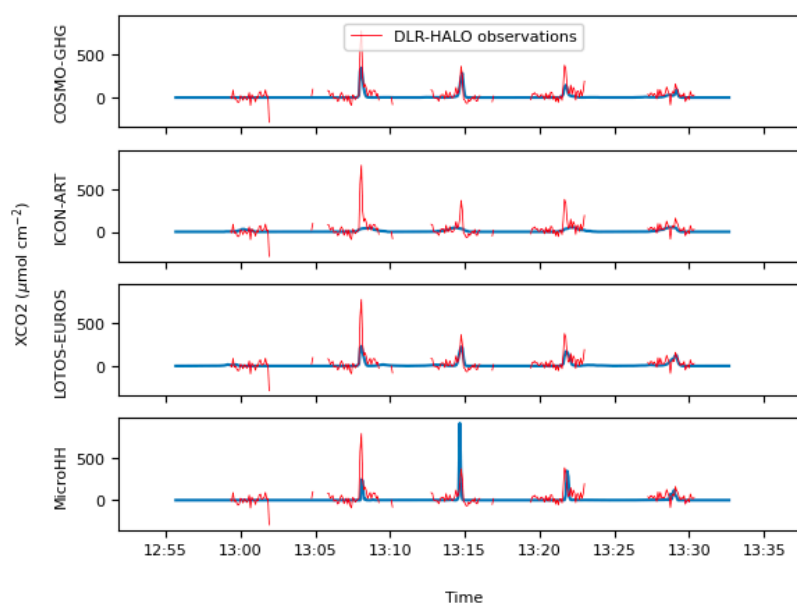


Figure 11. Observations of CO₂ column enhancements simulated and observed by CHARM-F along the HALO flight at Bełchatów on 7 June 2018.

4.1.1.4 Comparison against TROPOMI NO₂ images

A comparison with TROPOMI images was carried out by plotting the TROPOMI images (with a qa value of at least 0.75) against columns of NO₂ at an estimated overpass time of 12:00 (see Figure 12 and the zoomed version in Figure 13).

On the first day (2018-06-06), all models fit the observed TROPOMI image well, with only little diffusion of the plume in the downstream direction. Furthermore, the 'direction' of the plume is well-captured by all the models, including the slight up-ward downstream curvature, although the TROPOMI plume is directed slightly more southwards close to the source, compared to the simulated plumes. COSMO-GHG and LOTOS-EUROS additionally simulate the other anthropogenic sources in the area well; these were not simulated with MicroHH.

On the second day (2018-06-07), COSMO-GHG and LOTOS-EUROS have turbulent eddies with a length scale that is considerably larger than what can be seen in the TROPOMI plume, resulting in too much downstream diffusion. Conversely, the MicroHH result continues to fit the narrow plume on this second day well. In terms of general flow-direction, however, all models reproduce the TROPOMI image well.

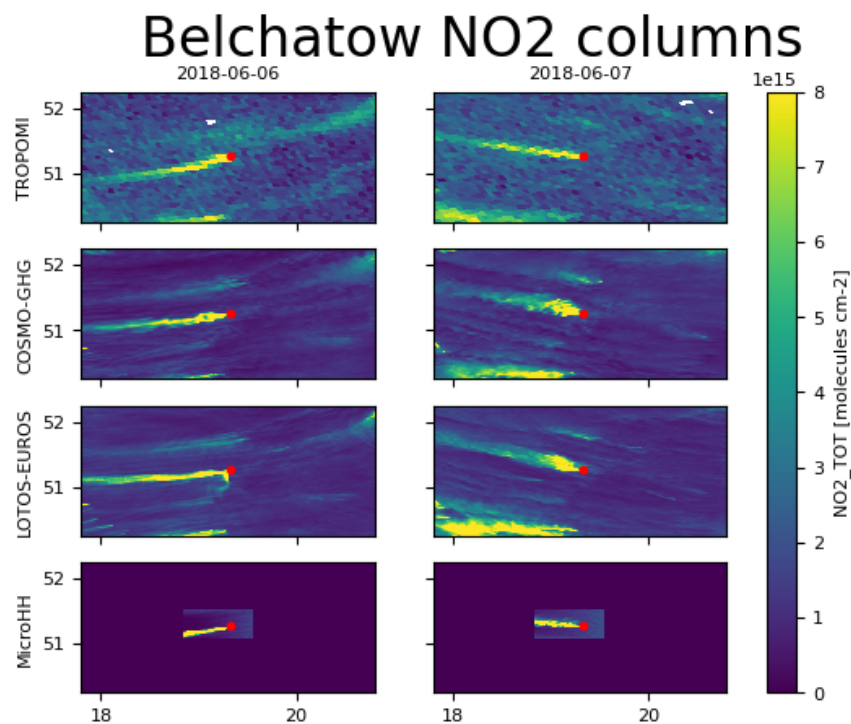


Figure 12. Comparison for TROPOMI columns with the total simulated NO₂. For COSMO-GHG, the NO₂ column was created based on an NO_x tracer (NO_x_PP_M + NO_x_ANTH + NO_x_BG) converted into an NO₂ tracer. For LOTOS-EUROS and MicroHH, the NO₂ column was modelled including full chemistry (NO₂_PP_M + NO₂_BG for MicroHH, and additionally NO₂_PP_ANTH + NO₂_BIO for LOTOS-EUROS).

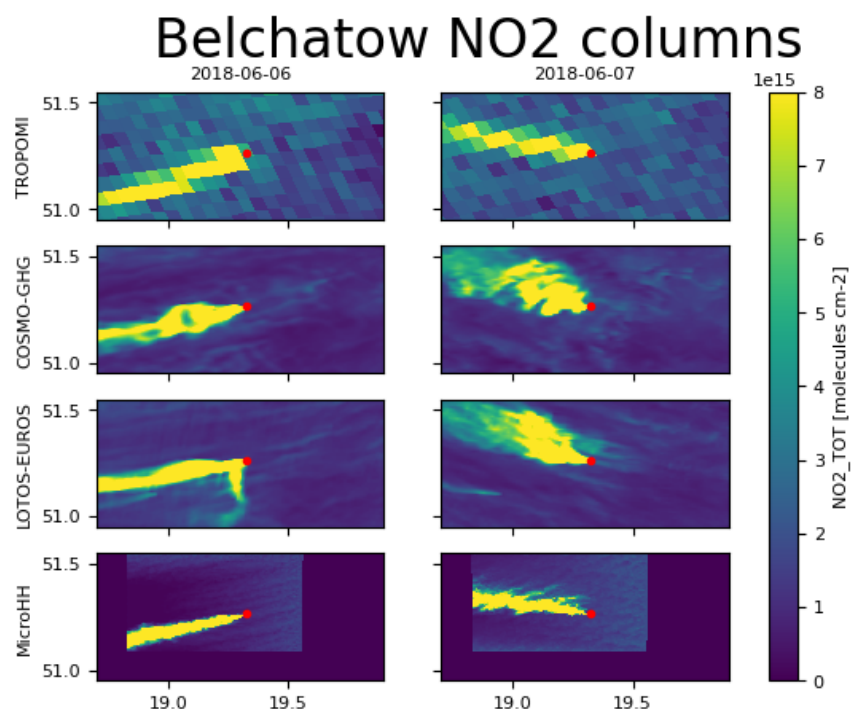


Figure 13. Zoom on the comparison for TROPOMI columns with the total simulated NO₂, see Figure 12.

4.1.1.5 Analysis of downwind NO₂ profile

As described in Section 3.3.4, through fitting a plume coordinate system to the data, and then taking the ratio of line densities between NO₂ or NO_x to CO₂ total columns, we can roughly quantify the evolution of the different quantities in the downstream direction. This type of analysis cannot account for differential reaction rates within or at the edges of the plume, but can nevertheless allow a level of comparison between the different modelling methods. Such computed downstream ratios are shown in Figure 14. Additionally shown in the plots is an estimate of the effective wind speed, which is the wind speed weighted with the vertical distribution of NO₂ or NO_x around the source position (i.e., if the wind speed around the source is given as $s(z)$ and the concentration as $\rho(z)$, then the effective wind speed was computed as $s_{eff} = \int s(z)\rho(z)dz / \int \rho(z)dz$). It can be noted that the effective wind speeds for all models and cases are roughly similar – except the LOTOS-EUROS wind on the 6th of June 2018 which is considerably higher than the other models. This can explain why the NO₂ as well as NO_x concentrations hardly decay in the downstream direction. The MicroHH result displays considerable 'spikiness' around the source location, before the decay ratio stabilizes in the downstream direction. This is both a result of the fact that further downstream there are more plume pixels than upstream of the source (leading to a smoothed out cross-sectional line density), as well as a result of the 'blobby' nature of eddies tearing off the jet. Different reaction rates may be expected within eddies compared to outside of the eddies, and in further downstream directions the plume becomes more well-mixed. COSMO-GHG only simulated an NO_x tracer with exponential decay, which is visible well in the NO_x:CO₂ ratio on the 6th of June. The parametrized relation to compute NO₂ from NO_x from Düring et al. (2011) appears to work well on the 6th of June, as the location of the peak for NO₂:CO₂ appears at a similar offset as for the chemistry models used in LOTOS-EUROS and MicroHH, while this peak is reached too early on the 7th of June.

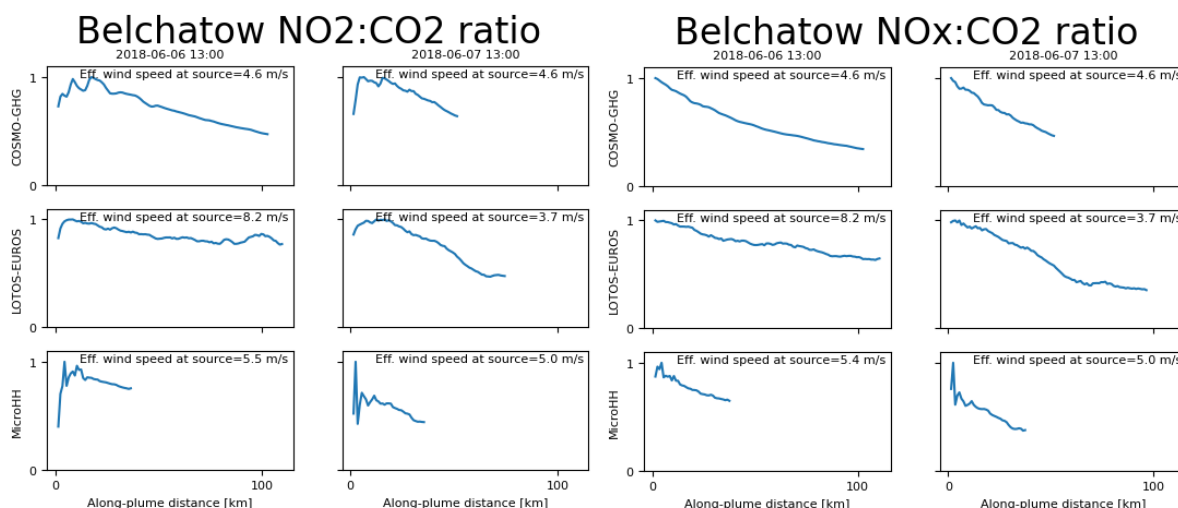


Figure 14. Comparison of downstream NO₂ and NO_x decay for Belchatów for the three models that submitted nitrogen oxide tracers. The ratios are normalized to 1. The effective wind speed is the wind speed weighted with the vertical distribution of NO₂ or NO_x around the source position.

4.1.1.6 Downwind dispersion of the plume

As described in Section 3.3.5, the width of the plume could be estimated by fitting a Gaussian function to plume cross-sections. This width has been plotted for the four models in the plume downstream direction, as shown in Figure 15. With the exception of ICON-ART, which appears to be well-modelled by a roughly Gaussian function (i.e., for which $\sigma(x) = \sqrt{2Kx/U}$ with K the eddy diffusivity coefficient and U the effective wind speed (Stockie, 2011)), the plumes on the 6th of June 2018 show an initial growth with distance, but then remain roughly at their size. Furthermore, some ‘growth’ followed by ‘shrinking’ of the plume can be observed in the downstream direction, which may be related to capturing the large-scale eddies. In the case of COSMO-GHG and LOTOS-EUROS, a width of $2\sigma = 4$ km is reached about 20 km downstream, while the MicroHH plume is only half that width at a comparable distance. The ICON-ART plume already starts off with a considerable non-zero size, this is an artefact of the modelling and source emission resolution (i.e., see in Figure 7 that the plume already appears present in the ‘upstream’ direction, due to the large triangular cell sizes). On 7 June 2018, we observe a similar Gaussian-like along-plume growth for ICON-ART, but observe a more erratic profile in the downwind directions for COSMO-GHG and LOTOS-EUROS. The Micro-HH plume remains, comparatively, very narrow.

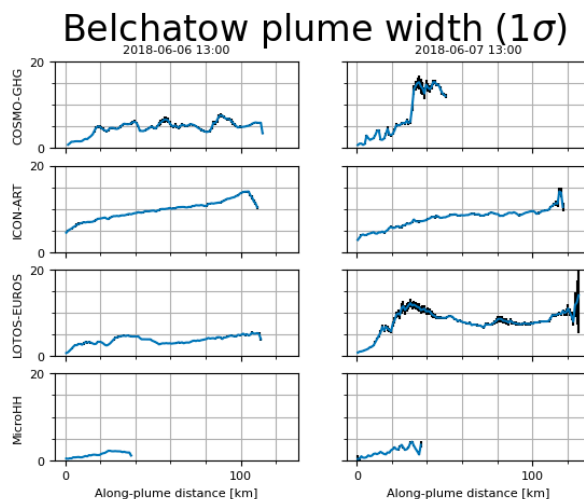


Figure 15. The downwind evolution of the plume width for the Belchatów power plant, following a Gaussian plume fit to the CO₂_PP_M tracer. The black line shows one standard deviation of the fitted plume width.

4.1.1.7 Synthetic CO₂M image

As explained in Section 3.3.2, it was possible to create a synthetic CO₂M image from the simulated data at an estimated overpass time of about 11:00 UTC, by extending the column vertically with CAMS CO₂ data, remapping the data onto 2×2 km² pixels, and adding 0.7 ppm Gaussian noise (the same pattern is applied on each image). Such images are shown in Figure 16. One apparent feature is that the ICON-ART simulated plume blends into the background considerably more than the plume modelled with the other methods due to its low enhancements over the background; similar to what we observed in the comparison against in-situ CO₂ and remotely sensed XCO₂ columns in an earlier section. The plume in the COSMO-GHG and LOTOS-EUROS images is primarily visible around the source location, after which it quickly blends into the background. Conversely, the MicroHH plume remains enhanced over the background for a longer time. However, between COSMO-GHG, LOTOS-EUROS and MicroHH, there is no considerable difference in the observable plume width for the 6th of June 2018, which is analogous to what was observed in the TROPOMI image in a previous subsection. The difference is larger on 7 June 2018, as the COSMO-GHG and LOTOS-EUROS plumes encounter large-scale turbulence (also visible on, e.g., Figure 5), and the resulting wide plume is of sufficiently low concentration that it quickly dissolves into the background. Conversely, the MicroHH plume on 7 June 2018 is readily visible along the entire image extent. Based on the comparisons with data made so far, it is likely that the MicroHH plume is slightly too narrow but generally in line with what could have been observed by a satellite.

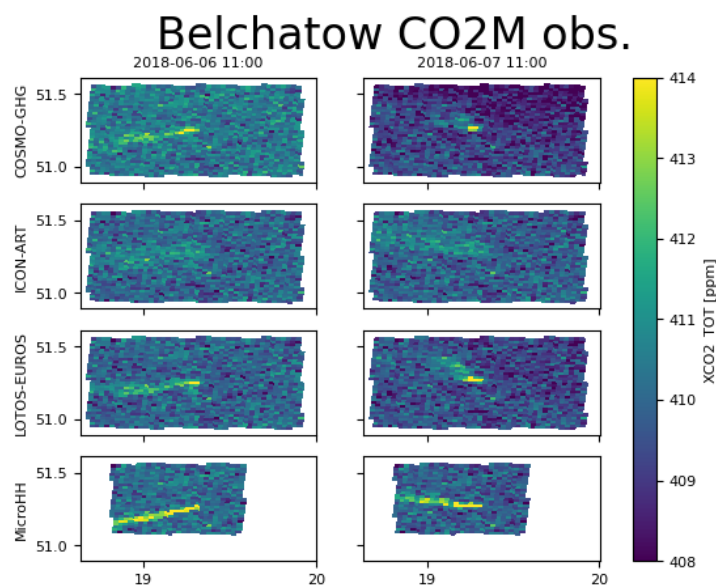


Figure 16. Synthetic CO₂M observation of the total CO₂ column around Bełchatów.

4.1.1.8 Conclusions for this case

In conclusion, we have seen the following: **to match in-situ data**, the best results are obtained using MicroHH (50 m horizontal resolution), then COSMO-GHG and LOTOS-EUROS (1.1 km horizontal resolution), then ICON-ART (6 km horizontal resolution). **To match XCO₂ and NO₂ column observations**, the results from COSMO-GHG, ICON-ART and LOTOS-EUROS generally produce plume transects that are too wide, while MicroHH produces transects that match very well with the observations.

4.1.2 Jänschwalde (2018-05-22 – 2018-05-23)

The Jänschwalde Power Station is a coal-fired power station in Germany, near the border with Poland. The same four models simulated its plume as the Bełchatów case (COSMO-GHG, ICON-ART, LOTOS-EUROS, and MicroHH). The LOTOS-EUROS model used the meteorology from COSMO-GHG. ICON-ART in this instance is run at 2 km resolution, instead of 6 km as for Bełchatów. The submitted tracers can be found in Table 3.

Table 3. Submitted tracers by the different models for the Jänschwalde case.

| Model | Submitted tracers |
|--------------------|--|
| COSMO-GHG | CO2_PP_M, CO2_PP_L, CO2_PP_H, CO2_ANTH, CO2_BG, CO2_BIO, CO_PP_M, CO_ANTH, CO_BG, NOX_PP_M, NOX_ANTH, NOX_BG |
| ICON-ART | CO2_PP_M, CO2_PP_L, CO2_PP_H |
| LOTOS-EUROS | CO2_PP_M, CO2_PP_L, CO2_PP_H, CO2_ANTH, CO2_BG, CO2_BIO, CO_PP_M, CO_PP_L, CO_PP_H, CO_ANTH, CO_BG, CO_BIO, NO_PP_M, NO_PP_L, NO_PP_H, NO_ANTH, NO_BG, NO_BIO, NO2_PP_M, NO2_PP_L, NO2_PP_H, NO2_ANTH, NO2_BG, NO2_BIO, OH, TNMVOC_PP_M, TNMVOC_PP_L, TNMVOC_H, TNMVOC_ANTH, TNMVOC_BG, TNMVOC_BIO, TPM10_PP_M, TPM10_PP_L, TPM10_PP_H, TPM10_ANTH, TPM10_BG, TPM10_BIO, TPM25_PP_M, TPM25_PP_L, TPM25_PP_H, TPM25_ANTH, TPM25_BG, TPM25_BIO |

| | |
|----------------|--|
| MicroHH | CO2_PP_M, CO2_BG, CO_PP_M, CO_BG, NO_PP_M, NO_BG, NO2_PP_M, NO2_BG, O3_PP_M, O3_BG, C3H6_PP_M, C3H6_BG, OH_PP_M, OH_BG |
|----------------|--|

4.1.2.1 Overview column images

The overview columns of the CO₂_PP_M tracer (middle release case) and CO₂_PP_L tracer (surface release case) can be found in Figure 17 and Figure 18, respectively. A zoom on the middle release case can be found in Figure 19. We note that the flow pattern up to the morning (00:00 to 08:00) is entirely different between the middle and low release cases, while at later times (12:00 to 20:00) the two release profiles produce very similar columns. This suggests again a case of strong mixing in the fully developed daytime ABL. The plume simulated with MicroHH shows considerable feather-like or density fingering features in the morning, while the other methods only show diffusion of the plume, indicating the stark difference between the turbulence-resolving resolution of the LES set-up of MicroHH versus the other NWP models. It can be seen that ICON-ART has considerably higher resolution in this case compared to the Bełchatów simulation, the triangular grid footprint can just barely be seen in the zoomed section of Figure 19.

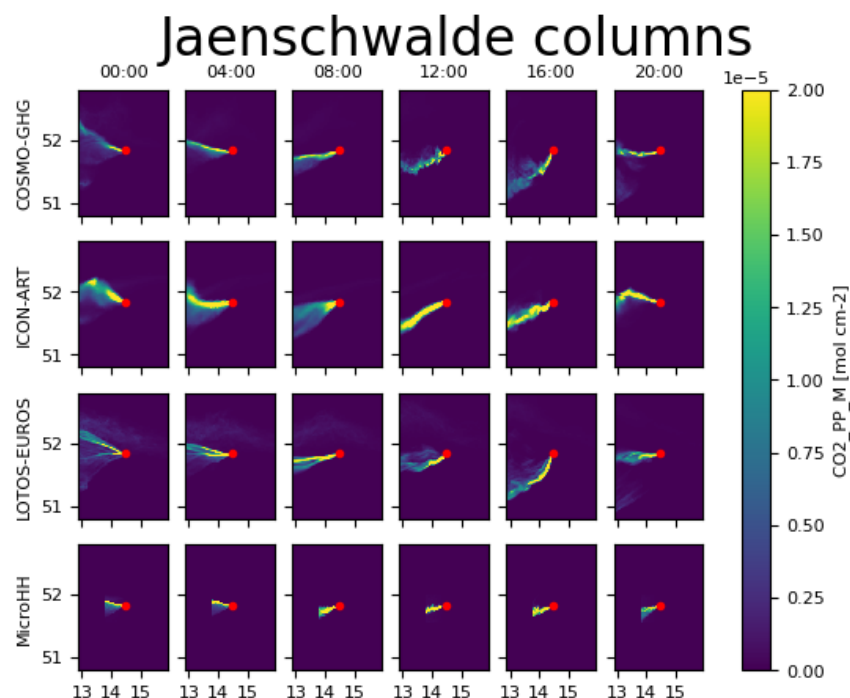


Figure 17. Total column images as generated by four modelling systems of the Jänschwalde powerplant plume, on May 23rd, 2018, for the "middle" emissions profile M. The location of the powerplant is indicated by the red dot.

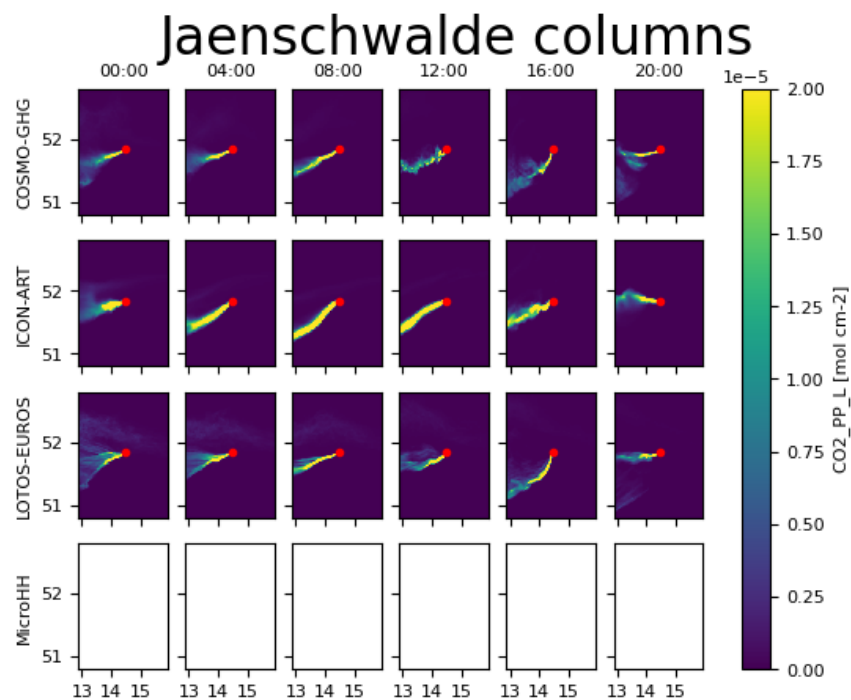


Figure 18. Total column images as generated by four modelling systems of the Jänschwalde powerplant plume, on May 23rd, 2018, for the "surface" emissions profile L. The location of the powerplant is indicated by the red dot. This emission profile case was not modelled in MicroHH.

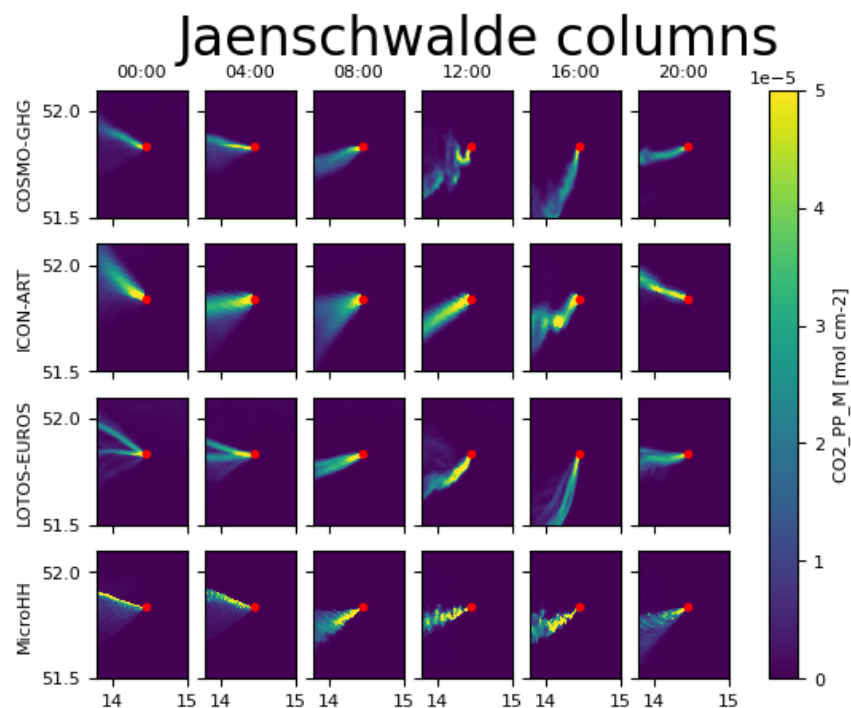


Figure 19. Zoom on the total column images as generated by four modelling systems of the Jänschwalde powerplant plume, on May 23rd, 2018, for the "middle" emissions profile M. The location of the powerplant is indicated by the red dot.

4.1.2.2 Comparison against in-situ CO₂ observations

In-situ CO₂ observations were made by a Los Gatos Research (LGR) CO₂ and CH₄ measuring instrument on the FUB-Cessna aircraft (Krautwurst et al., 2021). For the first ~80 minutes of

recordings (08:50 until 10:10), the aircraft flew just above the ABL, after which the aircraft descended into the ABL. As seen in the previous section, the atmospheric transport models struggled to reproduce concentrations above the ABL, and it is no different in this case. As visible for COSMO-GHG (Figure 20), ICON-ART (Figure 21), and LOTOS-EUROS (Figure 22), the height of the ABL appears to increase over the course of the morning, and the two large plume peaks in the observations around 09:15 are not well-recovered by these models. Conversely, MicroHH (Figure 23) captures these early observations partially, suggesting an already deeper ABL had developed at this stage. Plume transects afterwards, until about 10:05, are also reasonably represented by MicroHH while the other models do not match these observations at all. Focusing on just the transects after 10:05, they are captured moderately well by COSMO-GHG, although the simulated plumes are too wide compared to the observations. Unlike the Bełchatów case, there is less wind shear visible in the curtain. In ICON-ART, two plume transects at an altitude of ~1250 m are missed (at ~10:15), as the simulated ABL only extends to an altitude of about 1000 m at that time, which is lower than what COSMO-GHG predicts there. The plume transects that are captured within ICON-ART are generally a bit too wide, likely due to the modelling resolution, but the amplitude corresponds fairly well to the observed plumes. The plume transects by LOTOS-EUROS are similarly wide as in COSMO-GHG, but like ICON-ART, the transects around 10:15 are largely missed, indicating that the ABL is still developing around this time, or that the region is not well-mixed yet. The later plumes are matched well. The plume transects by MicroHH match best with the observations, particularly in placement and width of the plume, and partially also in the peak amplitudes simulated.

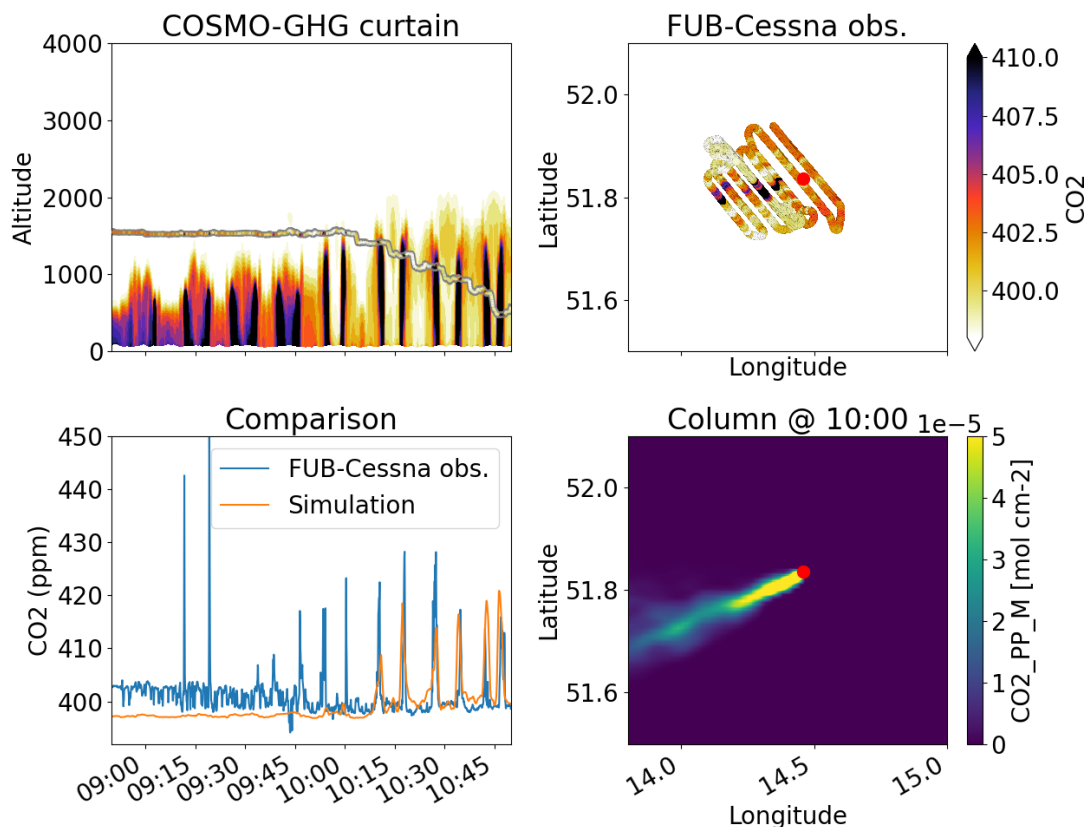


Figure 20. COSMO-GHG comparison against FUB-Cessna for Jänschwalde, 23 May 2018

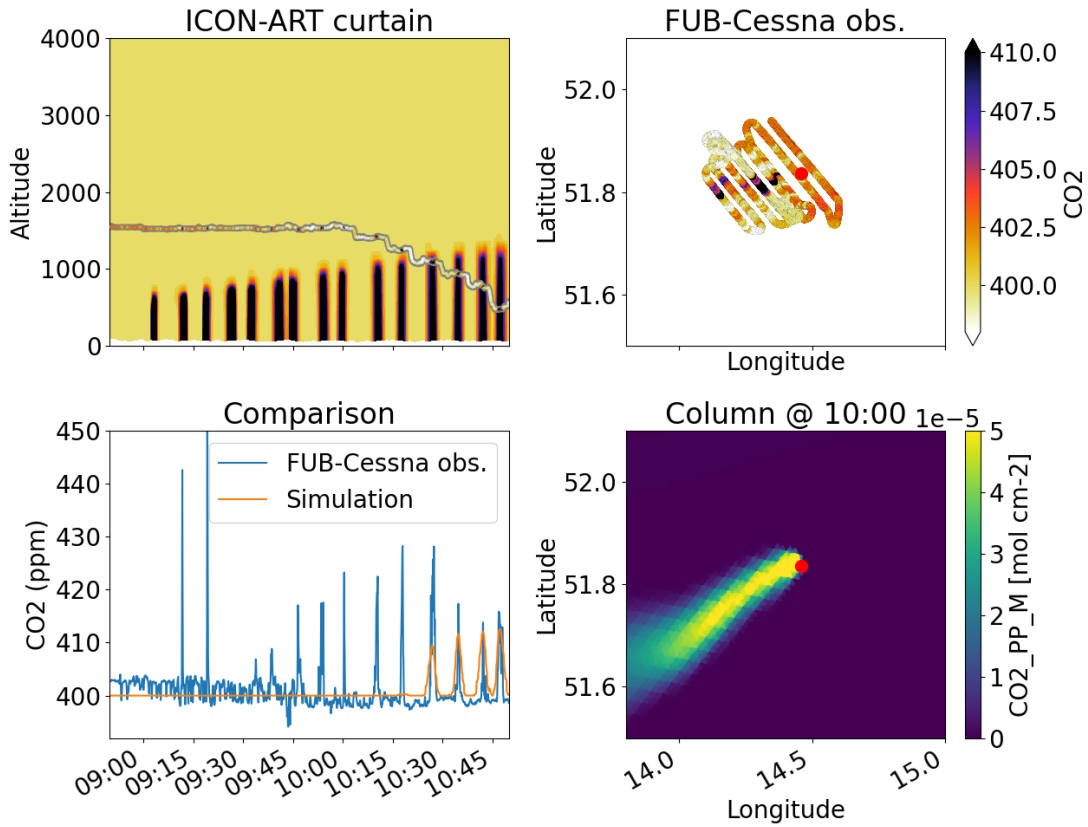


Figure 21. ICON-ART comparison against FUB-Cessna for Jämschwalde, 23 May 2018.

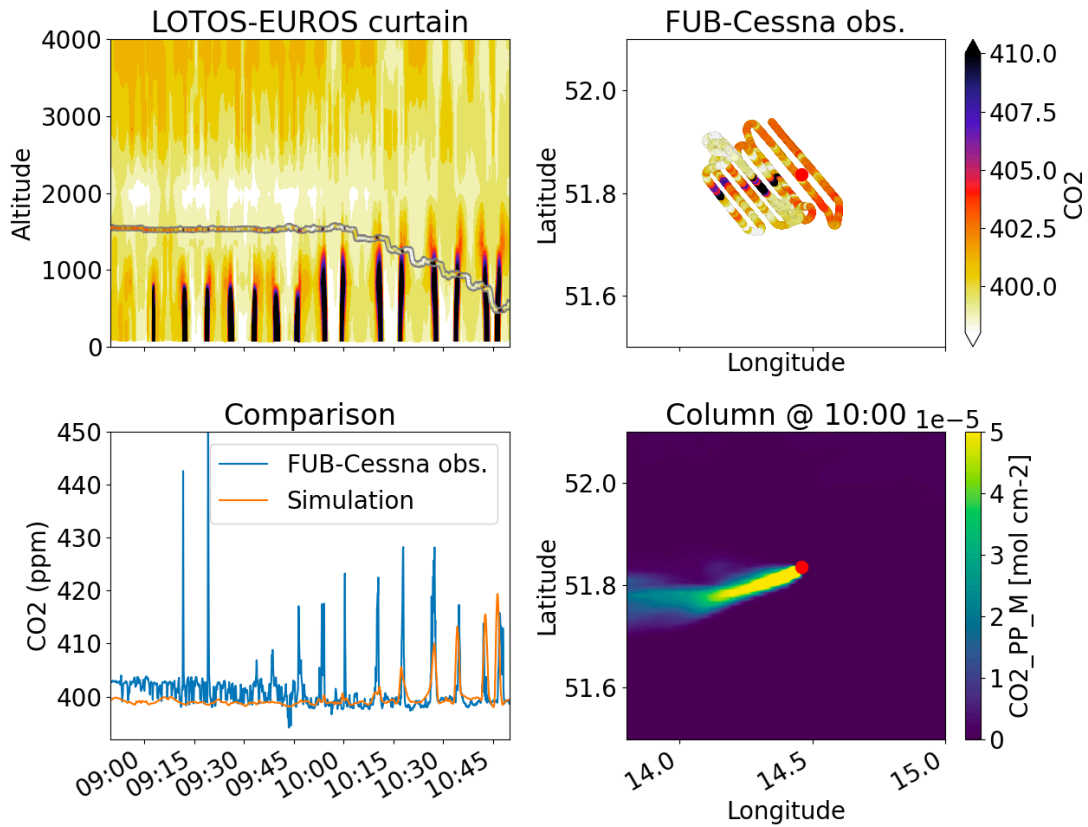


Figure 22. LOTOS-EUROS comparison against FUB-Cessna for Jämschwalde, 23 May 2018

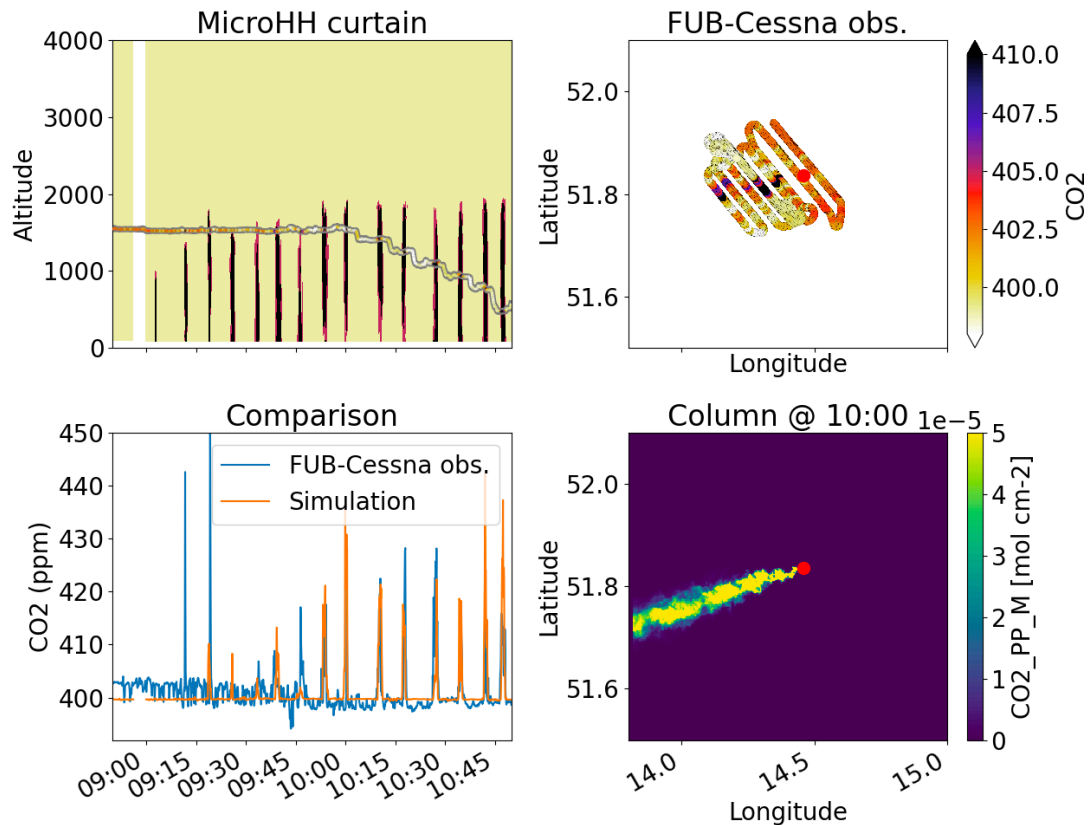


Figure 23. MicroHH comparison against FUB-Cessna for Jänschwalde, 23 May 2018.

By plotting the potential temperature ($\theta = T \cdot \left(\frac{10^5}{P}\right)^{0.286}$) as done in Figure 24, we get some insight into the boundary layer height of the various models. The capping inversion at the top of the ABL is relatively 'fuzzy' in COSMO-GHG and LOTOS-EUROS, but in general it appears that the ABL is about 1 km deep at the start of the measurements (and not very well-mixed), and the ABL height eventually grows to 1.5 km and well-mixed around 10:00. Conversely, in ICON-ART, the ABL is still developing over the course of the morning from an altitude of only about 500 m to 1500 m around 10:30. On the other hand, in MicroHH the ABL is already at an altitude of about 1300 m at the starting time (08:50). Hence, already at an early time of the flight the simulated MicroHH plumes mix within and around the ABL to high altitudes, while mixing to these altitudes is only possible later for the other models.

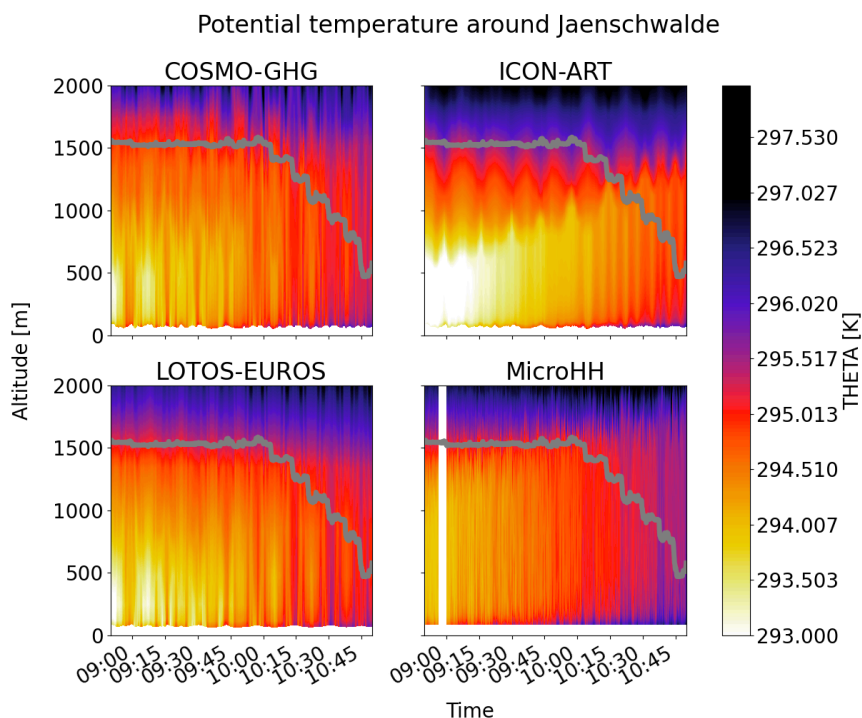


Figure 24. Plot of the potential temperature for the different models around Jänschwalde.

4.1.2.3 Comparison against remotely sensed XCO₂ columns

Like in the Bełchatów case, column observations were made around Jänschwalde from above the ABL, using the FUB-Cessna and the DLR-HALO aircraft, again with the respective MAMAP and CHARM-F Lidar instruments. Unlike the in-situ comparisons (where only the MicroHH model produced plume enhancements above the ABL), we now see that all models produce plume column enhancements in line with the observations (Figure 25, Figure 26). The CHARM-F Lidar instrument is noisy, but we can notice that all models measure all plume transects; except at ~09:18, a small plume enhancement is missing in the MicroHH model. The MAMAP instrument shows that the columns as produced by COSMO-GHG, ICON-ART and LOTOS-EUROS are a bit too wide and generally of too low amplitude, while the MicroHH model matches the plume width and plume amplitudes rather well.

Jaenschwalde column measurements

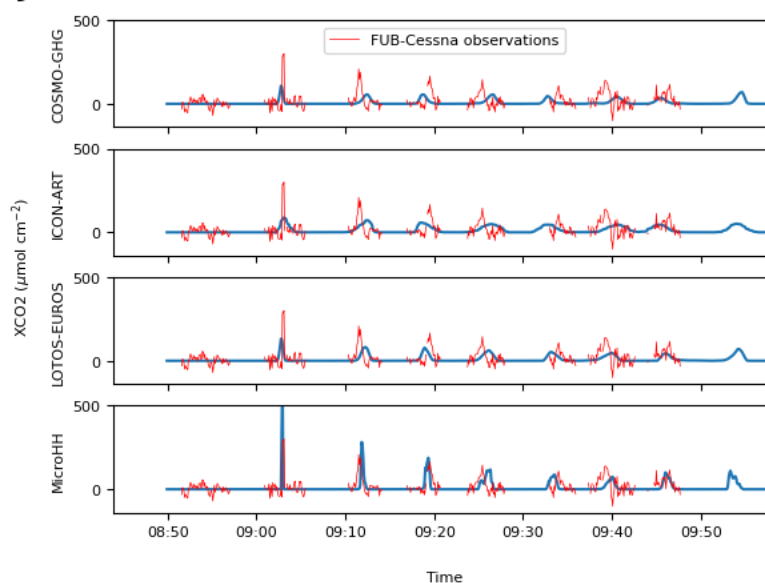


Figure 25. Time series of CO₂ column enhancements simulated and observed by MAMAP along the FUB-Cessna flight at Janschwalde on 23 May 2018.

Jaenschwalde column measurements

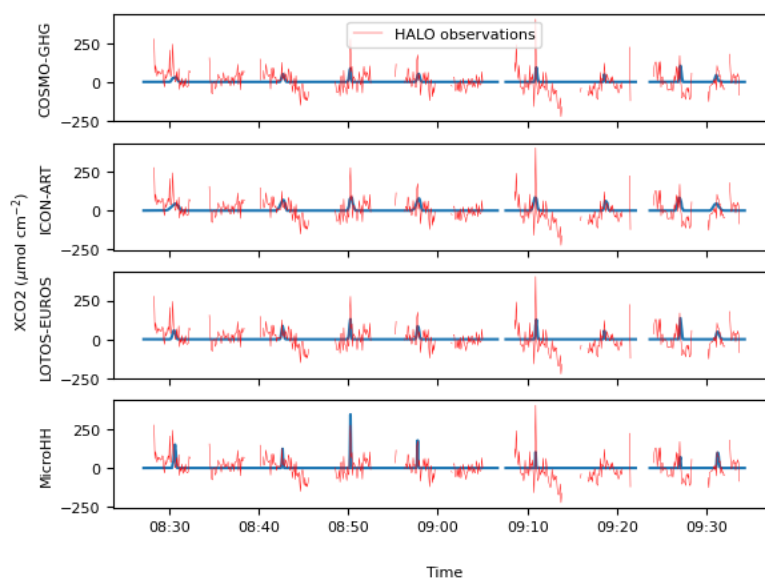


Figure 26. Observations of CO₂ column enhancements simulated and observed by CHARM-F along the HALO flight at Janschwalde on 23 May 2018.

4.1.2.4 Comparison against TROPOMI NO₂ image

Two TROPOMI images around Janschwalde are shown in Figure 27. A zoom in on a smaller area around the source is shown in Figure 28. On 23 May 2018, clouds obscure large parts of the domain (only pixels with a quality flag $qa > 0.75$ are displayed). However, on 22 May, the plume and close-by surrounding sources (e.g., Berlin in the top-left; and the Boxberg and Schwarze Pumpe power stations just below the Janschwalde power plant on Figure 27) are visible. All simulated plumes reasonably match the observed plumes (within the TROPOMI pixel size), despite differences in downwind turbulent structures between the various models.

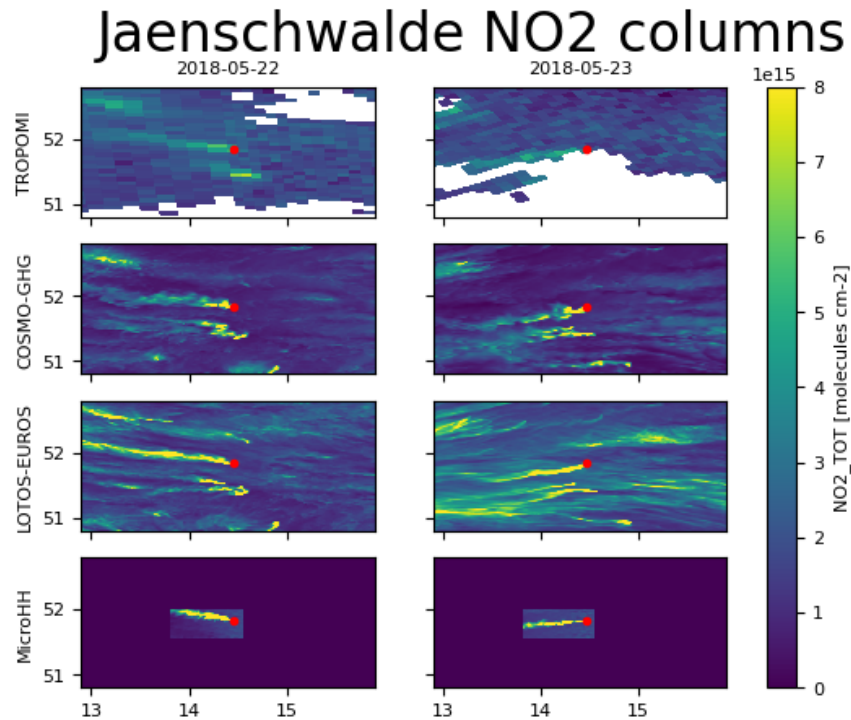


Figure 27. Comparison for TROPOMI columns with the total simulated NO₂. For COSMO-GHG, the NO₂ column was created based on an NO_x tracer (NO_x_PP_M + NO_x_ANTH + NO_x_BG) converted into an NO₂ tracer. For LOTOS-EUROS and MicroHH, the NO₂ column was modelled including full chemistry (NO₂_PP_M + NO₂_BG for MicroHH, and additionally NO₂_PP_ANTH + NO₂_BIO for LOTOS-EUROS).

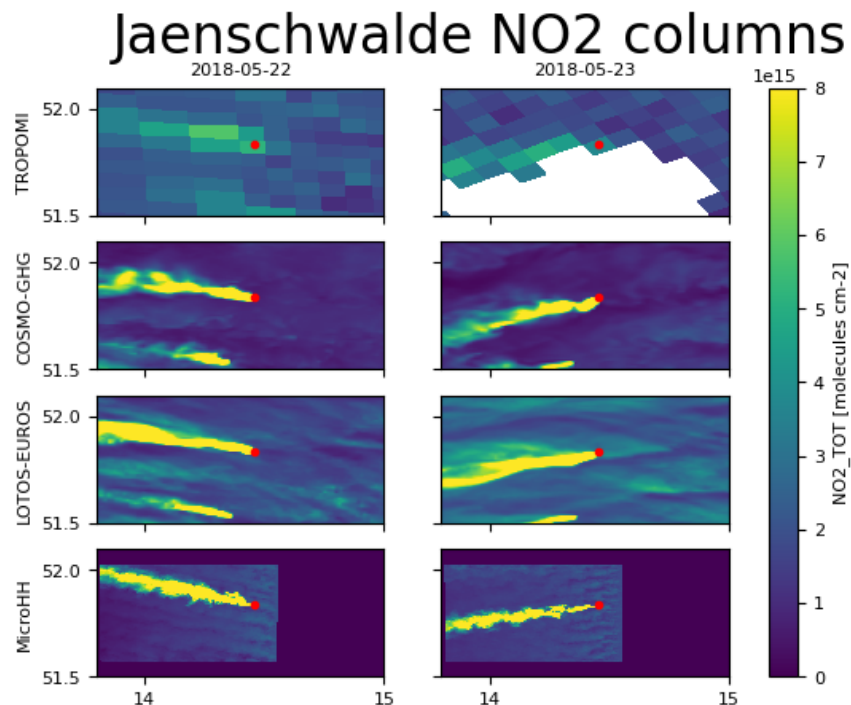


Figure 28. Zoom on the comparison for TROPOMI columns with the total simulated NO₂, see Figure 27.

4.1.2.5 Analysis of downwind NO₂ profile

A downwind analysis of NO₂ and NO_x cross-sectional profiles was carried out, with results shown in Figure 29. It is clearly visible that the MicroHH results appear 'noisy' close to the source location, as discussed for the Bełchatów case previously. Also, like in the Bełchatów case, the LOTOS-EUROS profile on the first analysed day shows relatively little decay of NO₂, together with a much larger effective (concentration-at-the-source-weighted) wind speed. Conversely, on the first day, the MicroHH effective wind speed is very low, leading to a very quick down-wind decay of both NO₂ and NO_x. The COSMO-GHG NO₂ tracer (which, we remind the reader, was computed from a decaying NO_x tracer through post-processing) appears to peak "too close" to the source on May 22, and "too far" away from the source on May 23, compared to the two other models. The LOTOS-EUROS NO_x column decays a bit slower than the other two methods on both days, even with the relatively low effective wind speed at the source.

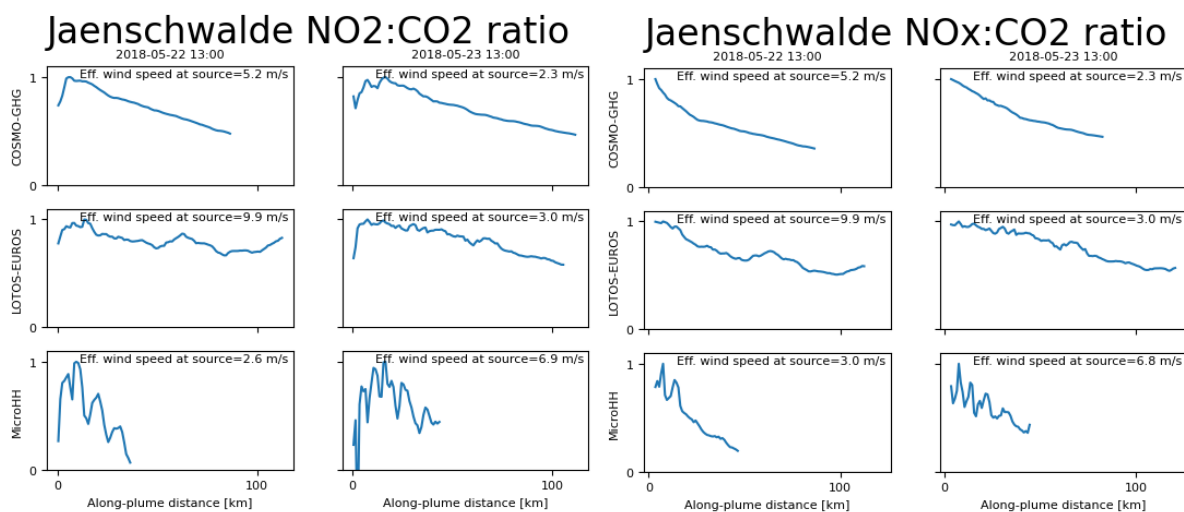


Figure 29. Comparison of downstream NO₂ and NO_x decay for Jänschwalde for the three models that submitted nitrogen oxide tracers. The ratios are normalized to 1. The effective wind speed is the wind speed weighted with the vertical distribution of NO₂ or NO_x around the source position.

4.1.2.6 Downwind dispersion of the plume

The plume width (as estimated through fitting a Gaussian function to cross-sections of the CO₂_PP_M tracer) for the Jänschwalde case is shown in Figure 30. Results as found in the previous case apply here too, in that a plume appears to grow initially, but then shows growing and shrinking patterns around a steady-state situation, likely related to turbulent eddies. The ICON-ART and LOTOS-EUROS plume widths on the second day are a bit of an exception to this case, as they appear to keep growing (i.e., diffusing) slowly in the downwind direction. This could be in line with the observation in Figure 19 (around 12:00) where both ICON-ART, LOTOS-EUROS show still few signs of turbulence at the scale of the target resolution, while COSMO-GHG and MicroHH contains discernible turbulent eddy structures. Hence, it appears that if turbulence is simulated in the form of diffusive mixing, plumes keep growing, while if turbulent eddies are resolved within the model, a somewhat steady-state size can be achieved (within the context of fitting Gaussian profiles to plume cross-sections).

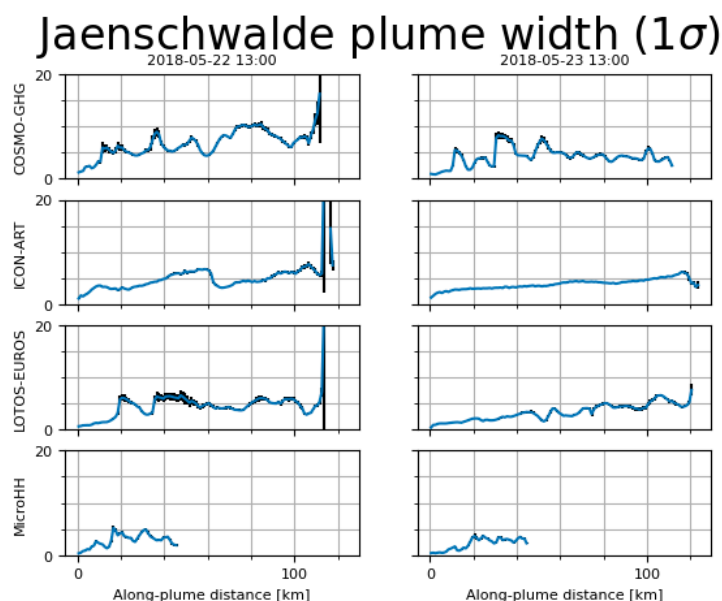


Figure 30. The downwind evolution of the plume width for the Jänschwalde power plant, following a Gaussian plume fit to the CO₂_PP_M tracer. The black line shows one standard deviation of the fitted plume width.

4.1.2.7 Synthetic CO₂M image

Through extending the columns with CAMS CO₂ profiles, we can again compute synthetic CO₂M images from the model results. Similar observations as for Bełchatów apply here; a notable difference is that the ICON-ART plume can be identified on this image in a similar fashion as the other methods, while it was considerably different in the Bełchatów case. The difference in modelling resolution (from 6 km to 2 km horizontally), means that the plume is now simulated with a narrower width and correspondingly higher concentrations, indicating that the 2 km setup for ICON-ART is more appropriate for use in (for example) inversions, than the 6 km resolution.

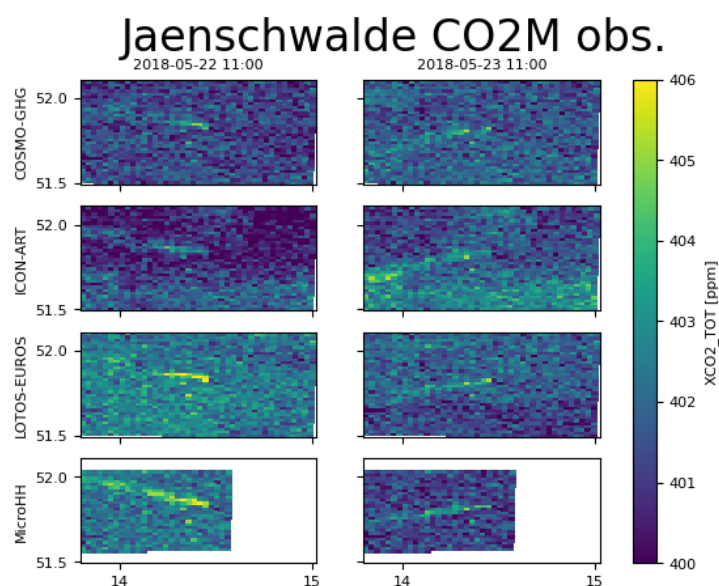


Figure 31. Synthetic CO₂M observation of the total CO₂ column around Jänschwalde.

4.1.2.1 Conclusions for this case

In conclusion, we have seen the following: **to match in-situ data**, the best results are obtained using MicroHH (50 m horizontal resolution), then COSMO-GHG and LOTOS-EUROS (1.1 km

horizontal resolution), then ICON-ART (2 km horizontal resolution). This was in no small part due to considerable differences in the modelled ABL height. **To match XCO₂ and NO₂ column observations**, the results from COSMO-GHG, ICON-ART and LOTOS-EUROS and MicroHH all generally produce transects in line with the observations.

4.1.3 Lipetsk (2019-06-12 – 2019-06-13)

The Lipetsk case focuses on the Novolipetsk Steel plant in Lipetsk, Russia. It was selected due to an isolated and clearly visible CO TROPOMI plume, related to blast furnace gas. Its plume was simulated by two models (COSMO-GHG and MicroHH). The submitted tracers can be found in Table 4.

Table 4. Submitted tracers by the different models for the Lipetsk case.

| Model | Submitted tracers |
|------------------|--|
| COSMO-GHG | CO2_PP_M, CO2_PP_L, CO2_PP_H, CO2_ANTH, CO2_BG, CO2_BIO, CO_PP_M, CO_ANTH, CO_BG, NOX_PP_M, NOX_ANTH, NOX_BG |
| MicroHH | CO2_PP_M, CO2_BG, CO_PP_M, CO_BG, NO_PP_M, NO_BG, NO2_PP_M, NO2_BG, O3_PP_M, O3_BG, C3H6_PP_M, C3H6_BG, OH_PP_M, OH_BG |

4.1.3.1 Overview column images

Figure 32 displays the Lipetsk column for the medium release case in both the large ('L') and zoomed-in small ('S') region. The two modelling systems show rather similar features in the morning, until around 12:00 a Kelvin-Helmholtz type large-scale instability becomes visible in the COSMO-GHG case, which becomes more stable again in the later evening, while the MicroHH plume remains more stable throughout the day, only to encounter wind shear in the evening as also visible in the COSMO-GHG case. At the periphery of the jets, there is turbulent mixing with the ambient air from an early time onwards.

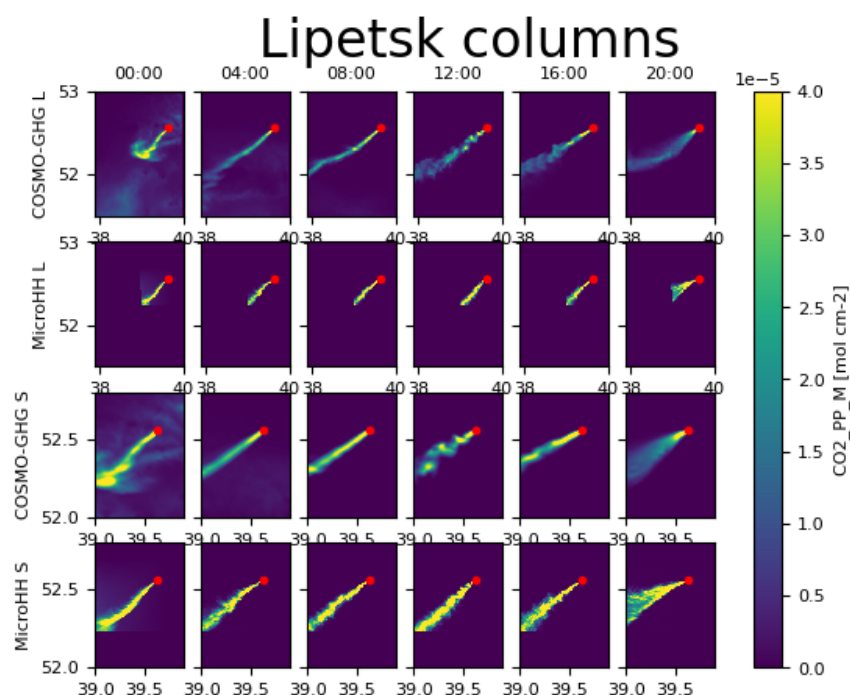


Figure 32. Total column images as generated by two modelling systems of the Lipetsk steel plant, on June 13th, 2019, for the "middle" emissions profile M in the large (L) and small (S) domains. The location of the steel plant is indicated by the red dot.

4.1.3.2 Comparison against TROPOMI CO image

On 12 June 2019, no quality TROPOMI CO overpass was found, but on 13 June 2019 a clear west-south-west directed plume could be observed. When comparing the TROPOMI observation with simulations (Figure 33 and a zoom in Figure 34), it is clear that the CO background in MicroHH is too small, but other than that, both modelling systems produce a narrow plume that appears to fit the observations relatively well (to within the pixel size of the TROPOMI data).

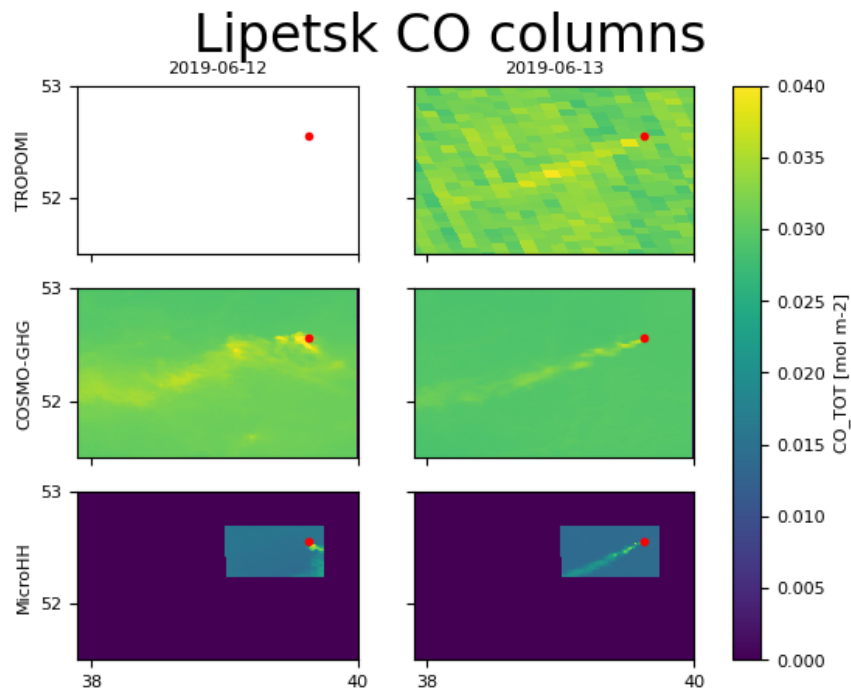


Figure 33. Comparison for TROPOMI columns with the total simulated CO. For MicroHH that is CO_PP_M + CO_BG, in COSMO-GHG additionally the other anthropogenic CO sources are included.

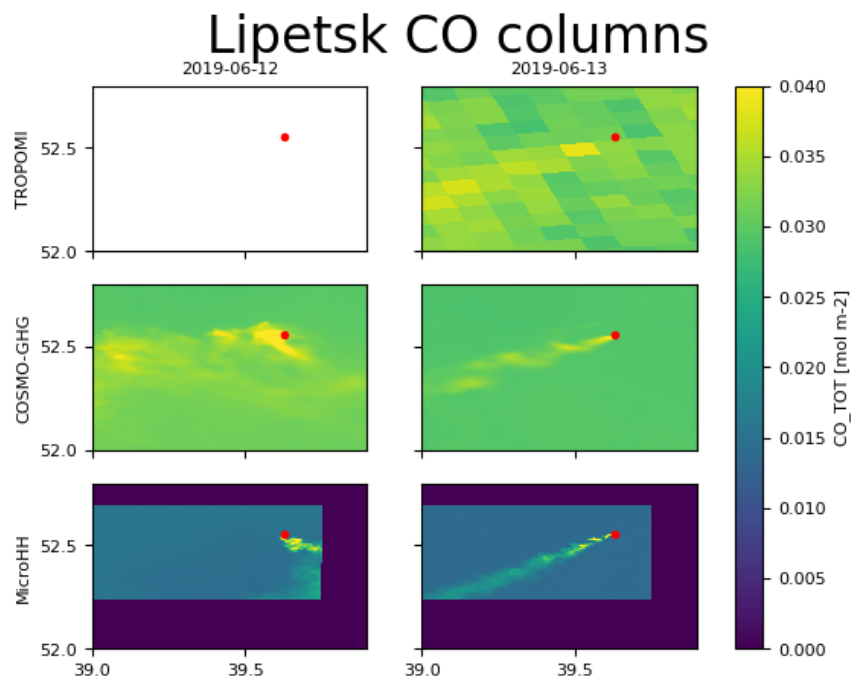


Figure 34. Zoom on the comparison for TROPOMI columns with the total simulated CO, see Figure 33.

4.1.3.3 Analysis of NO₂ profile downwind

In Figure 35, we illustrate the NO₂ profiles in the downwind direction. It must be noted that the results for 22 June 2019 come with large uncertainties, as the plume was undergoing a significant change of wind direction at the analysed time (e.g., see Figure 34), so fitting a plume coordinate system and obtaining sensible cross-sections was not trivial. Therefore, we focus on 23 June 2019, where we can see the NO₂:CO₂ ratio and NO_x:CO₂ ratios are similar between the two methods (although the decay is slightly slower in COSMO-GHG), if we see through the small-scale irregularities in the MicroHH results, likely due to turbulence (e.g., pinch off effects close to the source as visible in Figure 34).

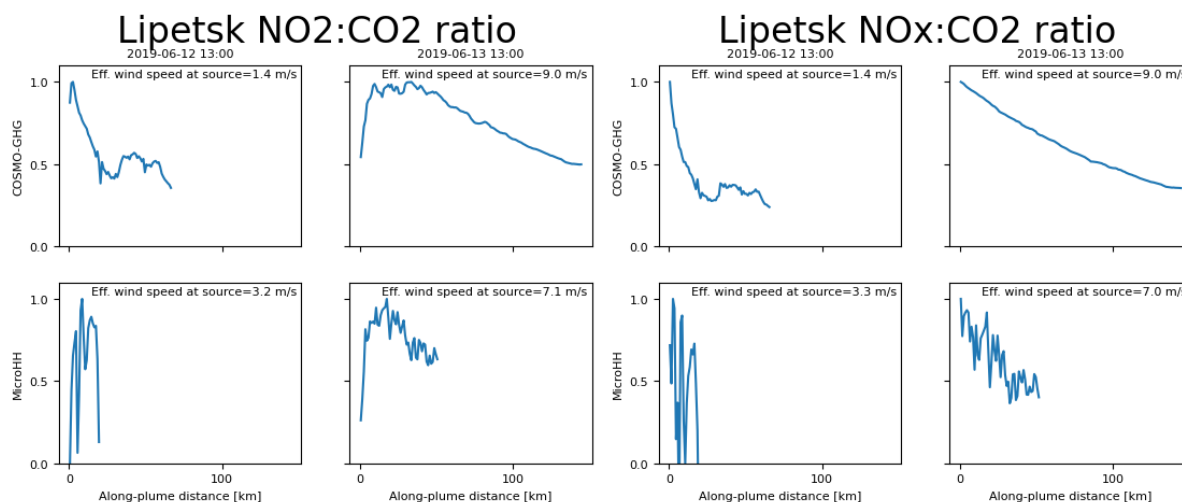


Figure 35. Comparison of downstream NO₂ and NO_x decay for Lipetsk. The ratios are normalized to 1. The effective wind speed is the wind speed weighted with the vertical distribution of NO₂ or NO_x around the source position

4.1.3.4 Downwind dispersion of the plume

As in the NO₂ downwind profiles, the plume detection for 12 June is not entirely reliable, so we will focus only on June 13th. There, we notice a plume that is slowly growing in its dimensions. We see that the growing trend for COSMO-GHG is rather irregular, as an effect of the large-scale turbulent eddies forming in the downwind direction (as also visible in Figure 34).

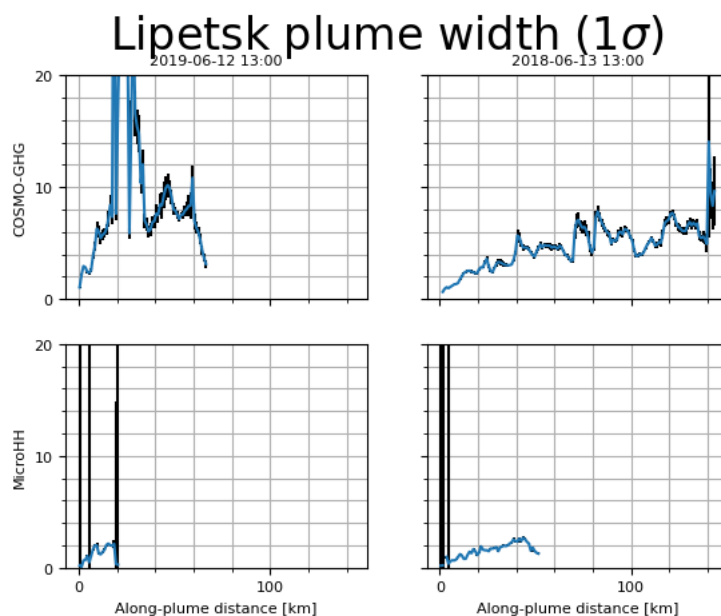


Figure 36. The downwind evolution of the plume width for the Lipetsk steel plant, following a Gaussian plume fit to the CO₂_PP_M tracer. The black line shows one standard deviation of the fitted plume width.

4.1.3.5 Synthetic CO₂M image

The synthetic CO₂M image, Figure 37, shows that the CO₂ plume simulated by the modelling methods is visibly elevated over the background, i.e., it can be seen in the synthetic image for both days, albeit again the plume is narrower in the MicroHH output than in the COSMO-GHG output.

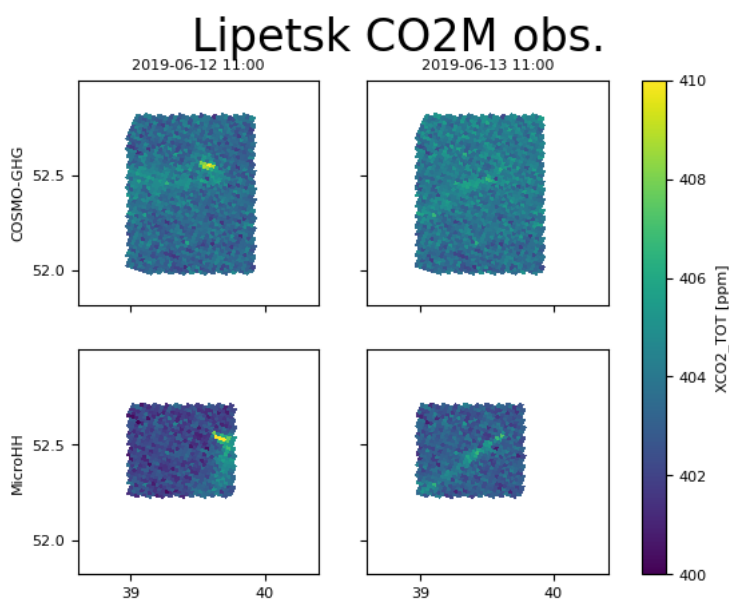


Figure 37. Synthetic CO₂M observation of the total CO₂ column around Lipetsk.

4.1.3.6 Conclusions for this case

In conclusion, we have seen the following: **To match CO column observations**, the results from COSMO-GHG, and MicroHH all generally produce column images in line with the observations.

4.1.4 Matimba (2020-07-24 – 2020-07-25)

The Matimba Power Station is a coal-fired power station in South Africa, near the border with Botswana. The same two models simulated its plume as the Lipetsk case (COSMO-GHG and MicroHH). NB: a powerplant with additional NO₂ emissions, the Medupi Power Station, was identified just 6 km away from the Matimba power station. It can thus be expected that modelled fields are underestimating the real emissions, as a reliable emissions inventory is missing in this area. The submitted tracers can be found in Table 5.

Table 5. Submitted tracers by the different models for the Matimba case.

| Model | Submitted tracers |
|------------------|--|
| COSMO-GHG | CO2_PP_M, CO2_PP_L, CO2_PP_H, CO2_ANTH, CO2_BG, CO2_BIO, CO_PP_M, CO_ANTH, CO_BG, NOX_PP_M, NOX_ANTH, NOX_BG |
| MicroHH | CO2_PP_M, CO2_BG, CO_PP_M, CO_BG, NO_PP_M, NO_BG, NO2_PP_M, NO2_BG, O3_PP_M, O3_BG, C3H6_PP_M, C3H6_BG, OH_PP_M, OH_BG |

4.1.4.1 Overview column images

Unlike the previous cases, there are considerable differences between the models in the overview column for the CO₂_PP_M tracer (Figure 38). COSMO-GHG is clearly modelling in unstable atmospheric conditions, winds turning at night from northeasterly to southeasterly, and a front passing in southerly direction around 12:00. In the evening, wind speeds fall considerably; CO₂ is simply building up around the power plant instead of being transported elsewhere. MicroHH undergoes some degree of turning winds during the day, but generally of a much smaller intensity than with COSMO-GHG. Only in the evening, the jet opens up and mixing of the plume intensifies. We note that FLEXPART model simulations driven with purely ERA5 fields, as shown in Hakkarainen et al. (2021), gave a good fit to the observations. It thus seems that the dynamics of the atmosphere were easy enough in this area, but that the free-running meteorology of the two models created a relatively complicated state of the atmosphere.

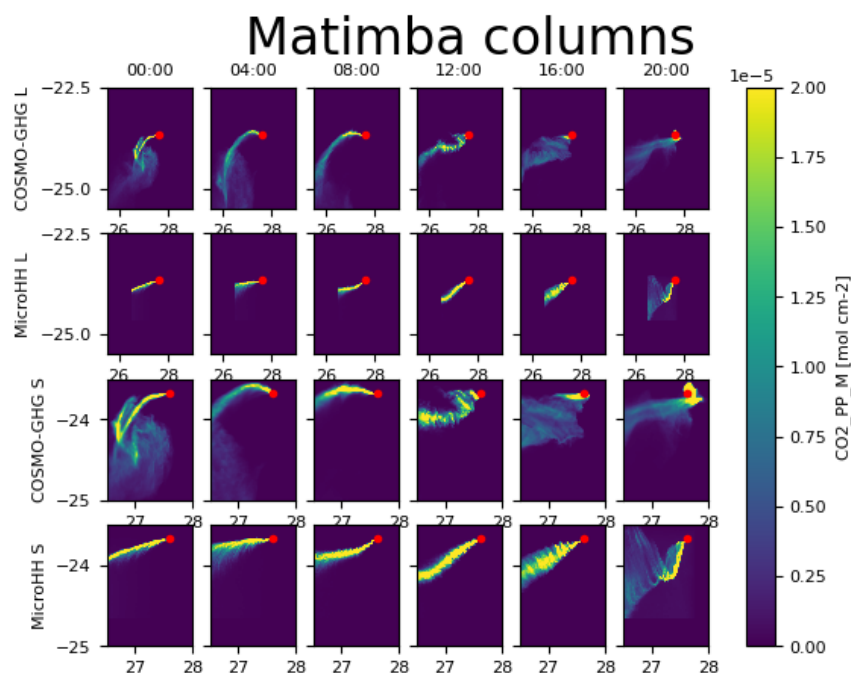


Figure 38. Total column images as generated by two modelling systems of the Matimba power plant, on July 25th, 2020, for the "middle" emissions profile M in the large (L) and small (S) domains. The location of the power plant is indicated by the red dot.

4.1.4.2 Comparison against TROPOMI NO₂ image

When comparing the simulations with TROPOMI NO₂ images (Figure 39 and Figure 40), it becomes clear that the COSMO-GHG results are far off the target, with entirely too large backgrounds, and other simulated sources in the area (due to EDGAR v.6) are not easily recognized on the corresponding TROPOMI image. MicroHH (which did not simulate further sources in the area) matches relatively well compared to the observed plume on the 24th of July, although the simulated plume appears to be thinner than the observed plume. The reasons for this (other than atmospheric and plume physics) may lie in the fact that the simulations are missing the additional Medupi Power Station source close by the Matimba power station. On the 25th, the MicroHH plume follows a different trajectory than the TROPOMI image (i.e., curving towards the right in the simulated column, while the plume curves towards the left on the TROPOMI observation).

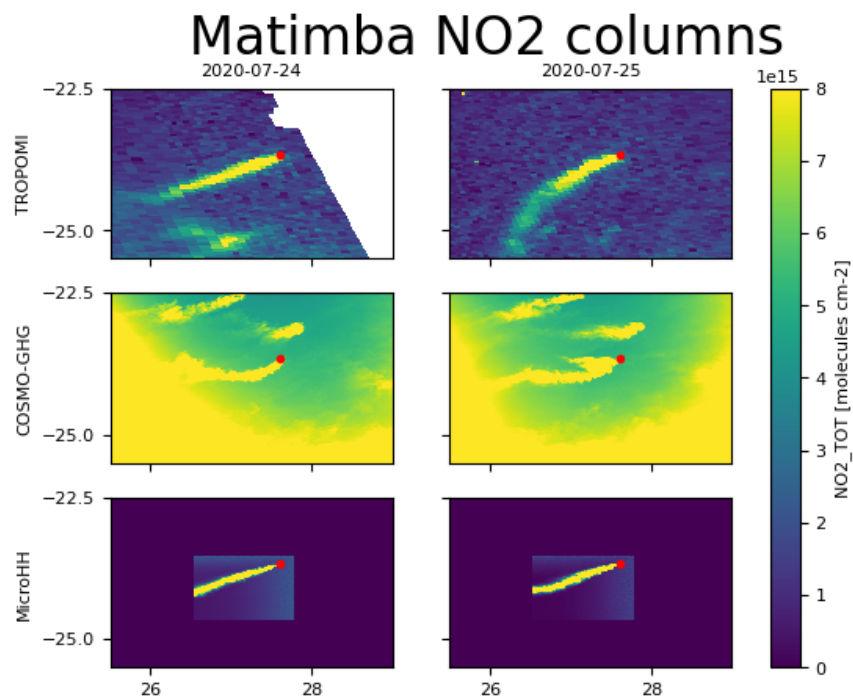


Figure 39. Comparison for TROPOMI columns with the total simulated NO₂. For COSMO-GHG, the NO₂ column was created based on an NO_x tracer (NOX_PP_M + NOX_ANTH + NOX_BG) converted into an NO₂ tracer. For MicroHH, the NO₂ column was modelled including full chemistry (NO2_PP_M + NO2_BG).

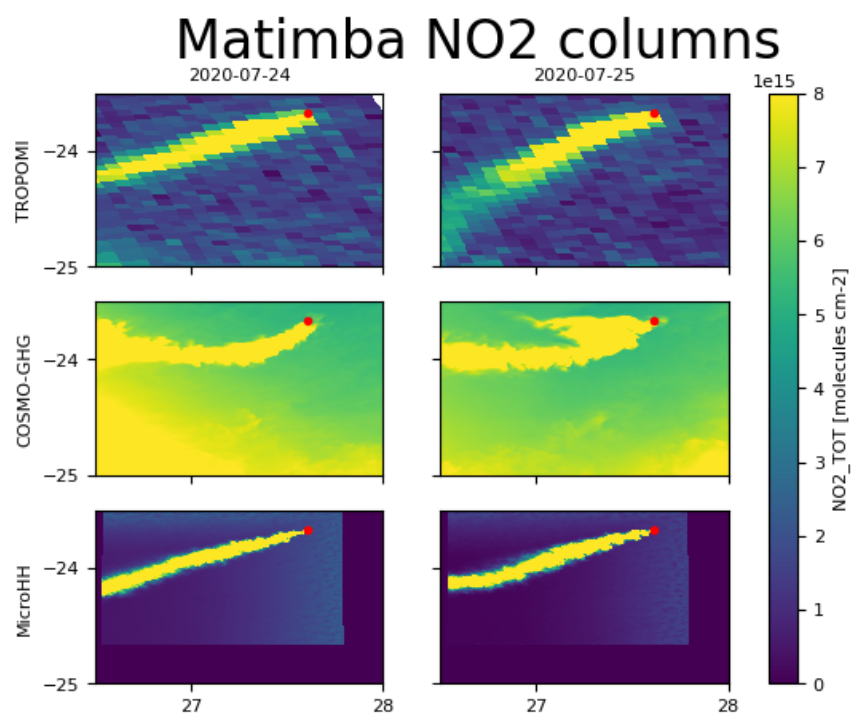


Figure 40. Zoom on the comparison for TROPOMI columns with the total simulated NO₂, see Figure 39.

4.1.4.3 Analysis of downwind NO₂ profile

When comparing the NO₂ and NO_x profiles downstream, we see that both COSMO-GHG and MicroHH simulated quite similar profiles on both days, with NO₂ concentrations peaking at a similar offset from the power plant stack in both models. A difference, however, lies in the NO_x

decay, which is clearly exponential in the COSMO-GHG case (which is, indeed, modelled with an exponential decay), while the decay simulated in MicroHH is essentially linear with distance, indicating that OH gets replenished in the downstream direction of the plume, to react further with the nitrogen oxides. This suggests that the assumption of an exponential decaying NO_x tracer for COSMO-GHG is too simplistic for this case.

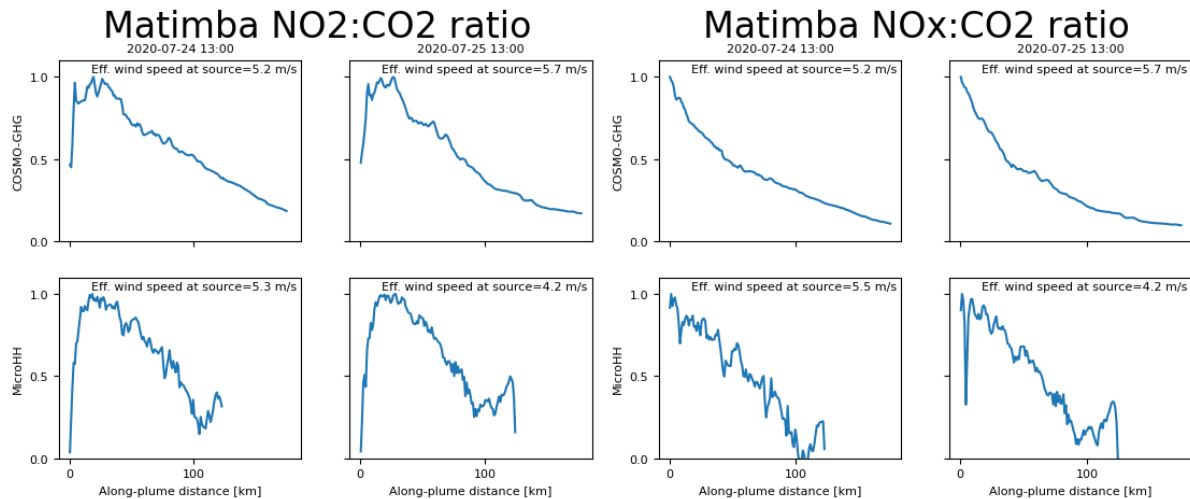


Figure 41. Comparison of downstream NO₂ and NO_x decay for Matimba. The ratios are normalized to 1. The effective wind speed is the wind speed weighted with the vertical distribution of NO₂ or NO_x around the source position.

4.1.4.4 Downwind dispersion of the plume

In the plume width plot (Figure 42) we can note a large downwind plume width deviation for COSMO-GHG on the 25th of July from about 30-70 km, which could already be seen on Figure 40. As in other cases, the COSMO-GHG plume is about twice as wide as the MicroHH plume, which again reaches a steady-state width that the width fluctuates around.

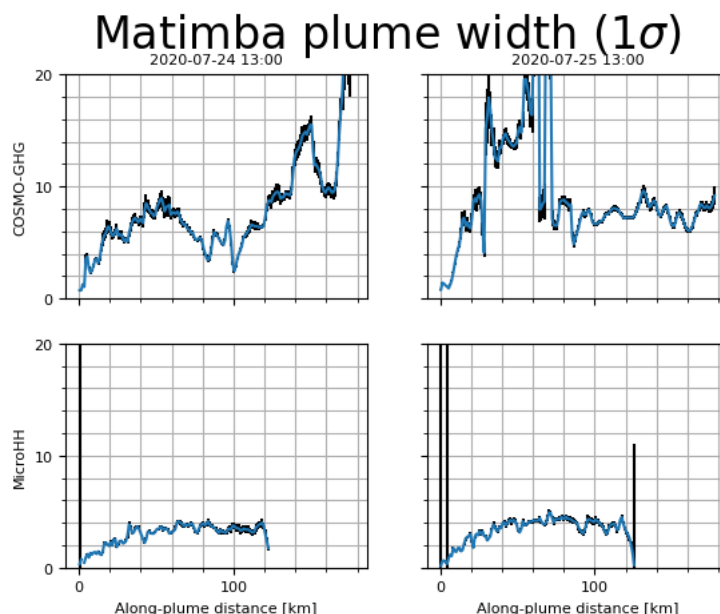


Figure 42. The downwind evolution of the plume width for the Matimba power plant, following a Gaussian plume fit to the CO₂_PP_M tracer. The black line shows one standard deviation of the fitted plume width

4.1.4.5 Synthetic CO₂M image

The Matimba plume can be seen well in synthetic CO₂M images (Figure 43) from both modelling systems and on both days.

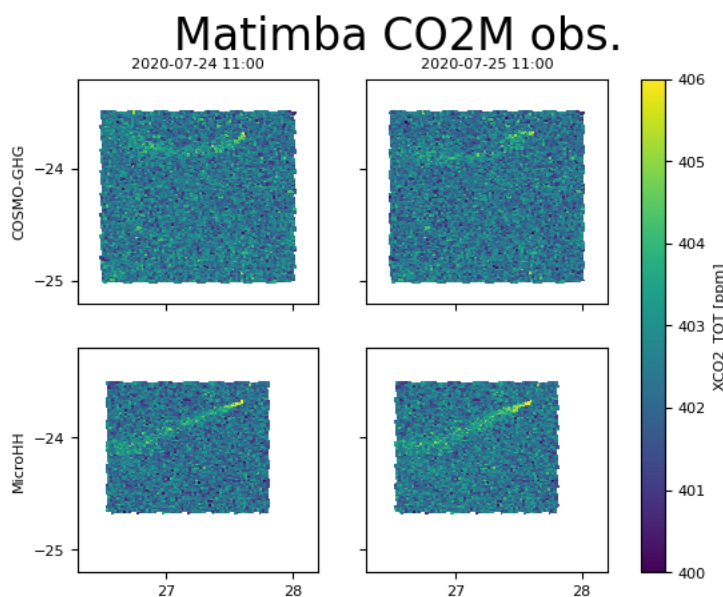


Figure 43. Synthetic CO₂M observation of the total CO₂ column around Matimba.

4.1.4.6 Conclusions for this case

In conclusion, we have seen the following: **To match NO₂ column observations**, the results from both models (but particularly COSMO-GHG) are not producing column images in line with the observations.

4.2 Cities

4.2.1 Berlin (2018-07-18 – 2018-07-26)

The Berlin urban area in Germany has been simulated with two models (COSMO-GHG and LOTOS-EUROS). The LOTOS-EUROS simulations were driven with meteorology from ICON simulations. The submitted tracers can be found in Table 6.

Table 6. Submitted tracers by the different models for the Berlin case.

| Model | Submitted tracers |
|--------------------|---|
| COSMO-GHG | CO ₂ _CITY, CO ₂ _ANTH, CO ₂ _BG, CO ₂ _BIO, CO_CITY, CO_ANTH, CO_BG, NOX_CITY, NOX_ANTH, NOX_BG |
| LOTOS-EUROS | CO ₂ _CITY, CO ₂ _ANTH, CO ₂ _BG, CO ₂ _BIO, CO_CITY, CO_ANTH, CO_BG, CO_BIO, NO_CITY, NO_ANTH, NO_BG, NO_BIO, NO ₂ _CITY, NO ₂ _ANTH, NO ₂ _BG, NO ₂ _BIO, OH, TNMVOC_CITY, TNMVOC_ANTH, TNMVOC_BG, TNMVOC_BIO |

4.2.1.1 Overview column images

In Figure 44, overview column images are given for the Berlin case on two of the simulated days. The two modelling systems now use a different meteorology (unlike what was the case for the power plants, before), but the two models transport the plume in essentially very similar patterns. One notable feature is that more of the turbulence is resolved in COSMO-GHG compared to LOTOS-EUROS (e.g., at 16:00 on both of the plotted days, the COSMO-GHG

plume contains distinguishable eddies, while the LOTOS-EUROS simulation shows opening of the plume only through diffusion around the edges). Unlike the power plant cases, the emissions now follow a temporal profile, and it can indeed be seen that emissions are considerably smaller in the night-time compared to the daytime.

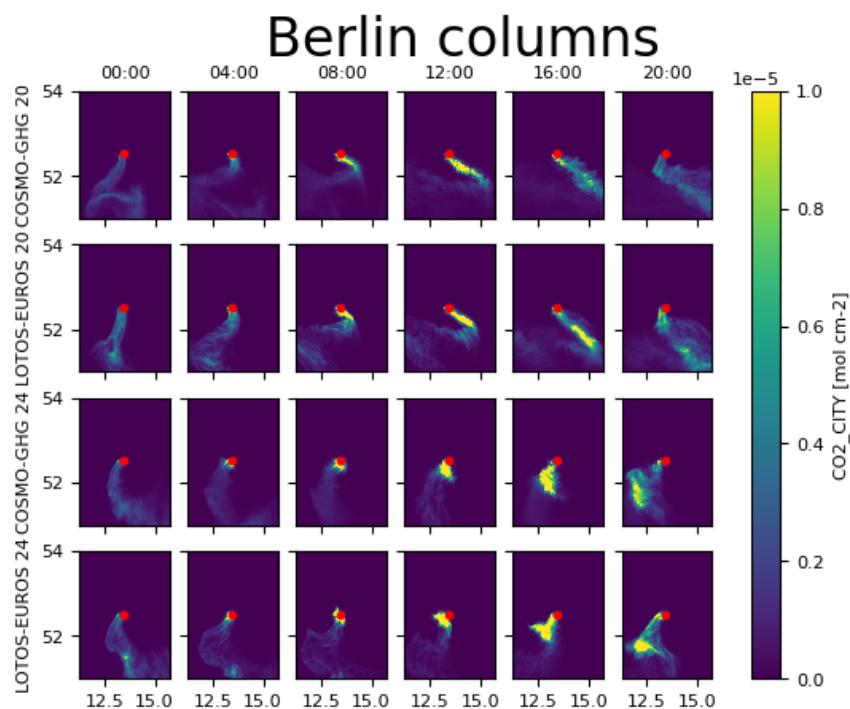


Figure 44. Total column images as generated by two modelling systems of the Berlin urban area, on July 20 and July 24, 2018. An approximate location centred within Berlin is indicated by the red dot.

4.2.1.2 Comparison against in-situ CO₂ measurements

In the context of the Urban Climate Under Change project [UC]², DLR-Cessna research flights were conducted around Berlin in July 2018 with the DLR-Cessna aircraft (Klausner, Mertens, et al., 2020; Scherer et al., 2019). Measurements of CO₂ were made with the Picarro G1301-m instrument (as also used in Section 4.1.1.2; the data for 20 and 24 July 2018 can be found under Klausner, Roiger, et al., 2020). Curtain and direct comparison plots were compiled for both aircraft flight days for COSMO-GHG (Figure 45 and Figure 47) and LOTOS-EUROS (Figure 46 and Figure 48). As the experiments took place during the afternoon, there is a considerable stochastic component in the measurements. However, it can be seen that the observations match to a very high degree with both simulations, for altitudes up to 3000 m, even though the ABL on both days is only about 1800 m deep.

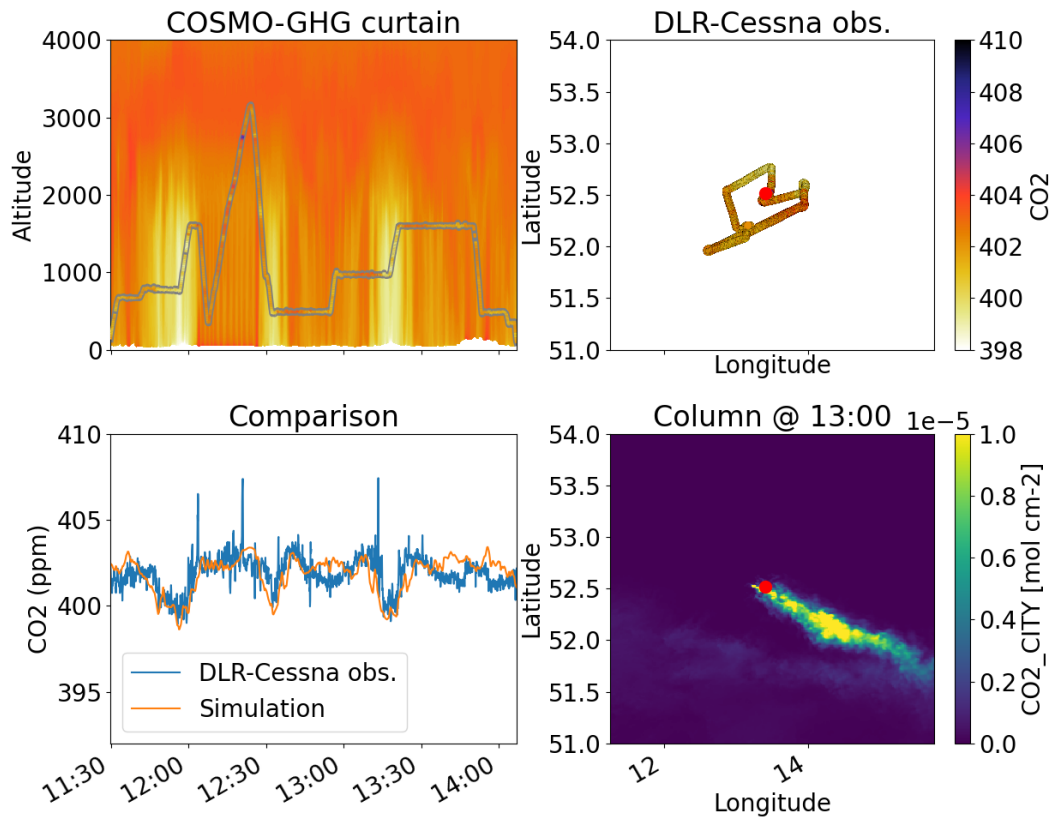


Figure 45. COSMO-GHG comparison against DLR-Cessna for Berlin, 20 July 2018.

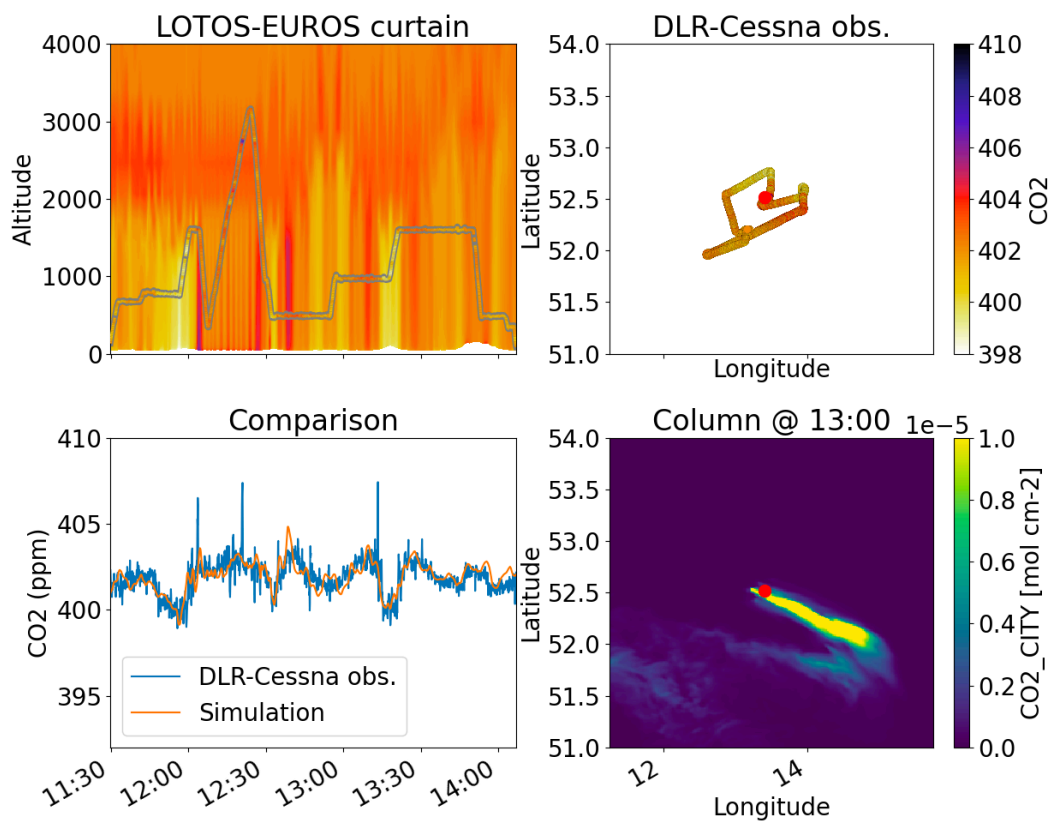


Figure 46. LOTOS-EUROS comparison against DLR-Cessna for Berlin, 20 July 2018.

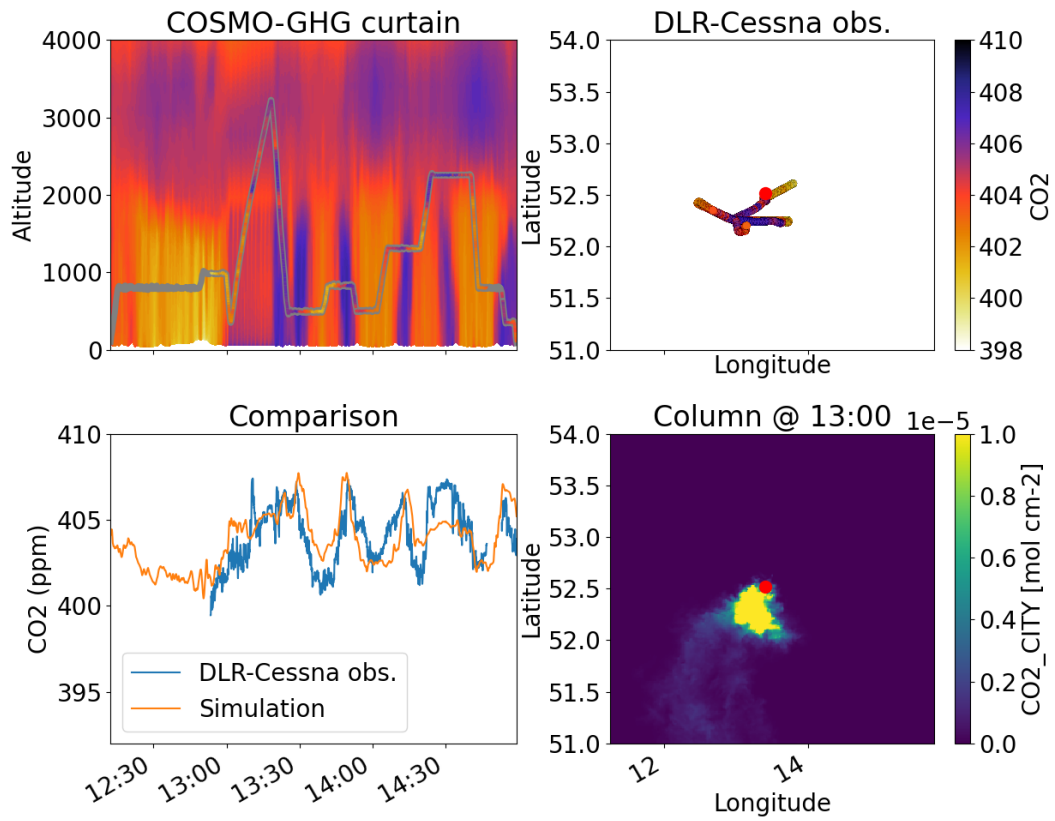


Figure 47. COSMO-GHG comparison against DLR-Cessna for Berlin, 24 July 2018.

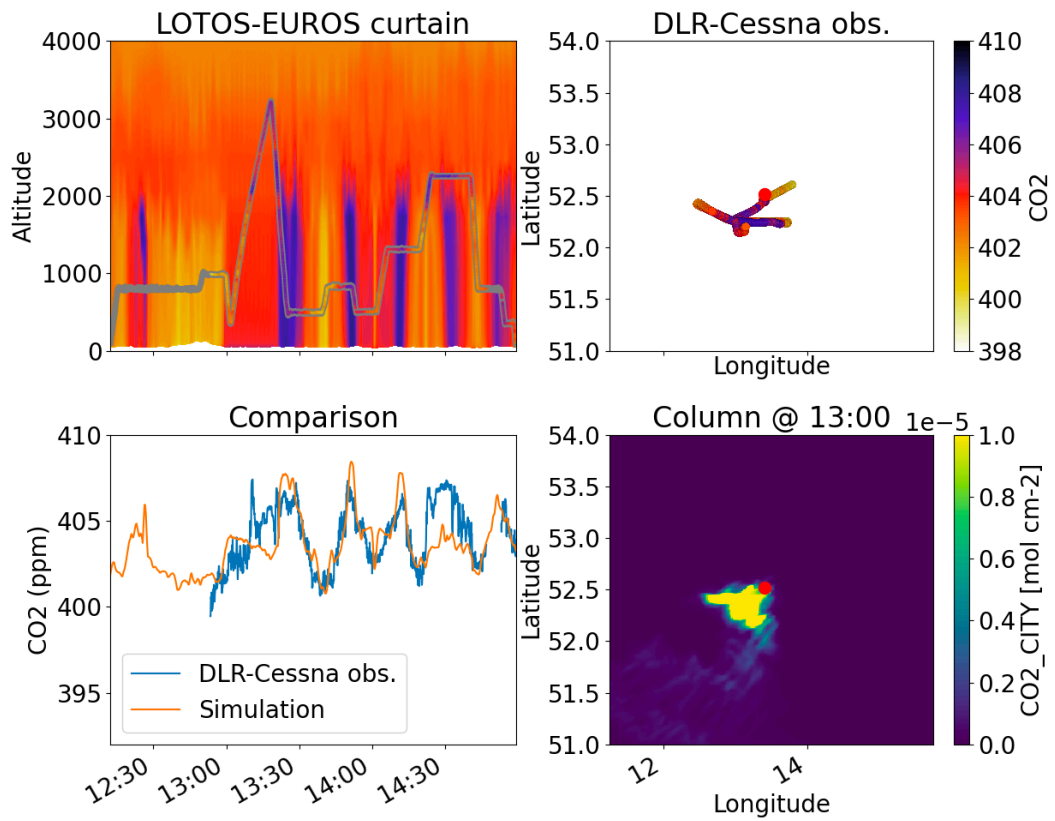


Figure 48. LOTOS-EUROS comparison against DLR-Cessna for Berlin, 24 July 2018.

4.2.1.3 Comparison against TROPOMI NO₂ image

The two best TROPOMI images for the simulated time series were selected as 23 and 26 July, 2018. A comparison for both days using both models can be seen in Figure 49. The right-bottom of the plot contains the Jänschwalde power plant, which we can also identify on both TROPOMI images, but also the Berlin plume itself is visible on the TROPOMI image. Both models are capable of explaining the TROPOMI image with equal skill; the only (visible) difference between the two models lies in their scale of resolved turbulence, and this is of a finer scale than what can be distinguished on the TROPOMI pixels.

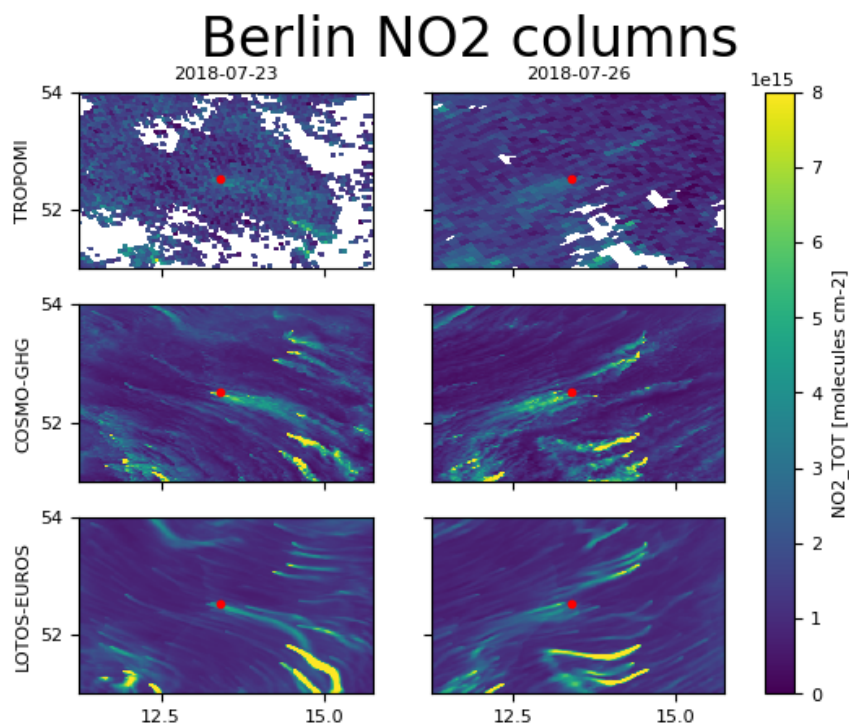


Figure 49. Comparison for TROPOMI columns with the total simulated NO₂. For COSMO-GHG, the NO₂ column was created based on an NO_x tracer (NOX_PP_M + NOX_ANTH + NOX_BG) converted into an NO₂ tracer. For LOTOS-EUROS, the NO₂ column was modelled including full chemistry (NO₂_CITY + NO₂_ANTH + NO₂_BG + NO₂_BIO).

4.2.1.4 Analysis of downwind NO₂ profile

Downwind NO₂ and NO_x column profiles for the same days as the displayed TROPOMI comparisons are shown in Figure 50. It is hard to discern a considerable difference between the NO₂ and the NO_x profile, likely due to (1) the ratio with CO₂ being not an ideal metric to test the downwind profiles, and (2) the fact that the first ~30 km in the “along-plume” direction are still within the city of Berlin, so decaying NO₂ and NO_x fields are being simultaneously being re-emitted (which is why the profiles are a bit jagged in the early part of the “along plume” direction). Hence, there is little conclusion that can be drawn from this figure. A more involved study could be of interest here (e.g., focussing on multiple times, various distances from the source, ...).

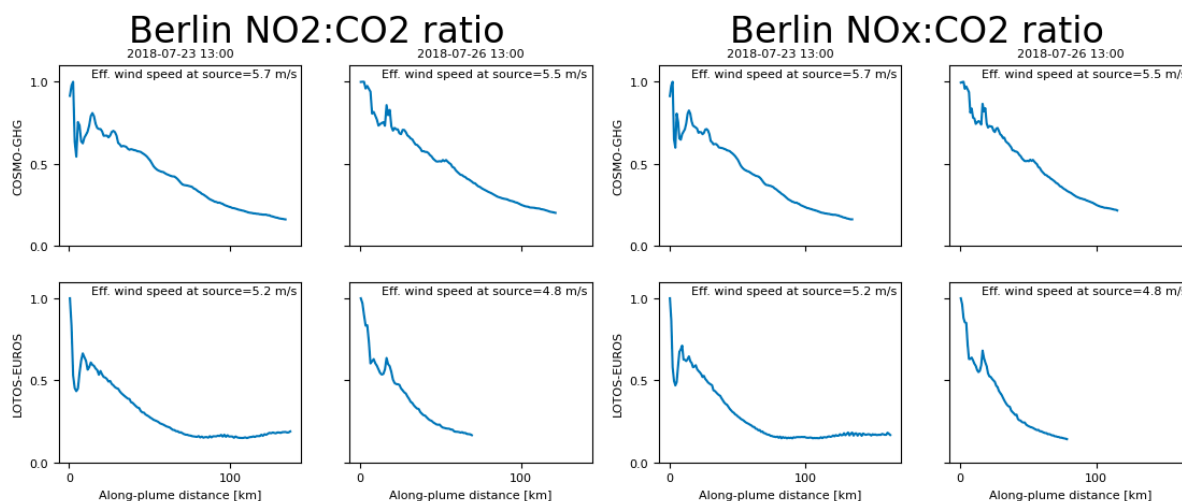


Figure 50. Comparison of downstream NO₂ and NO_x decay for the Berlin plume. The ratios are normalized to 1. The effective wind speed is the wind speed weighted with the vertical distribution of NO₂ or NO_x around the source position.

4.2.1.5 Downwind dispersion of the plume

The width of the plume has been estimated with a Gaussian fit, as plotted in Figure 51, and the results are in line with what was also visible on the TROPOMI image (Figure 49): the Berlin plume is opens up considerably more with COSMO-GHG than with LOTOS-EUROS on the 23rd of July, while both plumes becomes rather wide on the 26th of July. As also found in previous cases, the plume does not grow considerably in the downwind direction, after reaching a steady-state width.

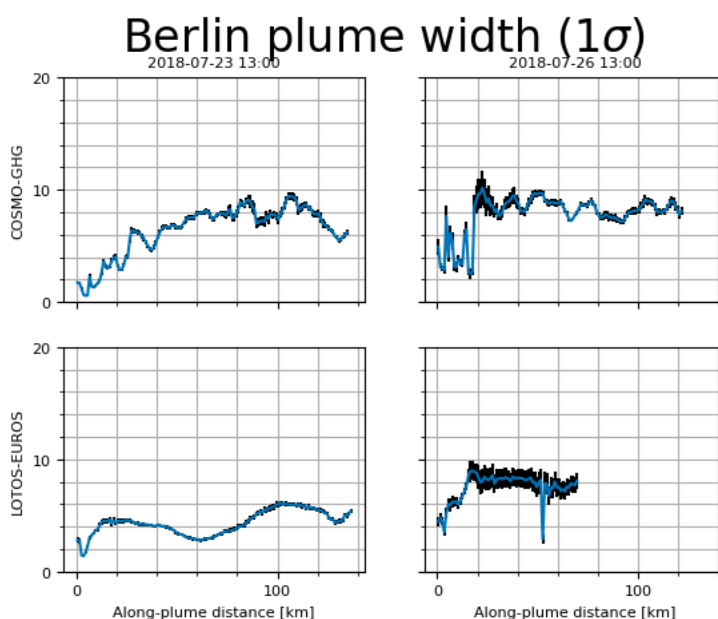


Figure 51. The downwind evolution of the plume width for the Berlin plume, following a Gaussian plume fit to the CO₂_CITY tracer. The black line shows one standard deviation of the fitted plume width

4.2.1.6 Synthetic CO₂M image

A synthetic CO₂M observation, as shown in Figure 52, shows a rather faint plume, particularly compared to, e.g., the Jämschwalde power plant as visible in the right-bottom corner.

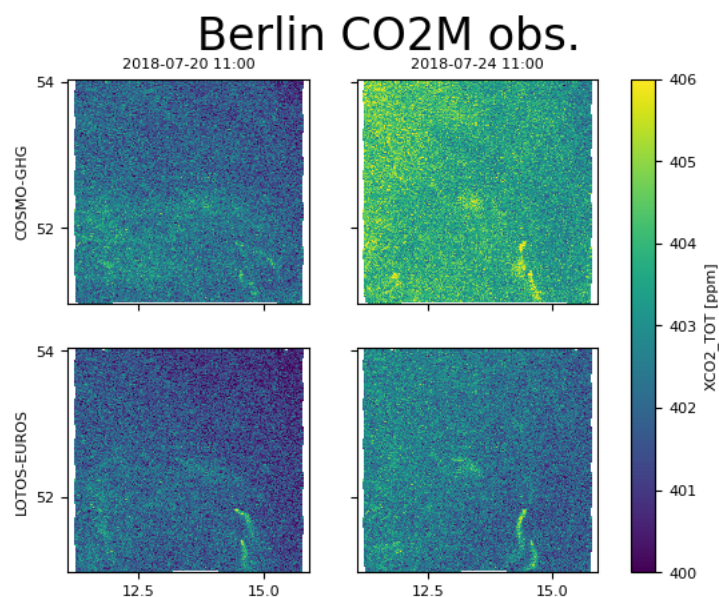


Figure 52. Synthetic CO₂M observation of the total CO₂ column around Berlin.

4.2.1.1 Conclusions for this case

In conclusion, we have seen the following: **to match in-situ data**, both models (COSMO-GHG and LOTOS-EUROS) yield results that match excellently with the observations. **To match NO₂ column observations**, the results from COSMO-GHG and LOTOS-EUROS yield results that match well to the observations.

4.2.2 Paris (2018-08-01 – 2018-08-08)

The Paris urban area in France has been simulated with two models (COSMO-GHG and WRF-CHEM). The submitted tracers can be found in Table 7.

Table 7. Submitted tracers by the different models for the Paris case.

| Model | Submitted tracers |
|------------------|--|
| COSMO-GHG | CO ₂ _CITY, CO ₂ _ANTH, CO ₂ _BG, CO ₂ _BIO, CO_CITY, CO_ANTH, CO_BG, NOX_CITY, NOX_ANTH, NOX_BG |
| WRF-CHEM | CO ₂ _CITY, CO ₂ _ANTH, CO ₂ _BG, CO ₂ _BIO |

4.2.2.1 Overview column images

In Figure 53, overview column images are given for the Paris case on two days. Despite showing plumes going in roughly similar directions, there are significant differences between the specifics of the two model outputs. For example, the WRF-CHEM plume is narrower at night and at morning times of the 1st of August (therefore appearing with higher magnitude) than the COSMO-GHG plume. During the evening of the 1st of August, COSMO-GHG predicts that the plume concentrations will transport northwards after a predominantly southward trajectory during the day, while in WRF-CHEM the southerly transport remains. The columns for the 5th of August show a very similar evolution up until 20:00, where the COSMO-GHG plume opens up considerably indicative of low wind speeds, while the WRF-CHEM plume remains narrow. Hence, it seems that the models agree relatively well during the daytime, but obtain different solutions in the night.

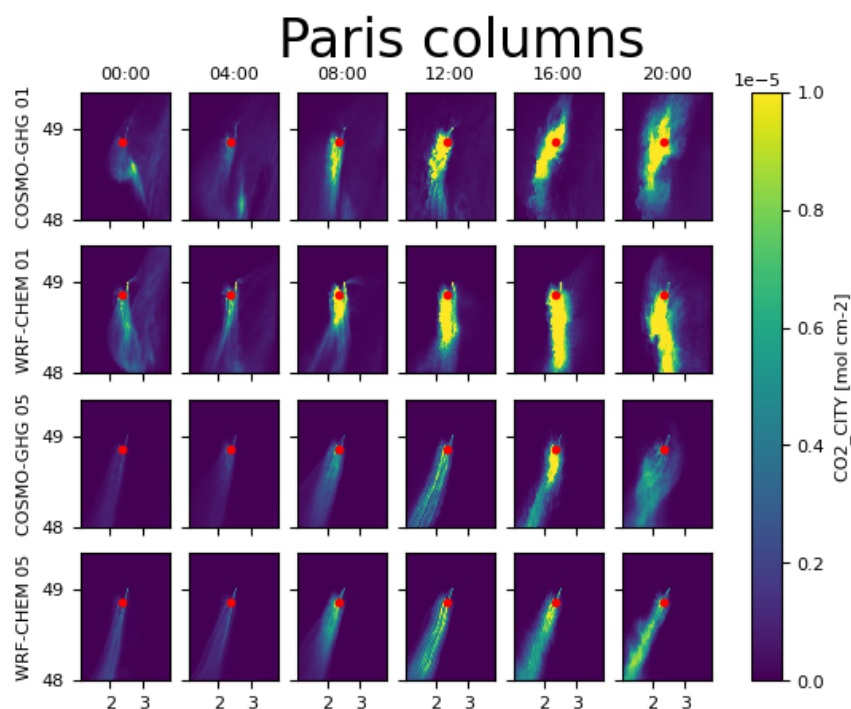


Figure 53. Total column images as generated by two modelling systems of the Paris urban area, on August 1 and August 5, 2018. An approximate location centred within Paris is indicated by the red dot.

4.2.2.2 Comparison against in-situ CO₂ measurements

CO₂ observation data was collected using Cavity Ring-Down Spectrometers (CRDSs) around Paris, with an hourly sampling rate (files were obtained from Michel Ramonet, LSCE). The station codes can be found in Table 8. Two stations (JUS and CDS) are located within the center of Paris in a dense urban environment where the emission density is the highest. The other five stations (AND, COU, GNS, OVS, SAC) are located at the edges of the urban and built-up areas in mixed urban–rural environments. All stations are from the LSCE / ICOS-Fr network (see Lian et al., 2022).

Table 8. CRDS measurement stations around Paris.

| Station code | Station name | Altitude |
|--------------|--|-----------|
| AND | Andilly | 60 m agl |
| CDS | Cité des Sciences | 34 m agl |
| COU | Coubron | 30 m agl |
| GNS | Gonesse | 36 m agl |
| JUS | Jussieu | 30 m agl |
| OVS | Observatoire de Versailles Saint-Quentin-en-Yvelines | 20 m agl |
| SAC | Saclay | 15 m agl |
| SAC | Saclay | 60 m agl |
| SAC | Saclay | 100 m agl |

Like the aircraft observational data in previous sections, we plot a curtain plot and point-wise comparison plot, to provide some context to the measurements. The resulting plot for

COSMO-GHG can be found in Figure 54, while the plot for WRF-CHEM may be found in Figure 55. In the curtain plots, we can see the daily build-up of the ABL towards an altitude of about 1500 m, or in particular the mixing of the city plume in the ABL. We can see the lower concentrations on the 4th and 5th of August 2018 (a weekend). The COSMO-GHG simulation generally overestimates the peak of the measurements for this station, while WRF-CHEM stays relatively close to the observations.

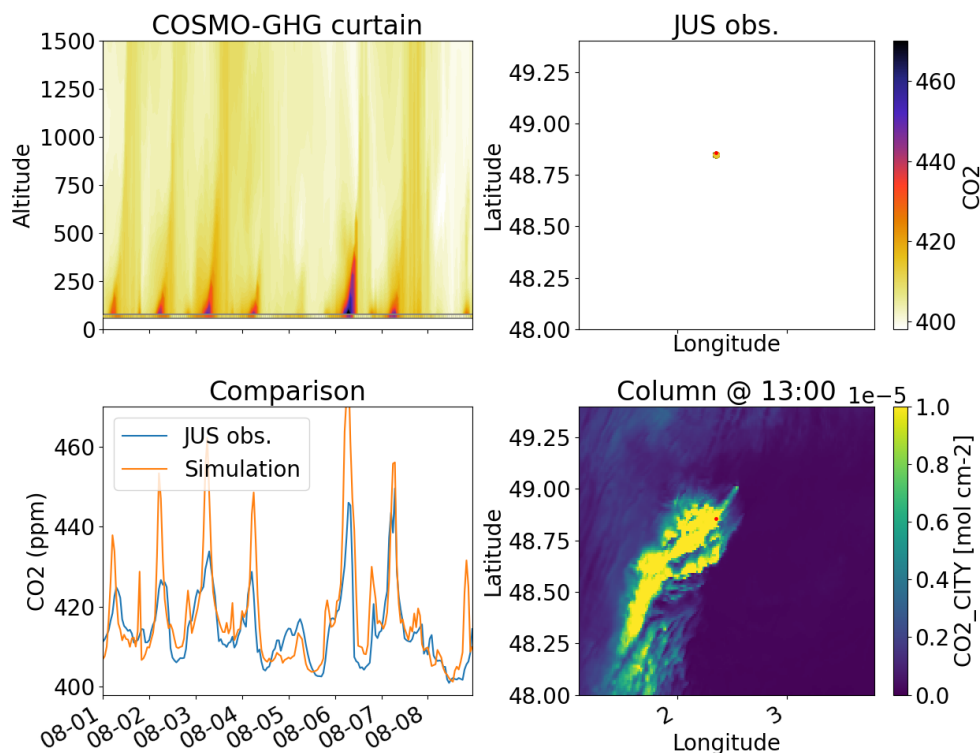


Figure 54. COSMO-GHG comparison against the Jussieu station for Paris, 01-08 August 2018.

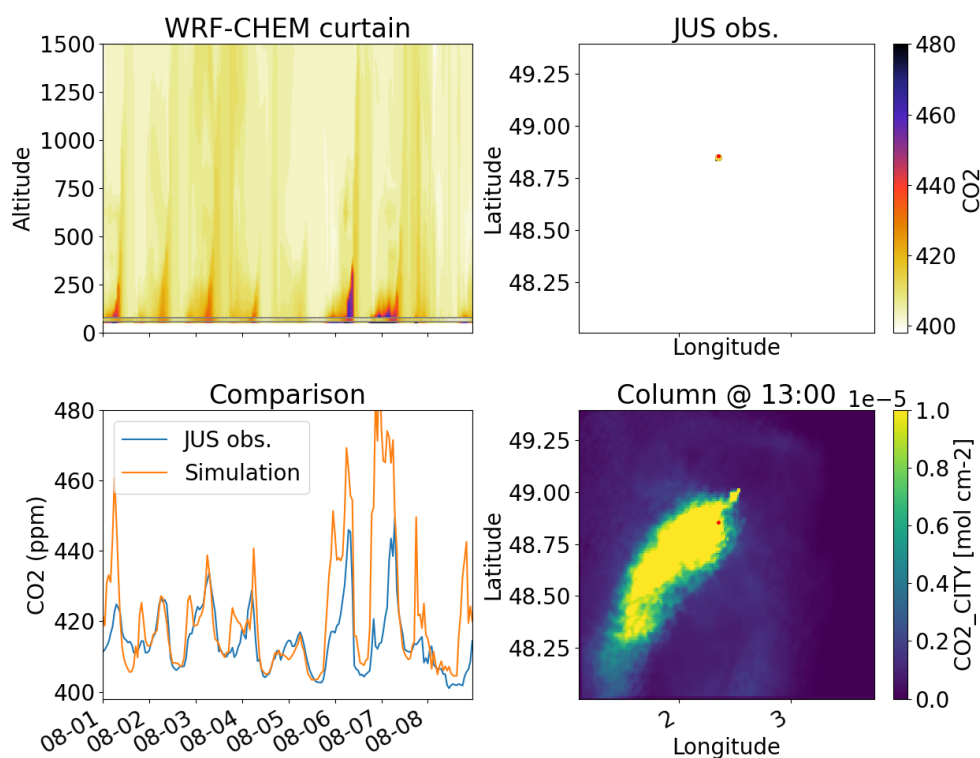


Figure 55. WRF-CHEM comparison against the Jussieu station for Paris, 01-08 August 2018.

We then turn our attention to the fit between observations and measurements for all stations. To quantify the fit, we use two metrics: the coefficient of determination

$$R^2 = 1 - \frac{\sum_t (\text{CO}_{2,obs}(t) - \text{CO}_{2,sim}(t))^2}{\sum_t (\text{CO}_{2,obs}(t) - \overline{\text{CO}_{2,obs}(t)})^2},$$

where $\overline{\text{CO}_{2,obs}(t)}$ is the mean of the observations over time, and the root-mean-square error

$$RMSE = \sqrt{(\text{CO}_{2,obs}(t) - \text{CO}_{2,sim}(t))^2}.$$

The results of the comparisons for all stations can be found in Figure 56. The cross-plots show that the simulations generally have a small tendency to overestimate the observations; except at the OVS and lowest SAC station where two peaks at the nights of the 5th to 6th and 6th to 7th of August can be observed which are not simulated with the same intensity. As these peaks are well-modelled in other cases (or even overestimated), this is likely not the case of a feature missing in the emissions inventory, but of a small mismatch between the simulated weather pattern and the real weather, deviating the trajectory of the enhanced concentrations slightly.

Paris in-situ data

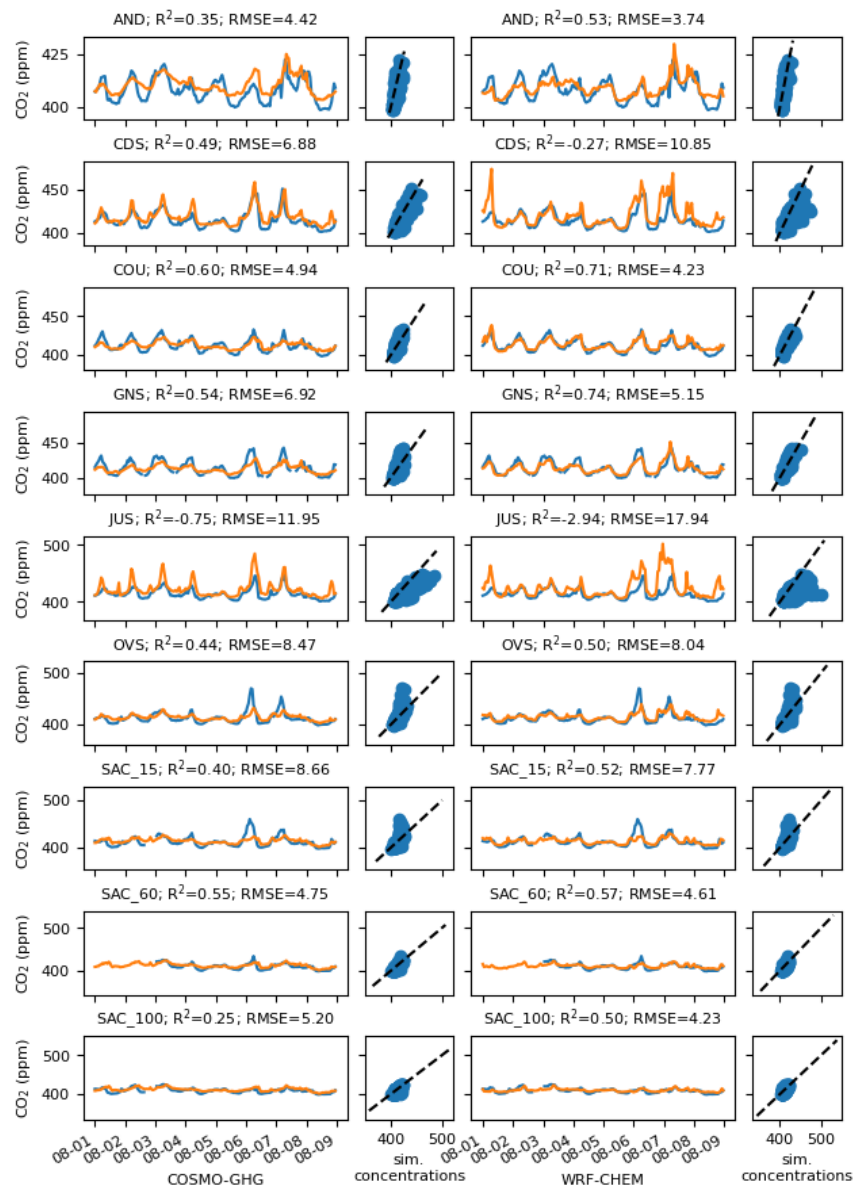


Figure 56. Comparison between the Paris CO₂ observations and simulations, shown both as a time-series and as a cross-plot. The observations are drawn in blue while the simulations are drawn in orange.

4.2.2.3 Comparison with TROPOMI NO₂

A TROPOMI comparison with the COSMO-GHG columns was made for every day of the observations, see Figure 57. Generally, we can see that the simulated concentrations lead to images remarkably similar to the TROPOMI images – certainly in terms of orientation of the plume, as well as the general shape of the plume.

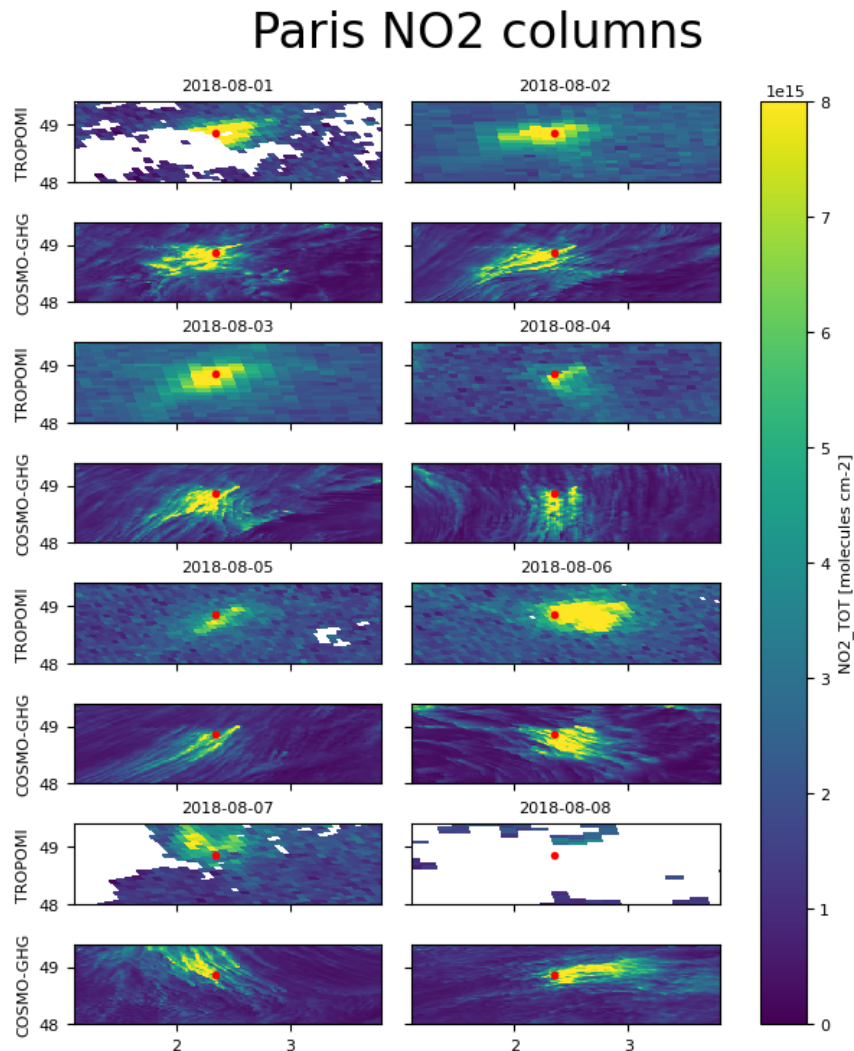


Figure 57. Comparison for TROPOMI columns with the total simulated NO₂. For COSMO-GHG, this NO₂ column was created based on an NO_x tracer (NOX_PP_M + NOX_ANTH + NOX_BG) converted into an NO₂ tracer.

4.2.2.4 Downwind dispersion of the plume

Figure 58 shows the downwind evolution of the width of the Paris city plume on the days also displayed in the overview columns. As already noted when describing the overview columns of Figure 53, the simulated plumes appear very similar during the daytime, and correspondingly we find plume widths very consistent between both models, for both days. In contrast to most other cases we considered thus far, the plume gradually widens in the downwind direction.

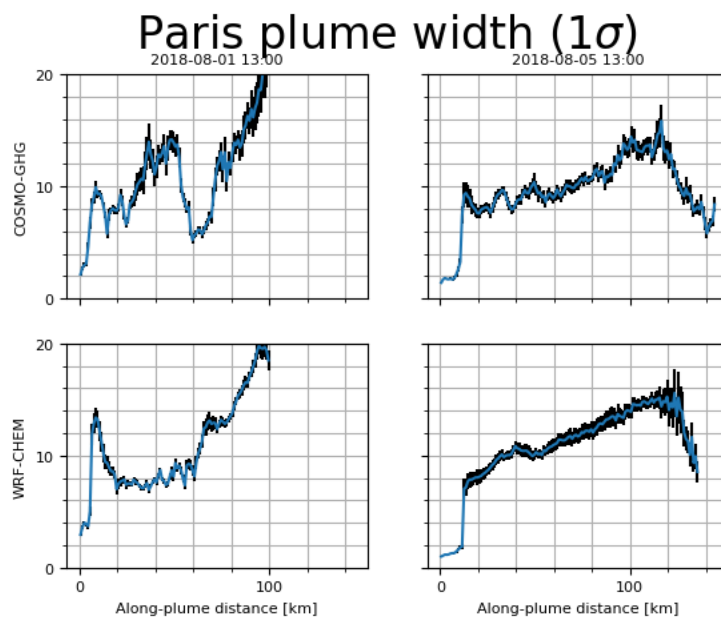


Figure 58. The downwind evolution of the plume width for the Paris plume, following a Gaussian plume fit to the CO_CITY tracer. The black line shows one standard deviation of the fitted plume width.

4.2.2.5 Synthetic CO₂M image

A synthetic CO₂M observation, as shown in Figure 59, shows a rather faint plume for Paris, which is only visibly discernible in the WRF-CHEM result on the 1st of August.

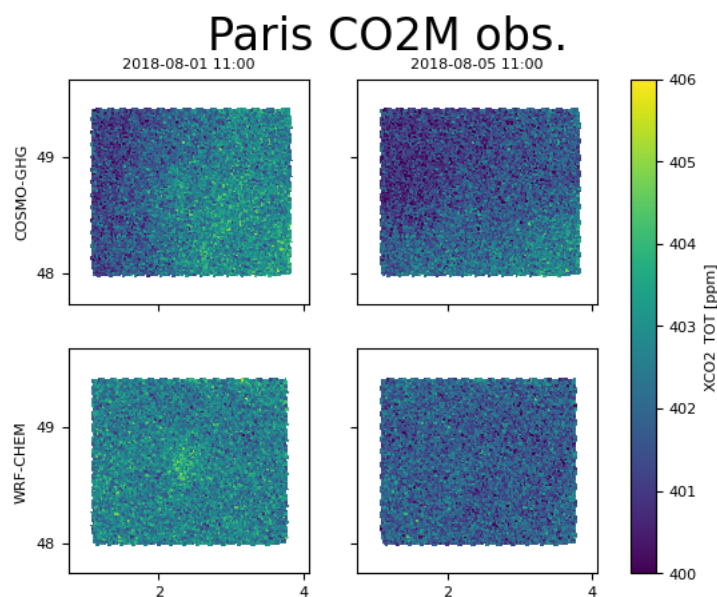


Figure 59. Synthetic CO₂M observation of the total CO₂ column around Paris.

4.2.2.6 Conclusions for this case

In conclusion, we have seen the following: **to match in-situ data**, both models (COSMO-GHG at 1.1 km resolution and WRF-CHEM at 1 km resolution) yield results that match well with the observations (though WRF-CHEM performs slightly better when the results are quantified). **To match NO₂ column observations**, the results from COSMO-GHG match extremely well with the TROPOMI images.

4.2.3 Randstad (2018-06-16 – 2018-06-23 & 2018-12-16 – 2018-12-23)

The Randstad urban area in the Netherlands has been simulated with one model (LOTOS-EUROS). The submitted tracers can be found in Table 9.

Table 9. Submitted tracers by one model for the Randstad case.

| Model | Submitted tracers |
|--------------------|--|
| LOTOS-EUROS | CO2_RS, CO2_ ANTH, CO2_BG, CO2_BIO, CO_RS, CO_ ANTH, CO_BG, CO_BIO, NO_RS, NO_ ANTH, NO_BG, NO_BIO, NO2_RS, NO2_ ANTH, NO2_BG, NO2_BIO, OH, TNMVOC_RS, TNMVOC_ ANTH, TNMVOC_BG, TNMVOC_BIO |

4.2.3.1 Overview column images

In the overview columns of Figure 60, two example days from both the ‘summer’ (S) and ‘winter’ (W) range of days are plotted. On the second day in each example, we can clearly see a range of point sources, with two particularly strong sources (related to Tata steel in the North, and the Port of Rotterdam in the South) standing out in particular.

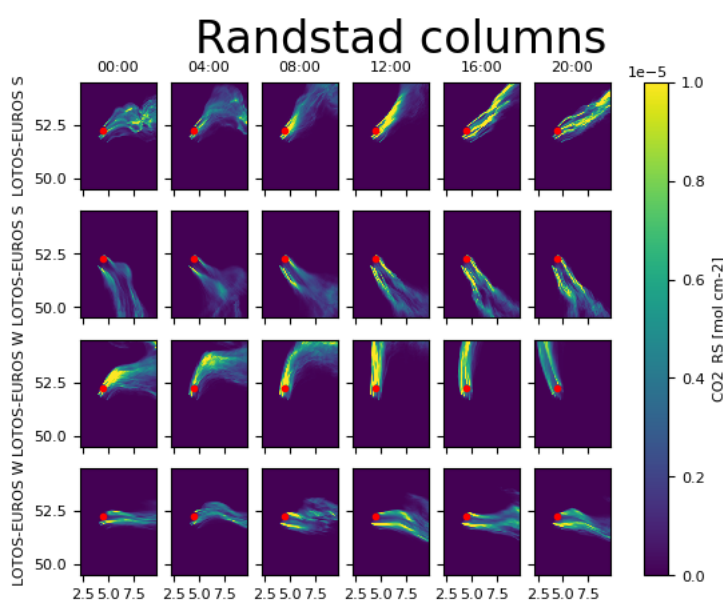


Figure 60. Total column images as generated by LOTOS-EUROS for the Randstad urban area with the CO₂_RS tracer, on 18th and 22nd of June (S) and 18th and 22nd of December (W). An approximate location centred within the Randstad area is indicated by the red dot.

4.2.3.2 Comparison against in-situ CO₂ measurements

A high-precision ICOS measurement station is located within the simulated domain, the KNMI-mast Cabauw. Data can be downloaded from the ICOS-CP (Frumau et al., 2022). This data is plotted in Figure 61, in a manner similar to the plotting of the Paris data. Unfortunately, a lot of the data is missing in both observational time ranges, but there is a reasonable fit between the observations and simulations where they are both available.

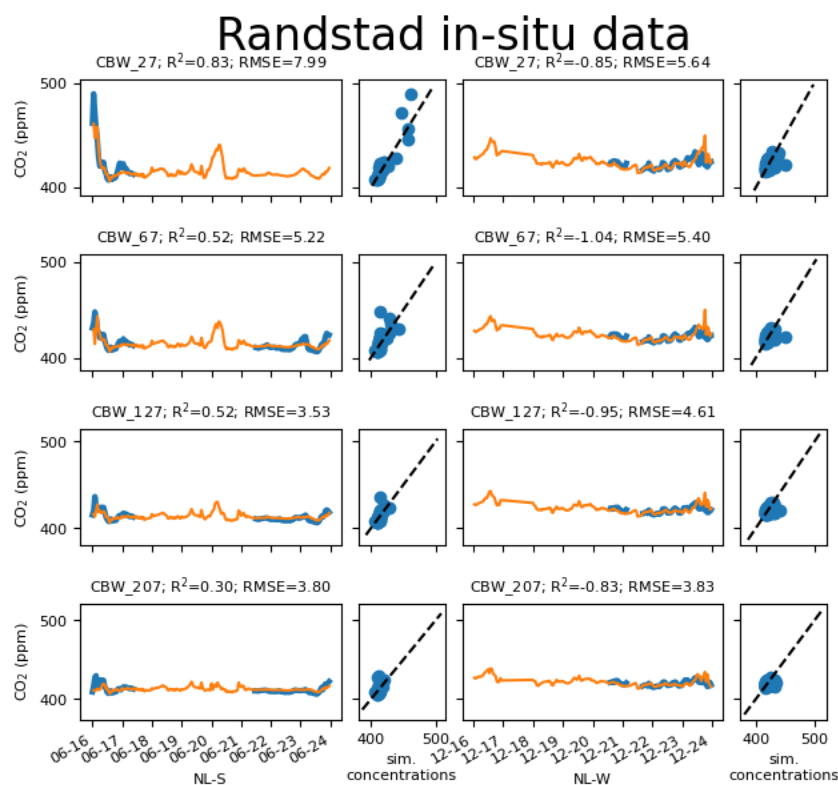


Figure 61. Comparison between the Cabauw CO₂ observations and simulations, shown both as a time-series and as a cross-plot. The observations are drawn in blue while the simulations are drawn in orange. The left panels shows the summer (S) days, while the right columns show the winter (W) days.

4.2.3.3 Comparison against in-situ NO₂ measurements

To verify also the simulated fields for this large domain more substantially, data from 43 Dutch urban, suburban and rural background NO₂ air quality sensors was downloaded (European Air Quality Portal, n.d.). A comparison of the data with the simulations can be found in Figure 62 for the summer data and Figure 63 for the winter data. We can observe that there are considerably more NO₂ in peaks the winter (likely due to combined effects of increased use of fossil fuels for heating and transport, less sunlight limiting the suitable conditions to break down NO₂, and a lower ABL height leading to less mixing into higher altitudes and thus higher concentrations near the ground). Correspondingly (e.g., as the ABL height cannot be accurately modelled), the fit to the NO₂ observations is generally poorer in the winter. Furthermore, there appears to be a slight underestimation of the observed concentrations in the winter. The signal in both the winter and summer is, however, rather well captured, indicating that the used meteorology, emission inventory and chemistry scheme combine to a rather accurate predictive system. To summarize, a density plot of the coefficient of determination (R^2) and root-mean-square error (RMSE) are given in Figure 64, which further confirm that the summer case is over-all predicted with a higher skill by the model than the winter case.

Randstad in-situ data

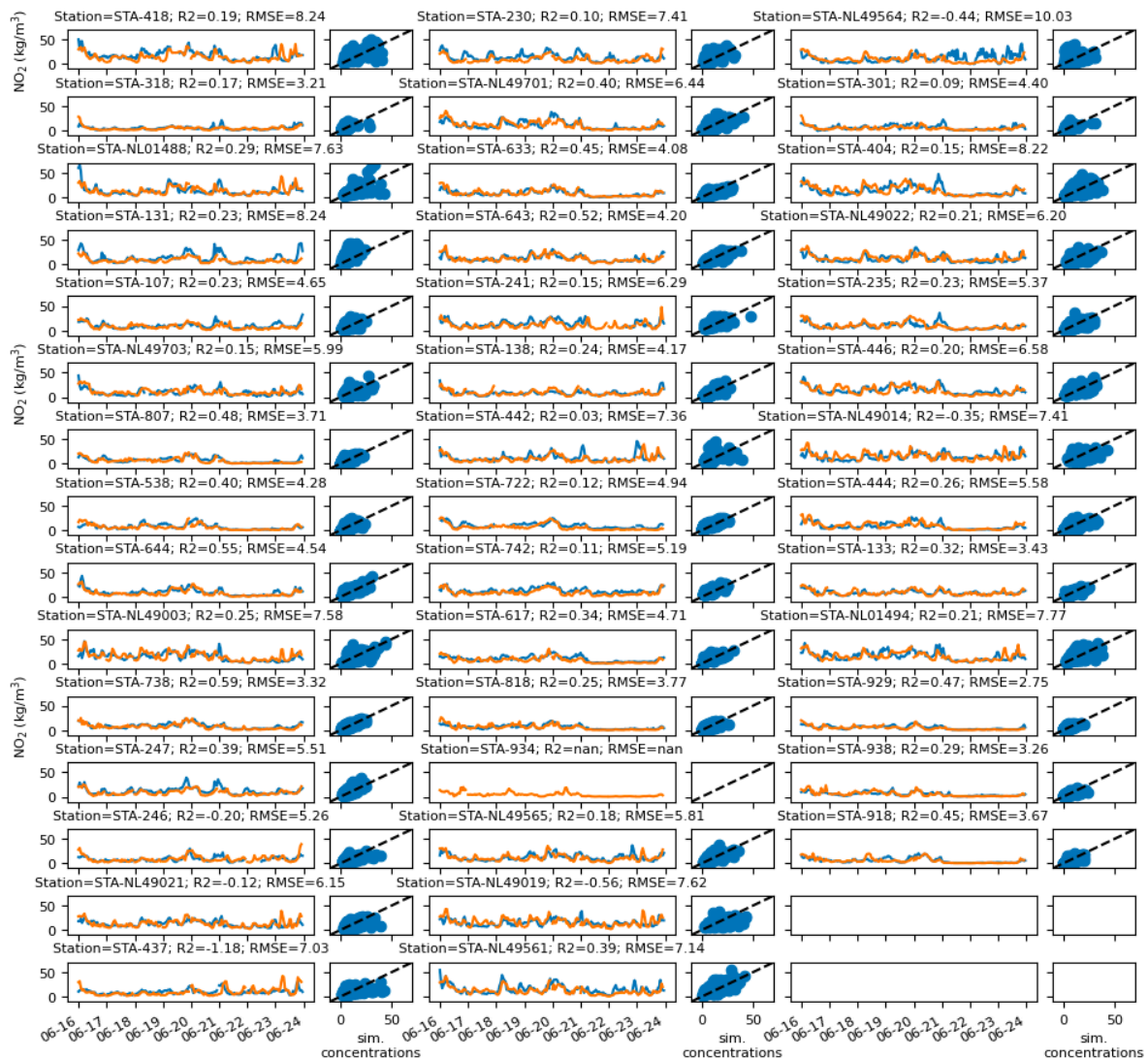


Figure 62. Comparison between Randstad NO₂ observations and simulations in the summer time, shown both as a time-series and as a cross-plot. The observations are drawn in blue while the simulations are drawn in orange. Identifying station IDs are given in the title for each subplot.

Randstad in-situ data

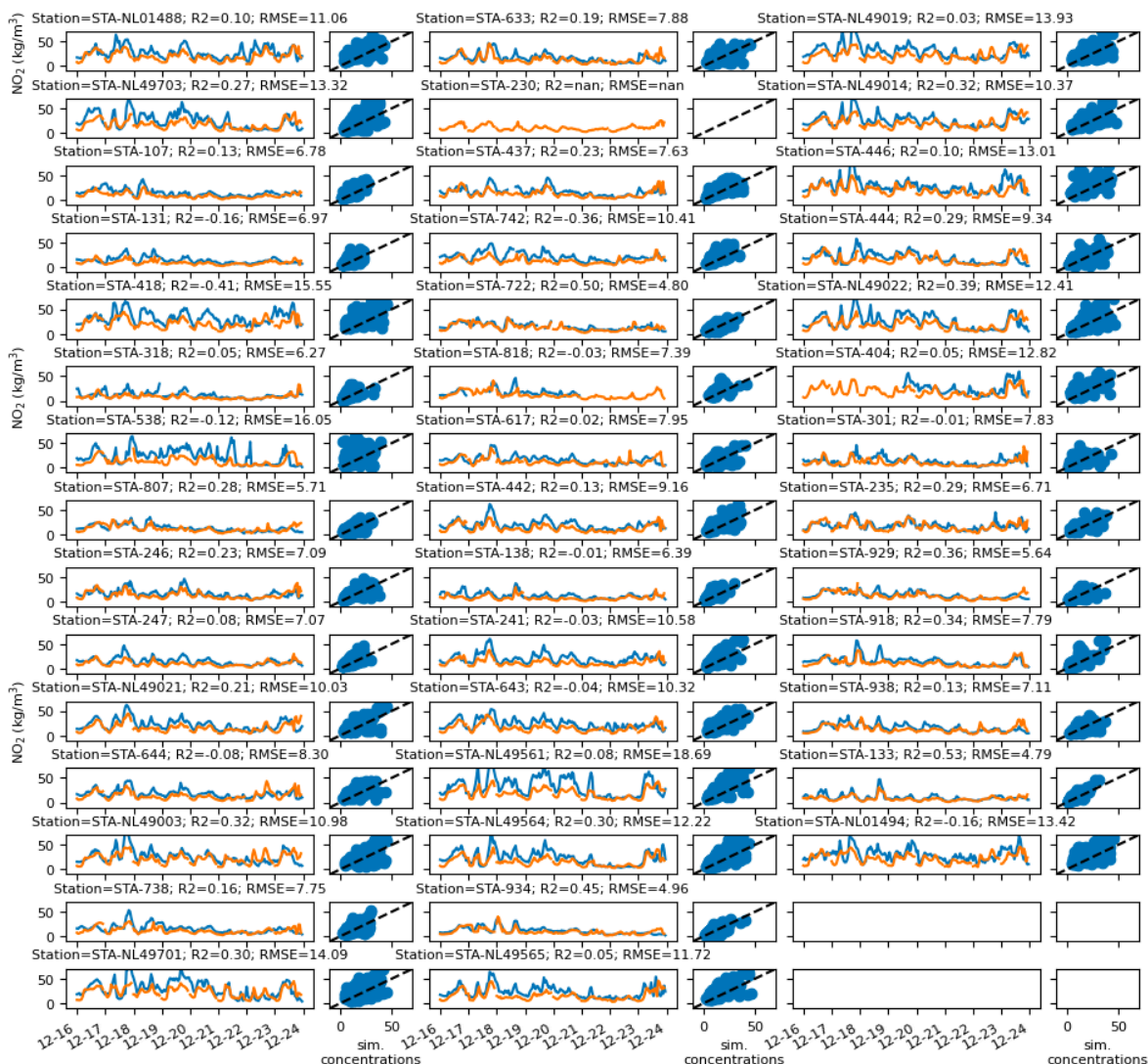


Figure 63. Comparison between Randstad NO₂ observations and simulations in the winter time, shown both as a time-series and as a cross-plot. The observations are drawn in blue while the simulations are drawn in orange. Identifying station IDs are given in the title for each subplot.

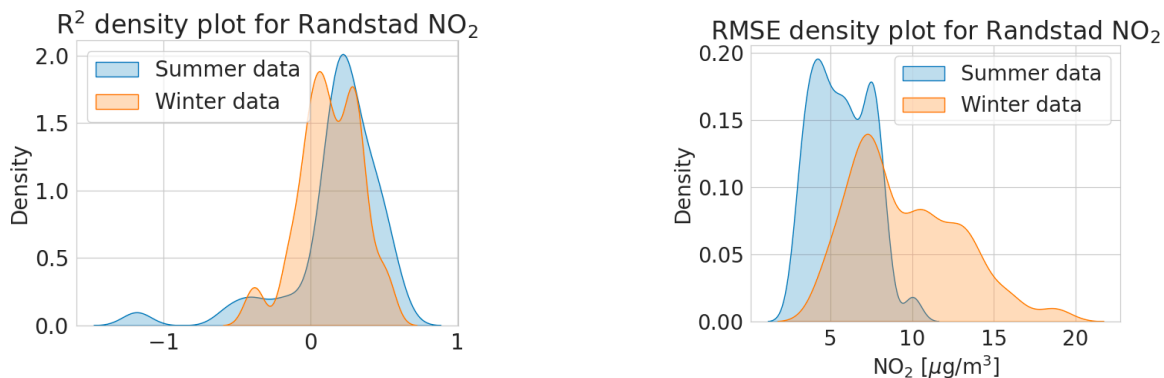


Figure 64. Density plot of the R² (higher is better) and RMSE (lower is better) scores, for the fit between NO₂ observations and simulated values, for the summer and winter dataset of the Randstad region.

4.2.3.4 Comparison against TROPOMI NO₂

In the entire considered time range (2018-06-16 – 2018-06-23 and 2018-12-16 – 2018-06-23), the two best TROPOMI images have been selected; however, even these two days had many pixels with a low qa value, so the comparison shown in Figure 65 does not allow for a significantly detailed analysis. The strongest plume modelled on the 20th of June corresponds to the Ruhr area, and a strong peak south of the Randstad area corresponds to the Port of Antwerp. Both the Ruhr area and Port of Antwerp can be seen on the TROPOMI image, while the Randstad area itself is not well captured on the TROPOMI image.

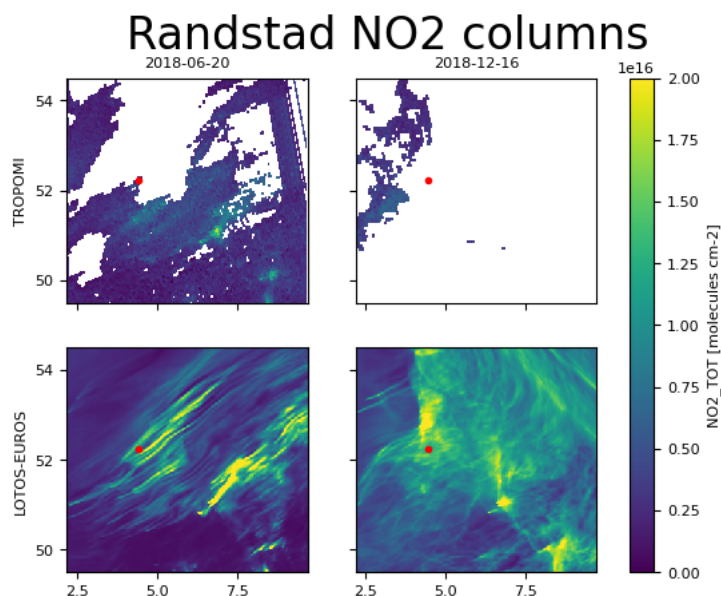


Figure 65. Comparison for TROPOMI columns with the total simulated NO₂. For LOTOS-EUROS, the NO₂ column was modelled including full chemistry (NO₂_RS + NO₂_ANTH + NO₂_BG + NO₂_BIO).

4.2.3.5 Synthetic CO₂M image

Finally, we show a synthetic CO₂M image for one summer day and one winter day for the Randstad area, Figure 66.

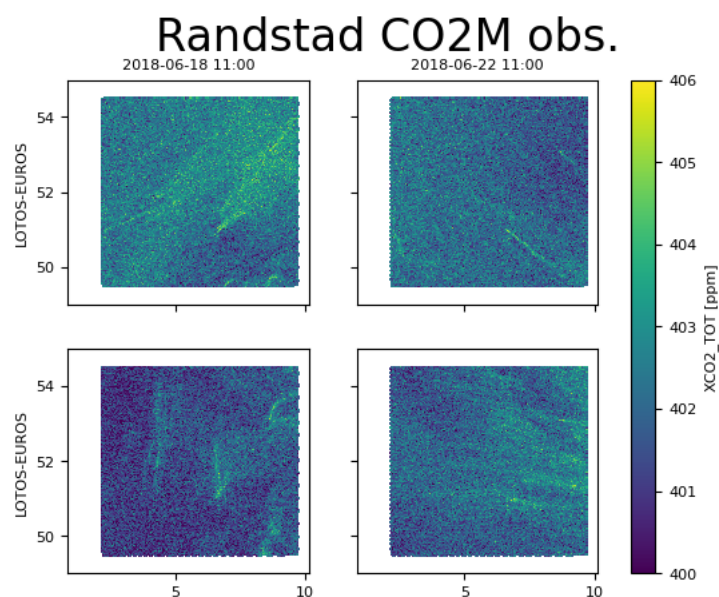


Figure 66. Synthetic CO₂M observation of the total CO₂ column around the Randstad area.

4.2.3.6 Conclusions for this case

In conclusion, we have seen the following: **to match in-situ data**, LOTOS-EUROS (at 2 km horizontal resolution) yields results that match well with the observations, but more so in the summer than in the winter. **To match NO₂ column observations**, there are generally too few good TROPOMI images available, but certainly similar trends are visible.

5 Conclusion

In this report, we have described the results of a model intercomparison for seven case studies of strong (conglomerates of) sources. In these case studies we have looked at the tracer trajectories generated by the various models (i.e., the combined effect of meteorology and tracer transport within the models), made comparisons against in-situ and remotely sensed data as well as TROPOMI images, analysed the downwind properties of the plume (e.g., the NO₂ or NO_x profile in the downstream direction, and the width of the plume), and demonstrated what a synthetic CO₂M image for these plumes would look like. Some concluding findings from the point source cases (Bełchatów, Jänschwalde, Lipetsk and Matimba) are:

- The best fit to in-situ data was obtained with the finest model, MicroHH with a 50 m horizontal resolution. The worst fit to in-situ data was obtained with the coarsest model, ICON-ART at 6 km horizontal resolution. This suggests that a plume-resolving model must be run at a resolution smaller than 6 km horizontally, to reproduce in-situ data.
- Considerable differences existed regarding the development of the atmospheric boundary layer (ABL), which could explain parts of the (mis)matches between simulations and observations. Hence, model resolution and numerically reproduced meteorology (rather than tracer transport modules) form the major component of inaccuracy between simulations and in-situ observations.
- The MicroHH plume was always considerably narrower and of higher amplitude than what the other models produced. Based on this study, one cannot say whether or not this is or is not realistic, though the MicroHH model was at times too narrow compared to in-situ data. However, the difference certainly had implications for the synthetic CO₂M images: plumes are considerably more visible on the synthetic CO₂M images computed from the MicroHH simulations than what results from the other models.
- Profiles of NO₂:CO₂ and NO_x:CO₂ in the direction downwind of plumes varied considerably between all three models submitting these gases, i.e., LOTOS-EUROS, MicroHH (both using a chemistry scheme) and COSMO-GHG (using a decaying NO_x tracer which was post-processed to NO₂ afterwards). A more robust study is probably required regarding this topic.
- Subsampled to CO₂M pixels, the MicroHH results show narrower and larger plume enhancements (as noted above) but, otherwise, images produced from the other model outputs look rather similar. One exception is that the CO₂M image based on the ICON-ART simulation at 6 km resolution deviated from the other results considerably, while the 2 km resolution looked rather similar to the other results. This suggests that a plume-resolving model must be run at a resolution smaller than 6 km, perhaps down to 2 km, to reproduce CO₂M images.

The models applied to the city cases (Berlin, Paris, and Randstad areas) all showed a relatively good fit with in-situ data. There are relatively little conclusions that can be drawn from these cases otherwise.

The synthetic CO₂M images have been collected into one large “library of plumes” which will be used within CoCO₂ WP4.2, and can be used by other researchers who want to test plume detection algorithms on this unique dataset.

6 Recommendations

The work carried out here was related to the open question: “how well can atmospheric transport models simulate individual plumes?” Based on the seven case studies considered here, the answer is “quite well”. With high-resolution models (e.g., the MicroHH LES model with 50 m horizontal resolution), very strong power plant plumes could be simulated excellently with respect to in-situ data, and with meso-scale models (e.g., COSMO-GHG at 1.1 km resolution) results are reasonable. Both scales of models generate reasonably similar synthetic CO₂M images, implying that for reasonable CO₂M images, a meso-scale model might be sufficient. However, if the resolution becomes too coarse (e.g., ICON-ART at 6 km horizontal resolution), the fit to in-situ observations decreases considerably and the synthetic CO₂M image ceases to be similar to what other models produce. Hence, for a local plume inversion system for CO₂M images, a resolution (considerably) smaller than 6 km must be used.

Two recommendations for future research are (amongst others):

- Online plume rise from the power plant stacks (rather than prescribing an emission profile) may allow for even more accurate simulations of strong power plant plumes. The buoyant released air takes some time to reach its final distribution in the atmosphere further downstream. An example of this phenomenon is shown in the figure below.

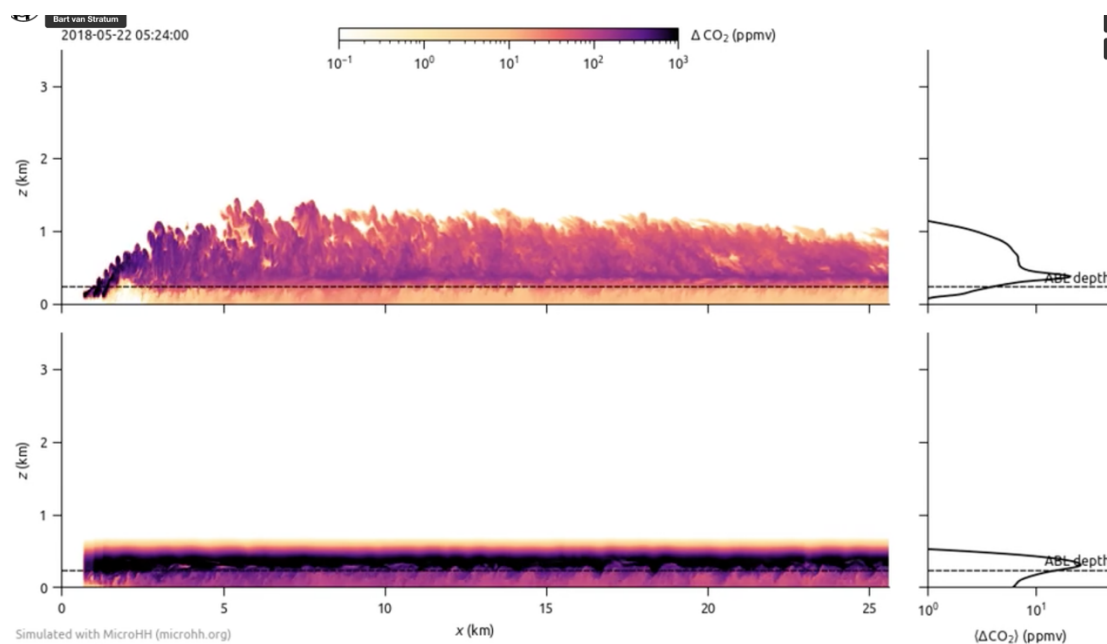


Figure 67. Example of online plume rise (top) versus a fixed emission profile (bottom) for a simplified 1D model around Jänschwalde, produced in MicroHH. The average vertically simulated profiles (right panels) differ considerably as a result.

- All three chemistry models (LOTOS-EUROS and MicroHH which use a chemistry module, and COSMO-GHG which uses a decaying NO_x tracer post-processed to NO₂) lead to quite different downstream NO₂ profiles. A closer look is required to disentangle (1) the effects of meteorology simply leading to a different plume shape and transport speeds, (2) model resolution affecting the chemistry effects on the edges of the plume [i.e., a LES model simulates more individual eddies which can undergo reactions on their edges, while a coarse NWP model simulates the same turbulence as merely a diffusive flow, which leads to less edges that can undergo reactions], (3) study the downstream NO₂ and NO_x profiles for more instances than done here (ideally with a high temporal sampling to remove an element of randomness), and to see whether or

not the decay processes are constant over the downwind direction of a plume or whether they change in a predictable way, (4) study when NO₂ signals are elevated over the background noise in synthetic CO₂M pixels [i.e., if the NO₂ signal can only be picked up a few pixels behind a source location, this affects plume detection methods like those described in Kuhlmann et al. (2021)].

7 References

- Ahmadov, R., Gerbig, C., Kretschmer, R., Koerner, S., Neininger, B., Dolman, A. J., & Sarrat, C. (2007). Mesoscale covariance of transport and CO₂ fluxes: Evidence from observations and simulations using the WRF-VPRM coupled atmosphere-biosphere model. *Journal of Geophysical Research: Atmospheres*, 112(D22). <https://doi.org/10.1029/2007JD008552>
- Balsamo, G., Beljaars, A., Scipal, K., Viterbo, P., Hurk, B. van den, Hirschi, M., & Betts, A. K. (2009). A Revised Hydrology for the ECMWF Model: Verification from Field Site to Terrestrial Water Storage and Impact in the Integrated Forecast System. *Journal of Hydrometeorology*, 10(3), 623–643. <https://doi.org/10.1175/2008JHM1068.1>
- Damian, V., Sandu, A., Damian, M., Potra, F., & Carmichael, G. R. (2002). The kinetic preprocessor KPP—a software environment for solving chemical kinetics. *Computers & Chemical Engineering*, 26(11), 1567–1579. [https://doi.org/10.1016/S0098-1354\(02\)00128-X](https://doi.org/10.1016/S0098-1354(02)00128-X)
- Denier van der Gon, H. & CoCO₂ WP2 team. (2021). *Prior Emission data 2018 documentation report* (D2.1; p. 22). CoCO₂. <https://confluence.ecmwf.int/download/attachments/208484410/CoCO2-D2.1-V1-0.pdf?version=1&modificationDate=1646232849545&api=v2>
- Düring, I., Bächlin, W., Ketzler, M., Baum, A., Friedrich, U., & Wurzler, S. (2011). A new simplified NO/NO₂ conversion model under consideration of direct NO₂-emissions. *Meteorologische Zeitschrift*, 67–73. <https://doi.org/10.1127/0941-2948/2011/0491>
- ECMWF. (n.d.). *L137 model level definitions*. Retrieved 28 November 2022, from <https://confluence.ecmwf.int/display/UDOC/L137+model+level+definitions>
- EEA, & JRC. (n.d.). *CLC 2018—Copernicus Land Monitoring Service* [Land item]. Retrieved 27 November 2022, from <https://land.copernicus.eu/pan-european/corine-land-cover/clc2018>
- EMPA. (n.d.). *Ddeq Gitlab repository*. GitLab. Retrieved 27 November 2022, from <https://gitlab.com/empa503/remote-sensing/ddeq>
- European Air Quality Portal. (n.d.). *Download of air quality data*. Retrieved 1 December 2022, from <https://discomap.eea.europa.eu/map/fme/AirQualityExport.htm>
- Fiehn, A., Kostinek, J., Eckl, M., Klausner, T., Gałkowski, M., Chen, J., Gerbig, C., Röckmann, T., Maazallahi, H., Schmidt, M., Korbeń, P., Necki, J., Jagoda, P., Wildmann, N., Mallaun, C., Bun, R., Nickl, A.-L., Jöckel, P., Fix, A., & Roiger, A. (2020). Estimating CH₄, CO₂ and CO emissions from coal mining and industrial activities in the Upper Silesian Coal Basin using an aircraft-based mass balance approach. *Atmospheric Chemistry and Physics*, 20(21), 12675–12695. <https://doi.org/10.5194/acp-20-12675-2020>
- Fiehn, A., Kostinek, Julian, Eckl, Maximillian, Klausner, T., Gałkowski, M., Chen, J., Gerbig, C., Röckmann, T., Maazallahi, H., Schmidt, M., Korbeń, P., Necki, Jarosław, Jagoda, P., Wildmann, N., Mallaun, C., Bun, R., Nickl, A.-L., Jöckel, P., Fix, A., & Rolger, A.

- (2020). *Data supplement to: Fiehn et al (2020): Estimating CH₄, CO₂, and CO emissions from coal mining and industrial activities in the Upper Silesian Coal Basin using an aircraft-based mass balance approach* (1.00, p. 7277067 bytes) [ZIP archive with ASCII CSV files]. ICOS ERIC - Carbon Portal. <https://doi.org/10.18160/0SFH-JJ93>
- Frumau, A., Hensen, A., & Vermeulen, A. (2022). *Atmospheric CO₂ product, Cabauw (207.0 m)*, 1992-10-23–2020-12-31. https://hdl.handle.net/11676/AkEZ2YpMsfej_GM8gDBx5G1p
- Gerbig, C. (2021). *Parameters for the Vegetation Photosynthesis and Respiration Model VPRM (1.1)* [Ascii text file]. ICOS-ERIC - Carbon Portal. <https://doi.org/10.18160/R9X0-BW7T>
- Hakkarainen, J., Szelaĝ, M. E., Ialongo, I., Retscher, C., Oda, T., & Crisp, D. (2021). Analyzing nitrogen oxides to carbon dioxide emission ratios from space: A case study of Matimba Power Station in South Africa. *Atmospheric Environment: X*, 10, 100110. <https://doi.org/10.1016/j.aeaoa.2021.100110>
- Hoyer, S., & Hamman, J. (2017). xarray: N-D labeled Arrays and Datasets in Python. *Journal of Open Research Software*, 5(1), Article 1. <https://doi.org/10.5334/jors.148>
- Huijnen, V., Flemming, J., Chabrillat, S., Errera, Q., Christophe, Y., Blechschmidt, A.-M., Richter, A., & Eskes, H. (2016). C-IFS-CB05-BASCOE: Stratospheric chemistry in the Integrated Forecasting System of ECMWF. *Geoscientific Model Development*, 9(9), 3071–3091. <https://doi.org/10.5194/gmd-9-3071-2016>
- Jähn, M., Kuhlmann, G., Mu, Q., Haussaire, J.-M., Ochsner, D., Osterried, K., Clément, V., & Brunner, D. (2020). An online emission module for atmospheric chemistry transport models: Implementation in COSMO-GHG v5.6a and COSMO-ART v5.1-3.1. *Geoscientific Model Development*, 13(5), 2379–2392. <https://doi.org/10.5194/gmd-13-2379-2020>
- Jung, M., Henkel, K., Herold, M., & Churkina, G. (2006). Exploiting synergies of global land cover products for carbon cycle modeling. *Remote Sensing of Environment*, 101(4), 534–553. <https://doi.org/10.1016/j.rse.2006.01.020>
- Klausner, T., Mertens, M., Huntrieser, H., Galkowski, M., Kuhlmann, G., Baumann, R., Fiehn, A., Jöckel, P., Pühl, M., & Roiger, A. (2020). Urban greenhouse gas emissions from the Berlin area: A case study using airborne CO₂ and CH₄ in situ observations in summer 2018. *Elementa: Science of the Anthropocene*, 8, 15. <https://doi.org/10.1525/elementa.411>
- Klausner, T., Roiger, A., Fiehn, A., Giez, A., Dreiling, V., Zöger, M., & Mallaun, C. (2020). *Aircraft measurement data obtained within the framework of the 3DO measurement campaign in summer 2018 over Berlin* [Data set]. Zenodo. <https://doi.org/10.5281/zenodo.3706726>
- Koene, E., & Brunner, D. (2022). *CoCO₂ WP4.1 Library of Plumes*. <https://doi.org/10.5281/zenodo.7448144>
- Kranenburg, R., Segers, A. J., Hendriks, C., & Schaap, M. (2013). Source apportionment using LOTOS-EUROS: Module description and evaluation. *Geoscientific Model Development*, 6(3), 721–733. <https://doi.org/10.5194/gmd-6-721-2013>
- Krautwurst, S., Gerilowski, K., Borchardt, J., Wildmann, N., Gałkowski, M., Swolkień, J., Marshall, J., Fiehn, A., Roiger, A., Ruhtz, T., Gerbig, C., Necki, J., Burrows, J. P., Fix, A., & Bovensmann, H. (2021). Quantification of CH₄ coal mining emissions in Upper Silesia by passive airborne remote sensing observations with the Methane Airborne MAPper (MAMAP) instrument during the CO₂ and Methane (CoMet) campaign.

- Atmospheric Chemistry and Physics*, 21(23), 17345–17371.
<https://doi.org/10.5194/acp-21-17345-2021>
- Krol, M., & van Stratum, B. (2021). *Definition of simulation cases and model system for building a library of plumes* (D4.1; p. 20). CoCO₂. <https://www.coco2-project.eu/node/293>
- Kuhlmann, G., Broquet, G., Marshall, J., Clément, V., Löscher, A., Meijer, Y., & Brunner, D. (2019). Detectability of CO₂ emission plumes of cities and power plants with the Copernicus Anthropogenic CO₂ Monitoring (CO₂M) mission. *Atmospheric Measurement Techniques*, 12(12), 6695–6719. <https://doi.org/10.5194/amt-12-6695-2019>
- Kuhlmann, G., Brunner, D., Broquet, G., & Meijer, Y. (2020). Quantifying CO₂ emissions of a city with the Copernicus Anthropogenic CO₂ Monitoring satellite mission. *Atmospheric Measurement Techniques*, 13(12), 6733–6754. <https://doi.org/10.5194/amt-13-6733-2020>
- Kuhlmann, G., Henne, S., Meijer, Y., & Brunner, D. (2021). Quantifying CO₂ Emissions of Power Plants With CO₂ and NO₂ Imaging Satellites. *Frontiers in Remote Sensing*, 2. <https://www.frontiersin.org/articles/10.3389/frsen.2021.689838>
- Lauritzen, P. H., Ullrich, P. A., Jablonowski, C., Bosler, P. A., Calhoun, D., Conley, A. J., Enomoto, T., Dong, L., Dubey, S., Guba, O., Hansen, A. B., Kaas, E., Kent, J., Lamarque, J.-F., Prather, M. J., Reinert, D., Shashkin, V. V., Skamarock, W. C., Sørensen, B., ... Tolstykh, M. A. (2014). A standard test case suite for two-dimensional linear transport on the sphere: Results from a collection of state-of-the-art schemes. *Geoscientific Model Development*, 7(1), 105–145. <https://doi.org/10.5194/gmd-7-105-2014>
- Lian, J., Bréon, F.-M., Broquet, G., Zaccheo, T. S., Dobler, J., Ramonet, M., Staufer, J., Santaren, D., Xueref-Remy, I., & Ciais, P. (2019). Analysis of temporal and spatial variability of atmospheric CO₂ concentration within Paris from the GreenLITE™ laser imaging experiment. *Atmospheric Chemistry and Physics*, 19(22), 13809–13825. <https://doi.org/10.5194/acp-19-13809-2019>
- Lian, J., Lauvaux, T., Utard, H., Bréon, F.-M., Broquet, G., Ramonet, M., Laurent, O., Albarus, I., Cucchi, K., & Ciais, P. (2022). Assessing the Effectiveness of an Urban CO₂ Monitoring Network over the Paris Region through the COVID-19 Lockdown Natural Experiment. *Environmental Science & Technology*, 56(4), 2153–2162. <https://doi.org/10.1021/acs.est.1c04973>
- Madronich, S., & Flocke, S. (1999). The Role of Solar Radiation in Atmospheric Chemistry. In P. Boule (Ed.), *Environmental Photochemistry* (pp. 1–26). Springer. https://doi.org/10.1007/978-3-540-69044-3_1
- Mahadevan, P., Wofsy, S. C., Matross, D. M., Xiao, X., Dunn, A. L., Lin, J. C., Gerbig, C., Munger, J. W., Chow, V. Y., & Gottlieb, E. W. (2008). A satellite-based biosphere parameterization for net ecosystem CO₂ exchange: Vegetation Photosynthesis and Respiration Model (VPRM). *Global Biogeochemical Cycles*, 22(2). <https://doi.org/10.1029/2006GB002735>
- Manders, A. M. M., Bultjes, P. J. H., Curier, L., Denier van der Gon, H. A. C., Hendriks, C., Jonkers, S., Kranenburg, R., Kuenen, J. J. P., Segers, A. J., Timmermans, R. M. A., Visschedijk, A. J. H., Wichink Kruit, R. J., van Pul, W. A. J., Sauter, F. J., van der Swaluw, E., Swart, D. P. J., Douros, J., Eskes, H., van Meijgaard, E., ... Schaap, M. (2017). Curriculum vitae of the LOTOS–EUROS (v2.0) chemistry transport model.

- Geoscientific Model Development*, 10(11), 4145–4173. <https://doi.org/10.5194/gmd-10-4145-2017>
- Miura, H. (2007). An Upwind-Biased Conservative Advection Scheme for Spherical Hexagonal–Pentagonal Grids. *Monthly Weather Review*, 135(12), 4038–4044. <https://doi.org/10.1175/2007MWR2101.1>
- National Centers For Environmental Prediction/National Weather Service/NOAA/U.S. Department Of Commerce. (2004). *NCEP ADP Global Surface Observational Weather Data, October 1999—Continuing* (p. 124.584 Gbytes) [WMO BUFR,LITTLE R]. UCAR/NCAR - Research Data Archive. <https://doi.org/10.5065/4F4P-E398>
- Neggers, R. a. J., Siebesma, A. P., & Heus, T. (2012). Continuous Single-Column Model Evaluation at a Permanent Meteorological Supersite. *Bulletin of the American Meteorological Society*, 93(9), 1389–1400. <https://doi.org/10.1175/BAMS-D-11-00162.1>
- Pincus, R., Mlawer, E. J., & Delamere, J. S. (2019). Balancing Accuracy, Efficiency, and Flexibility in Radiation Calculations for Dynamical Models. *Journal of Advances in Modeling Earth Systems*, 11(10), 3074–3089. <https://doi.org/10.1029/2019MS001621>
- Q. Errera, M. Ramonet, N. Sudarchikova, M. Schulz, H.J. Eskes, S. Basart, A. Benedictow, Y. Bennouna, A.-M. Blechschmidt, S. Chabrillat, Y. Christophe, E. Cuevas, A. El-Yazidi, H. Flentje, P. Fritzsche, K.M. Hansen, U. Im, J. Kapsomenakis, B. Langerock, ... C. Zerefos. (2021). *Validation report of the CAMS near-real-time global atmospheric composition service: Period March – May 2021* [EQC Report]. Copernicus Atmosphere Monitoring Service. <https://atmosphere.copernicus.eu/node/714>
- Sandu, A., Sander, R., Long, M. S., Yantosca, R. M., Lin, H., Shen, L., & Jacob, D. J. (2022). *KineticPreProcessor/KPP: The Kinetic PreProcessor (KPP) 3.0.0*. Zenodo. <https://doi.org/10.5281/zenodo.7308373>
- Satellite Services Division/Office Of Satellite Data Processing And Distribution/NESDIS/NOAA/U.S. Department Of Commerce, & National Centers For Environmental Prediction/National Weather Service/NOAA/U.S. Department Of Commerce. (2004). *NCEP ADP Global Upper Air Observational Weather Data, October 1999—Continuing* (p. 529.245 Gbytes) [WMO BUFR,LITTLE R]. UCAR/NCAR - Research Data Archive. <https://doi.org/10.5065/39C5-Z211>
- Scherer, D., Antretter, F., Bender, S., Cortekar, J., Emeis, S., Fehrenbach, U., Gross, G., Halbig, G., Hasse, J., Maronga, B., Raasch, S., & Scherber, K. (2019). Urban Climate Under Change [UC]2 – A National Research Programme for Developing a Building-Resolving Atmospheric Model for Entire City Regions. *Meteorologische Zeitschrift*, 95–104. <https://doi.org/10.1127/metz/2019/0913>
- Schröter, J., Rieger, D., Stassen, C., Vogel, H., Weimer, M., Werchner, S., Förstner, J., Prill, F., Reinert, D., Zängl, G., Giorgetta, M., Ruhnke, R., Vogel, B., & Braesicke, P. (2018). ICON-ART 2.1: A flexible tracer framework and its application for composition studies in numerical weather forecasting and climate simulations. *Geoscientific Model Development*, 11(10), 4043–4068. <https://doi.org/10.5194/gmd-11-4043-2018>
- Schulzweida, U. (2022). *CDO User Guide*. <https://doi.org/10.5281/zenodo.7112925>
- Stockie, J. M. (2011). The Mathematics of Atmospheric Dispersion Modeling. *SIAM Review*, 53(2), 349–372. <https://doi.org/10.1137/10080991X>
- Sweeney, C., Karion, A., Wolter, S., Newberger, T., Guenther, D., Higgs, J. A., Andrews, A. E., Lang, P. M., Neff, D., Dlugokencky, E., Miller, J. B., Montzka, S. A., Miller, B. R., Masarie, K. A., Biraud, S. C., Novelli, P. C., Crotwell, M., Crotwell, A. M., Thoning, K., & Tans, P. P. (2015). Seasonal climatology of CO₂ across North America from aircraft

- measurements in the NOAA/ESRL Global Greenhouse Gas Reference Network. *Journal of Geophysical Research: Atmospheres*, 120(10), 5155–5190. <https://doi.org/10.1002/2014JD022591>
- van Heerwaarden, C. C., van Stratum, B. J. H., Heus, T., Gibbs, J. A., Fedorovich, E., & Mellado, J. P. (2017). MicroHH 1.0: A computational fluid dynamics code for direct numerical simulation and large-eddy simulation of atmospheric boundary layer flows. *Geoscientific Model Development*, 10(8), 3145–3165. <https://doi.org/10.5194/gmd-10-3145-2017>
- Virtanen, P., Gommers, R., Oliphant, T. E., Haberland, M., Reddy, T., Cournapeau, D., Burovski, E., Peterson, P., Weckesser, W., Bright, J., van der Walt, S. J., Brett, M., Wilson, J., Millman, K. J., Mayorov, N., Nelson, A. R. J., Jones, E., Kern, R., Larson, E., ... van Mulbregt, P. (2020). SciPy 1.0: Fundamental algorithms for scientific computing in Python. *Nature Methods*, 17(3), Article 3. <https://doi.org/10.1038/s41592-019-0686-2>
- Wolff, S., Ehret, G., Kiemle, C., Amediek, A., Quatrevalet, M., Wirth, M., & Fix, A. (2021). Determination of the emission rates of CO₂ point sources with airborne lidar. *Atmospheric Measurement Techniques*, 14(4), 2717–2736. <https://doi.org/10.5194/amt-14-2717-2021>
- Zängl. (2013, September). *ICON: The Icosahedral Nonhydrostatic Modelling framework of DWD and MPI-M*. Seminar on Recent Developments in Numerical Methods for Atmosphere and Ocean Modelling. <https://www.ecmwf.int/en/elibrary/76999-icosahedral-nonhydrostatic-modelling-framework-dwd-and-mpi-m>
- Zängl, G., Reinert, D., Rípodas, P., & Baldauf, M. (2015). The ICON (ICOsahedral Non-hydrostatic) modelling framework of DWD and MPI-M: Description of the non-hydrostatic dynamical core. *Quarterly Journal of the Royal Meteorological Society*, 141(687), 563–579. <https://doi.org/10.1002/qj.2378>

Document History

| Version | Author(s) | Date | Changes |
|---------|---|------------|--|
| 0.1 | Erik Koene (EMPA) | 01/12/2022 | |
| 0.2 | Erik Koene (EMPA) and all collaborating authors | 16/12/2022 | Made modifications based on input from partners within the project |
| 0.3 | Erik Koene (EMPA) | 18/01/2023 | Modifications based on input from Janne Hakkarainen |
| | | | |
| | | | |

Internal Review History

| Internal Reviewers | Date | Comments |
|-------------------------|------------|-------------------------------|
| Janne Hakkarainen (FMI) | 10/01/2023 | Some technical/minor comments |
| | | |
| | | |
| | | |
| | | |

Estimated Effort Contribution per Partner

| Partner | Effort |
|--------------|------------------------|
| Organisation | effort in person month |
| | |
| | |
| | |
| Total | |

This publication reflects the views only of the author, and the Commission cannot be held responsible for any use which may be made of the information contained therein.

8 Modelling protocols

Protocol for CoCO₂ Power Plant Plume Simulations

Author: Dominik Brunner, Erik Koene

Version: v1.0, 28 February 2021

Table of Contents

| | |
|--|---|
| Protocol for CoCO ₂ Power Plant Plume Simulations | 1 |
| 1. Simulations | 2 |
| 2. Input Data | 3 |
| 2.1. Meteorology | 3 |
| 2.2 Emissions | 3 |
| 2.3 Background fields | 4 |
| 2.4 Other anthropogenic emissions in the modelling domain | 5 |
| 2.5 Photosynthesis and biospheric fluxes | 5 |
| 2.6 Possible outputs | 5 |
| 3. Output | 6 |
| 4. Observations | 7 |
| 5. Logistics | 7 |

1. Simulations

Since the protocol should be applicable to a wide range of models with different resolutions and associated computational costs, the protocol defines a set of minimal requirements plus a set of options.

Table 1 describes the minimum domain and time period that has to be covered by the simulations. The main day of interest is **07 June** (changes w.r.t. the Jaenschwalde protocol are highlighted in yellow, i.e., the rest has stayed the same!), when the plume was observed from multiple aircraft around noon. The simulation's time period thus includes 1 day of spin-up, but modellers may choose a longer spin-up period if required to obtain robust results not affected by the initialization.

Table 1. Simulations

| ID | Power plant | Domain | | Time period (time in UTC, dates in 2018) |
|-----|-------------|-------------|---------------|---|
| | | lon range | lat range | |
| BEL | Belchatow | 18.7–19.9°E | 50.95–51.55°N | 06/06 00:00 – 08/06 00:00 |

The model domain can be larger than the minimum domain specified in Table 1. Simulations should be performed at a typical resolution of the model and on the model's specific projection. Output needs to be generated on, or projected to, a regular latitude-longitude grid (see section 3).

Each simulation needs to include at least three CO₂ tracers representing three different release altitudes and optionally tracers for CO, NO₂ and NO (or NO_x, for models that do not consider a non-linear chemistry) for the reference release altitude:

Table 2. Power plant emission tracers included in each simulation

| High release case | Middle release case (reference) | Low release case (at the surface) | Mandatory |
|-------------------|------------------------------------|--------------------------------------|-----------|
| CO2_PP_H | CO2_PP_M | CO2_PP_L | Yes |
| | CO_PP_M | | No |
| | NO2_PP_M | | No |
| | NO_PP_M (Or NOX_PP_M) | | No |

Additional optional tracers for CO₂, CO and NO and NO₂ (or NO_x, for models without non-linear chemistry) representing background concentrations and other fluxes within the model domain are denoted as follows:

Table 3. Optional tracers relating to background fields, anthropogenic emissions and biospheric fluxes

| Background fields transported from outside the domain ¹ | Other anthropogenic emissions in the modelling domain (except those from Belchatow) ² | Biospheric fluxes (photosynthesis and respiration) ³ | Total anthropogenic emissions (background fields + other anthropogenic emissions + Belchatow emissions) |
|--|--|---|---|
| CO2_BG | CO2_ANTH | CO2_BIO | CO2_TOT_ANTH |
| CO_BG | CO_ANTH | | CO_TOT_ANTH |
| NO2_BG | NO2_ANTH | | NO2_TOT_ANTH |
| NO_BG NOX_BG | NO_ANTH NOX_ANTH | | NO_TOT_ANTH NOX_TOT_ANTH |

¹ See section 2.3

² See section 2.4

³ See section 2.5

These tracers are optional but recommended to produce realistic concentration fields in the surroundings of the power plant.

Simulations with full chemistry should only provide CO_TOT_ANTH, NO2_TOT_ANTH and NO_TOT_ANTH, rather than the individual components in the other columns of the table. Models with no or idealized chemistry (e.g. constant NO_x lifetime) should provide the individual components. For CO₂, the three tracers CO2_BG, CO2_ANTH and CO2_BIO should be provided separately whenever possible.

High-resolution models may include additional tracers representing emissions from individual stacks (see section 2.2).

2. Input Data

2.1. Meteorology

The changing meteorological conditions during the simulation period should be captured as accurately as possible. Models should, therefore, be driven or constrained by meteorological (re-)analysis fields from ECMWF, either from the operational stream or from ERA5.

Online models should use ECMWF meteorological fields as initial and boundary conditions. In case of multiple nested domains, ECMWF fields should constrain the outermost domain. It is also recommended to turn on standard meteorological data assimilation/nudging, in order to keep the simulated meteorology as close to observed meteorology as possible.

2.2 Emissions

The power plant **Belchatow** releases emissions from **two stacks**.

All models need to include the tracers representing the total emissions from the power plant as a single source (denoted as "single" in Table 4). These tracers should be named according to Table 2. Models with resolutions better than 300 m may include additional tracers released from the individual stacks to test the sensitivity of the results to this choice. These additional tracers should be simulated for the middle (reference) release height and should be called CO2_PP_M_E and CO2_PP_M_W, respectively. The same naming convention can be used for the optional other tracers.

Table 4. Source locations and strengths

| Power plant | Stack/tower | Coordinate longitude, latitude | Emission rate [kg CO ₂ /s] | [kg CO/s] | [kg NO ₂ /s] | [kg NO/s] | NO _x tracer [NO ₂ mass equivalent/s] |
|------------------|---------------|-----------------------------------|--|--------------|-------------------------|--------------|--|
| Belchatow | Single | 19.3261°E, 51.2660°N | 1217.7 | 0.789 | 0.0458 | 0.567 | 0.916 |
| Belchatow | East | 19.3285°E, 51.2660°N | 608.8 | 0.395 | 0.0229 | 0.284 | 0.458 |
| Belchatow | West | 19.3237°E, 51.2660°N | 608.8 | 0.395 | 0.0229 | 0.284 | 0.458 |

The locations and the suggested emission strengths are listed in Table 4. Note that the coordinates provided in E-PRTR are not the exact coordinates of the emissions but rather of the postal address of the plant. The source strengths correspond to the latest values reported to Dominik Brunner for the year 2018, and the **finalized TNO emission dataset for 2018 from CoCO2 WP2**.

For models that do not consider any (non-linear) chemistry, it is fine to submit NO_x tracers rather than the separate NO₂ and NO components. To convert between NO₂, NO, and NO_x we use the relation

$\text{NO} = 0.95 \cdot \text{NO}_x \cdot (30/46)$ and $\text{NO}_2 = 0.05 \cdot \text{NO}_x$, where 30 and 46 are the molar masses of NO and NO₂ respectively, and NO_x is given in NO₂ mass equivalent units (as, e.g., in the TNO dataset). Again, the CO/NO/NO₂/NO_x tracers are not mandatory.

Vertical emission profiles

Emissions from the power plants undergo plume rise due to the momentum and buoyancy of the flue gas. Plume rise depends on stack and effluent parameters as well as on meteorological conditions (wind speed, stability).

Plume rise and the vertical extent of the plumes were calculated using the empirical equations recommended by the Association of German Engineers (VDI – Fachbereich Umweltmeteorologie, 1985), which are based on the original work of Briggs (1984). Typical stack parameters were obtained from Pregger et al. (2009), considering typical power plant capacities and fuel types, and from site descriptions (Table 5).

Table 5. Stack parameters used in plume rise calculation.

| Site | Stack height (m) | Stack diameter (m) | Effluent temperature (K) | Volume flux (m ³ s ⁻¹) | Comment |
|------|------------------|--------------------|--------------------------|---|--|
| BEL | 299 | NA | 432 | 330 | direct emissions through stack from combustion process |

All models need to simulate tracers with fixed vertical emission profiles representing a high, middle and a low (i.e., surface) release case (tracers *_PP_H, *_PP_M and *_PP_L as described in section 1). The middle release case corresponds to the plume rise calculation for the approximate time of the aircraft measurement flights (07 June 2018 12:00 UTC for Belchatow), whereas the high case represents an upper limit of the plume rise calculation during the last 24 hour before the flights. The low release height corresponds to emissions at the surface.

The vertical profiles for the High, and Middle release cases are provided in the file:

plume_rise_BEL.csv

The columns in the file are

tracer, E0_50, E50_100, E100_150, E150_200, ... , E1450_1500

where EXXX-YYY is the fractional emission from the altitude layer between XXX m and YYY m above ground. The sum over all layers is 1. Altitudes are meters above ground.

Models which simulate additional tracers for individual stacks should use the middle vertical profile for these tracers.

Temporal emission profiles

For these simulations, we will not assume a temporal evolution, i.e., constant emissions over time.

2.3 Background fields

For the modelling of optional background tracers, corresponding to the fields transported from outside the model domain into the model, we *recommend* using the CAMS reanalysis dataset (at a horizontal resolution of 80 km), which is available both for greenhouse gases like CO₂ and for reactive gases (CO, NO_x). The CAMS global GHG reanalysis (EGG4) as well as the CAMS global atmospheric composition reanalysis (EAC4) can be obtained from the Copernicus Atmosphere Data

Store (ADS) on fixed pressure levels or on the model levels, and at 0.75°x0.75° horizontal and 3-hourly temporal resolution. For details see

<https://ads.atmosphere.copernicus.eu/cdsapp#!/dataset/cams-global-ghg-reanalysis-egg4>

<https://ads.atmosphere.copernicus.eu/cdsapp#!/dataset/cams-global-reanalysis-eac4>

2.4 Other anthropogenic emissions in the modelling domain

For the optional modelling of anthropogenic emissions in the modelling domain (except for the power plant itself, which is modelled with its separate tracer), we prescribe the high-resolution (1 km x 1 km) prior emissions dataset (PED) from TNO for the year 2018 (these were shared by Hugo Denier van der Gon by e-mail on 23 December 2021 with all WP2 and WP4 participants, including info regarding FTP access). The point source emissions for Belchatow must be set to 0 – this entry corresponds to line 841875 in the CSV file (if line '1' corresponds to the header line), or entry 841874 in the NetCDF file (if the first row of data is indexed with '1'). To convert the NO_x emissions to separate NO and NO₂ fields, use the conversion relation given on the previous page. These emissions will be released at the surface.

2.5 Photosynthesis and biospheric fluxes

For the optional modelling of biospheric fluxes in the modelling domain, each group should use its standard approach.

2.6 Possible outputs

To summarize, table 6 lists all possible tracers that may be computed.

Table 6. List of all possible tracers for which output may be computed. NO_x fields can be supplied in place of separate NO₂ and NO tracers, if no (non-linear) chemistry is considered.

| | |
|--------------|--------------|
| CO2_PP_H | |
| CO2_PP_M | |
| CO2_PP_L | |
| CO_PP_M | |
| NO2_PP_M | NOX_PP_M |
| NO_PP_M | |
| CO2_BG | |
| CO_BG | |
| NO2_BG | NOX_BG |
| NO_BG | |
| CO2_ANTH | |
| CO_ANTH | |
| NO2_ANTH | NOX_ANTH |
| NO_ANTH | |
| CO2_BIO | |
| CO2_TOT_ANTH | |
| CO_TOT_ANTH | |
| NO2_TOT_ANTH | NOX_TOT_ANTH |
| NO_TOT_ANTH | |
| CO2_PP_M_E | |
| CO2_PP_M_W | |

| | |
|------------|------------|
| CO_PP_M_E | |
| CO_PP_M_W | |
| NO2_PP_M_E | NOX_PP_M_E |
| NO_PP_M_E | |
| NO2_PP_M_W | NOX_PP_M_W |
| NO_PP_M_W | |

3. Output

To facilitate the processing and inter-comparison of the simulations, please follow the following guidelines for the file content and formats as closely as possible. Only gridded output is requested. Interpolation to the measurements will be done centrally in a unified way. Output should be generated on the native vertical grid of the model but horizontally interpolated to a regular latitude-longitude grid (using the WGS84 geodetic reference). Output frequency should be at least hourly. Output every 15 minutes is recommended.

To account for the different resolutions and domain sizes, output should be provided for two different domains. The smaller inner domain fully encompasses the aircraft measurements and targets the near-field of the plumes. The larger outer domain extends about 100 km on all sides of the power plant.

Table 6. Output grids (all coordinates denote grid cell centers) and output frequency.

| Power plant | Domain | Longitude range | Latitude range | resolution dlon x dlat | Size nx x ny | Freq. hr |
|-------------|--------|-----------------|-----------------|---------------------------|-----------------|-------------------|
| Belchatow | SMALL | 18.7 – 19.9°E | 50.95 – 51.55°N | 0.003° x 0.002° | 401 x 301 | 0.25 ⁴ |
| Belchatow | LARGE | 17.8 – 20.8°E | 50.25 – 52.25°N | 0.015° x 0.01° | 201 x 201 | 1.00 |

We ask you to provide output in netCDF format with **one file per day** containing the following dimensions and variables:⁵

File name format: **BEL_[Domain]_[yyyymmdd]_[group]_[model].nc**

Where domain is either SMALL or LARGE. Group can be e.g. LSCE, model e.g. CHIMERE. Please use capital letters. In case of multiple simulations, please include the simulation version in the model name, e.g. CHIMERE-SIM1.

Dimensions:

- latitude: Number of grid points in zonal direction
- longitude: Number of grid points in meridional direction
- level: Number of full (cell center) vertical levels
- levelh: Number of half (cell edge) vertical levels
- time: Number of time steps

⁴ ARTM can only provide hourly output

⁵ See also the deliverable D4.1, section 5, and an example for the Jänschwalde output placed at <https://confluence.ecmwf.int/display/CoCO2/Overview+of+simulations+and+model+systems>

Variables:

| VARIABLE | DESCRIPTION | UNITS | DIMENSIONS | COMMENTS |
|----------------|---|-----------------------|-----------------------------------|--|
| time | Time | UTC | time | Hours since 06 June 2018 00:00 (UTC) |
| longitude | Zonal location | degrees | latitude, longitude | |
| latitude | Meridional location | degrees | latitude, longitude | |
| p | Air pressure at cell center | Pa | time, level, latitude, longitude | |
| z | Height above surface at cell center | m | time, level, latitude, longitude | Even for models that do not have a time-varying grid |
| ph | Air pressure at cell edge | Pa | time, levelh, latitude, longitude | |
| zh | Height above surface at cell edge | m | time, levelh, latitude, longitude | |
| ta | Air temperature | K | time, level, latitude, longitude | |
| hus | Specific humidity | kg kg ⁻¹ | time, level, latitude, longitude | |
| ua | Eastward wind | m s ⁻¹ | time, level, latitude, longitude | |
| va | Northward wind | m s ⁻¹ | time, level, latitude, longitude | |
| wa | Vertical wind | m s ⁻¹ | time, level, latitude, longitude | |
| ps | Surface pressure | Pa | time, latitude, longitude | |
| zsurf | Surface elevation | m | time, latitude, longitude | |
| CO2_PP_H | CO ₂ tracer mole fraction high release | mol mol ⁻¹ | time, level, latitude, longitude | |
| CO_PP_H | CO tracer mole fraction high release | mol mol ⁻¹ | time, level, latitude, longitude | |
| ...Etcetera... | | | | |

For hourly output, a daily file should contain output for 0 UTC, 1 UTC, ... , 23 UTC, where the time corresponds to the instantaneous model fields (or center of an averaging interval). Output at 15 minute resolution should be provided in an analogous way for 00 UTC, 00:15 UTC, 00:30 UTC etc.

The vertical model domain should at least cover altitudes up to 2400 m above sea level. The atmospheric boundary layer height was about 1800 m on 07 June 2018.

4. Observations

Aircraft measurements include in situ and remote sensing observations. In situ measurements include CO₂ and other trace gases as well as meteorological parameters. Remote sensing observations include CO₂ column anomalies from the MAMAP spectrometer and CO₂ column mixing ratios from the CHARM-F Lidar. In both cases, the measurements are representative for the CO₂ columns below the aircraft.

Interpolation to aircraft measurements for model evaluation will be done centrally by Empa.

5. Logistics

Input

Inputs are available from the CoCO2 ftp server

ftp [coco2@ftp.ecmwf.int](ftp://coco2@ftp.ecmwf.int)

in the following subdirectories:

/WP4/Plume_Simulations/**Belchatow**: Inputs specific for Jänschwalde case (including protocol)

The TNO data is available at

ftp [CoCO2@ftp0015.web-ftp81@web-ftp81.tno.nl](ftp://CoCO2@ftp0015.web-ftp81@web-ftp81.tno.nl)

/WP2/CoCO2_inventory_2018_v1_0: 1 km emission data set from TNO Europe

Output

Output should be uploaded to the [ICOS Fileshare](#).

Please submit your results by [31 March 2021](#).

Protocol for CoCO₂ Power Plant Plume Simulations

Author: Dominik Brunner, Erik Koene

Version: v4.0, 11 November 2021

Table of Contents

| | |
|--|---|
| Protocol for CoCO ₂ Power Plant Plume Simulations | 1 |
| 1. Simulations | 2 |
| 2. Input Data | 3 |
| 2.1. Meteorology | 3 |
| 2.2 Emissions | 3 |
| 2.3 Background fields | 4 |
| 2.4 Other anthropogenic emissions in the modelling domain | 5 |
| 2.5 Photosynthesis and biospheric fluxes | 5 |
| 2.6 Possible outputs | 5 |
| 3. Output | 6 |
| 4. Observations | 7 |
| 5. Logistics | 7 |

1. Simulations

Since the protocol should be applicable to a wide range of models with different resolutions and associated computational costs, the protocol defines a set of minimal requirements plus a set of options.

Table 1 describes the minimum domain and time period that has to be covered by the simulations. The main day of interest is 23 May, when the plume was observed from multiple aircraft around noon. The simulation's time period thus includes 1 day of spin-up, but modellers may choose a longer spin-up period if required to obtain robust results not affected by the initialization.

Table 1. Simulations

| ID | Power plant | Domain | | Time period (time in UTC, dates in 2018) |
|-----|-------------|-------------|---------------|---|
| | | lon range | lat range | |
| JAE | Jämschwalde | 13.8–15.0°E | 51.50–52.10°N | 22/05 00:00 – 24/05 00:00 |

The model domain can be larger than the minimum domain specified in Table 1. Simulations should be performed at a typical resolution of the model and on the model's specific projection. Output needs to be generated on, or projected to, a regular latitude-longitude grid (see section 3).

Each simulation needs to include at least three CO₂ tracers representing three different release altitudes and optionally tracers for CO, NO₂ and NO (or NO_x, for models that do not consider a non-linear chemistry) for the reference release altitude:

Table 2. Power plant emission tracers included in each simulation

| High release case | Middle release case (reference) | Low release case (at the surface) | Mandatory |
|-------------------|------------------------------------|--------------------------------------|-----------|
| CO2_PP_H | CO2_PP_M | CO2_PP_L | Yes |
| | CO_PP_M | | No |
| | NO2_PP_M | (Or NOX_PP_M) | No |
| | NO_PP_M | | No |

Additional optional tracers for CO₂, CO and NO and NO₂ (or NO_x, for models without non-linear chemistry) representing background concentrations and other fluxes within the model domain are denoted as follows:

Table 3. Optional tracers relating to background fields, anthropogenic emissions and biospheric fluxes

| Background fields transported from outside the domain ¹ | Other anthropogenic emissions in the modelling domain (except those from the powerplant) ² | Biospheric fluxes (photosynthesis and respiration) ³ | Total anthropogenic emissions (background fields + other anthropogenic emissions + power plant emissions) |
|--|---|---|---|
| CO2_BG | CO2_ANTH | CO2_BIO | CO2_TOT_ANTH |
| CO_BG | CO_ANTH | | CO_TOT_ANTH |
| NO2_BG | NO2_ANTH | | NO2_TOT_ANTH |
| NO_BG | NO_ANTH | | NO_TOT_ANTH |
| NOX_BG | NOX_ANTH | | NOX_TOT_ANTH |

These tracers are optional but recommended to produce realistic concentration fields in the surroundings of the power plant.

¹ See section 2.3

² See section 2.4

³ See section 2.5

Simulations with full chemistry should only provide CO_TOT_ANTH, NO2_TOT_ANTH and NO_TOT_ANTH, rather than the individual components in the other columns of the table. Models with no or idealized chemistry (e.g. constant NO_x lifetime) should provide the individual components. For CO₂, the three tracers CO2_BG, CO2_ANTH and CO2_BIO should be provided separately whenever possible.

High-resolution models may include additional tracers representing emissions from individual stacks (see section 2.2).

2. Input Data

2.1. Meteorology

The changing meteorological conditions during the simulation period should be captured as accurately as possible. Models should, therefore, be driven or constrained by meteorological (re-)analysis fields from ECMWF, either from the operational stream or from ERA5.

Online models should use ECMWF meteorological fields as initial and boundary conditions. In case of multiple nested domains, ECMWF fields should constrain the outermost domain. It is also recommended to turn on standard meteorological data assimilation/nudging, in order to keep the simulated meteorology as close to observed meteorology as possible.

2.2 Emissions

The power plant Jämschwalde does not have any emission stacks anymore but the flue gas is released directly through the cooling towers. In total, there are 9 cooling towers arranged in 3 groups (East, Centre, West). In each group, emissions are released from 2 of the 3 cooling towers. The distance between the groups is much larger (~300 m) than the distance between the towers (~110 m) in each group.

All models need to include the tracers representing the total emissions from the power plant as a single source (denoted as "single" in Table 4). These tracers should be named according to Table 2. Models with resolutions better than 300 m may include additional tracers released from the individual stacks to test the sensitivity of the results to this choice. These additional tracers should be simulated for the middle (reference) release height and should be called CO2_PP_M_E, CO2_PP_M_C, and CO2_PP_M_W, respectively. The same naming convention can be used for the optional other tracers.

Table 4. Source locations and strengths

| Power plant | Stack/tower | Coordinate longitude, latitude | Emission rate | | | | NO _x tracer [NO ₂ mass equivalent/s] |
|-------------|-------------|-----------------------------------|-------------------------|-----------|-------------------------|-----------|--|
| | | | [kg CO ₂ /s] | [kg CO/s] | [kg NO ₂ /s] | [kg NO/s] | |
| Jämschwalde | Single | 14.4580°E, 51.8361°N | 732.5 | 0.223 | 0.0289 | 0.359 | 0.579 |
| Jämschwalde | East | 14.4622°E, 51.8360°N | 244.2 | 0.0745 | 0.00965 | 0.120 | 0.193 |
| Jämschwalde | Centre | 14.4580°E, 51.8361°N | 244.2 | 0.0745 | 0.00965 | 0.120 | 0.193 |
| Jämschwalde | West | 14.4538°E, 51.8362°N | 244.2 | 0.0745 | 0.00965 | 0.120 | 0.193 |

The locations and the suggested emission strengths are listed in Table 4. Note that the coordinates provided in E-PRTR are not the exact coordinates of the emissions but rather of the postal address of the plant. The source strengths correspond to the latest values reported to Dominik Brunner for the year 2018, and the preliminary TNO emission dataset for 2018.

For models that do not consider any (non-linear) chemistry, it is fine to submit NO_x tracers rather than the separate NO₂ and NO components. To convert between NO₂, NO, and NO_x we use the relation $NO = 0.95 \cdot NO_x \cdot (30/46)$ and $NO_2 = 0.05 \cdot NO_x$, where 30 and 46 are the molar masses of NO and NO₂ respectively, and NO_x is given in NO₂ mass equivalent units (as, e.g., in the TNO dataset). Again, the CO/NO/NO₂/NO_x tracers are not mandatory.

Vertical emission profiles

Emissions from the power plants undergo plume rise due to the momentum and buoyancy of the flue gas. Plume rise depends on stack and effluent parameters as well as on meteorological conditions (wind speed, stability).

Plume rise and the vertical extent of the plumes were calculated using the empirical equations recommended by the Association of German Engineers (VDI – Fachbereich Umweltmeteorologie, 1985), which are based on the original work of Briggs (1984). Typical stack parameters were obtained from Pregger et al. (2009), considering typical power plant capacities and fuel types, and from site descriptions (Table 5).

Table 5. Stack parameters used in plume rise calculation.

| Site | Stack height (m) | Stack diameter (m) | Effluent temperature (K) | Volume flux (m ³ s ⁻¹) | Comment |
|------|------------------|--------------------|--------------------------|---|--|
| JAE | 120 | NA | 322 | 790 | emission of filtered flue gas through cooling towers |

All models need to simulate tracers with fixed vertical emission profiles representing a high, middle and a low (i.e., surface) release case (tracers *_PP_H, *_PP_M and *_PP_L as described in section 1). The middle release case corresponds to the plume rise calculation for the approximate time of the aircraft measurement flights (23 May 2018 09:00 UTC for Jänschwalde), whereas the high case represents an upper limit of the plume rise calculation during the last 24 hour before the flights. The low release height corresponds to emissions at the surface.

The vertical profiles for the High, and Middle release cases are provided in the file:

[plume_rise_JAE.csv](#)

The columns in the file are

[tracer](#), [E0_50](#), [E50_100](#), [E100_150](#), [E150_200](#), ..., [E1450_1500](#)

where EXXX-YYY is the fractional emission from the altitude layer between XXX m and YYY m above ground. The sum over all layers is 1. Altitudes are meters above ground.

Models which simulate additional tracers for individual stacks should use the middle vertical profile for these tracers.

Temporal emission profiles

For these simulations, we will not assume a temporal evolution, i.e., constant emissions over time.

2.3 Background fields

For the modelling of optional background tracers, corresponding to the fields transported from outside the model domain into the model, we *recommend* using the CAMS reanalysis dataset (at a horizontal resolution of 80 km), which is available both for greenhouse gases like CO₂ and for reactive gases (CO, NO_x). The CAMS global GHG reanalysis (EGG4) as well as the CAMS global

atmospheric composition reanalysis (EAC4) can be obtained from the Copernicus Atmosphere Data Store (ADS) on fixed pressure levels or on the model levels, and at 0.75°x0.75° horizontal and 3-hourly temporal resolution. For details see

<https://ads.atmosphere.copernicus.eu/cdsapp#!/dataset/cams-global-ghg-reanalysis-egg4>

<https://ads.atmosphere.copernicus.eu/cdsapp#!/dataset/cams-global-reanalysis-eac4>

2.4 Other anthropogenic emissions in the modelling domain

For the optional modelling of anthropogenic emissions in the modelling domain (except for the power plant itself, which is modelled with its separate tracer, we prescribe the high-resolution (1 km x 1 km) emissions dataset from TNO extrapolated for the year 2018 (see Section 5 for access to the data set). These are only preliminary data from TNO, and an updated dataset will become available in CoCO2 project WP2, later on. The point source emissions for Jämschwalde must be set to 0 – this entry corresponds to line 4895818 in the CSV file (if line '1' corresponds to the header line), or entry 4895817 in the NetCDF file (if the first data point is indexed with '1'). To convert the NO_x emissions to separate NO and NO₂ fields, use the conversion relation given on the previous page.

2.5 Photosynthesis and biospheric fluxes

For the optional modelling of biospheric fluxes in the modelling domain, each group should use its standard approach.

2.6 Possible outputs

To summarize, table 6 lists all possible tracers that may be computed.

Table 6. List of all possible tracers for which output may be computed. NO_x fields can be supplied in place of separate NO₂ and NO tracers, if no (non-linear) chemistry is considered.

| | |
|--------------|--------------|
| CO2_PP_H | |
| CO2_PP_M | |
| CO2_PP_L | |
| CO_PP_M | |
| NO2_PP_M | NOX_PP_M |
| NO_PP_M | |
| CO2_BG | |
| CO_BG | |
| NO2_BG | NOX_BG |
| NO_BG | |
| CO2_ANTH | |
| CO_ANTH | |
| NO2_ANTH | NOX_ANTH |
| NO_ANTH | |
| CO2_BIO | |
| CO2_TOT_ANTH | |
| CO_TOT_ANTH | |
| NO2_TOT_ANTH | NOX_TOT_ANTH |
| NO_TOT_ANTH | |
| CO2_PP_M_E | |

| | |
|------------|------------|
| CO2_PP_M_C | |
| CO2_PP_M_W | |
| CO_PP_M_E | |
| CO_PP_M_C | |
| CO_PP_M_W | |
| NO2_PP_M_E | NOX_PP_M_E |
| NO_PP_M_E | |
| NO2_PP_M_C | NOX_PP_M_C |
| NO_PP_M_C | |
| NO2_PP_M_W | NOX_PP_M_W |
| NO_PP_M_W | |

3. Output

To facilitate the processing and inter-comparison of the simulations, please follow the following guidelines for the file content and formats as closely as possible. Only gridded output is requested. Interpolation to the measurements will be done centrally in a unified way. Output should be generated on the native vertical grid of the model but horizontally interpolated to a regular latitude-longitude grid (using the WGS84 geodetic reference). Output frequency should be at least hourly. Output every 15 minutes is recommended.

To account for the different resolutions and domain sizes, output should be provided for two different domains. The smaller inner domain fully encompasses the aircraft measurements and targets the near-field of the plumes. The larger outer domain extends about 100 km on all sides of the power plant.

Table 6. Output grids (all coordinates denote grid cell centers) and output frequency.

| Power plant | Domain | Longitude range | Latitude range | resolution dlon x dlat | Size nx x ny | Freq. hr |
|-------------|--------|-----------------|-----------------|---------------------------|-----------------|-------------------|
| Jänschw. | SMALL | 13.8 – 15.0°E | 51.50 – 52.10°N | 0.003° x 0.002° | 401 x 301 | 0.25 ⁴ |
| Jänschw. | LARGE | 12.9 – 15.9°E | 50.80 – 52.80°N | 0.015° x 0.01° | 201 x 201 | 1.00 |

We ask you to provide output in netCDF format with **one file per day** containing the following dimensions and variables:⁵

File name format: **JAE_[Domain]_[yyyymmdd]_[group]_[model].nc**

Where domain is either SMALL or LARGE. Group can be e.g. LSCE, model e.g. CHIMERE. Please use capital letters. In case of multiple simulations, please include the simulation version in the model name, e.g. CHIMERE-SIM1.

Dimensions:

- latitude: Number of grid points in zonal direction
- longitude: Number of grid points in meridional direction
- level: Number of full (cell center) vertical levels
- levelh: Number of half (cell edge) vertical levels
- time: Number of time steps

⁴ ARTM can only provide hourly output

⁵ See also the deliverable D4.1, section 5, and an example for the Jänschwalde output placed at <https://confluence.ecmwf.int/display/CoCO2/Overview+of+simulations+and+model+systems>

Variables:

| VARIABLE | DESCRIPTION | UNITS | DIMENSIONS | COMMENTS |
|----------------|---|-----------------------|-----------------------------------|--|
| time | Time | UTC | time | Hours since 22 May 2018 00:00 (UTC) |
| longitude | Zonal location | degrees | latitude, longitude | |
| latitude | Meridional location | degrees | latitude, longitude | |
| p | Air pressure at cell center | Pa | time, level, latitude, longitude | |
| z | Height above surface at cell center | m | time, level, latitude, longitude | Even for models that do not have a time-varying grid |
| ph | Air pressure at cell edge | Pa | time, levelh, latitude, longitude | |
| zh | Height above surface at cell edge | m | time, levelh, latitude, longitude | |
| ta | Air temperature | K | time, level, latitude, longitude | |
| hus | Specific humidity | kg kg ⁻¹ | time, level, latitude, longitude | |
| ua | Eastward wind | m s ⁻¹ | time, level, latitude, longitude | |
| va | Northward wind | m s ⁻¹ | time, level, latitude, longitude | |
| wa | Vertical wind | m s ⁻¹ | time, level, latitude, longitude | |
| ps | Surface pressure | Pa | time, latitude, longitude | |
| zsurf | Surface elevation | m | time, latitude, longitude | |
| CO2_PP_H | CO ₂ tracer mole fraction high release | mol mol ⁻¹ | time, level, latitude, longitude | |
| CO_PP_H | CO tracer mole fraction high release | mol mol ⁻¹ | time, level, latitude, longitude | |
| ...Etcetera... | | | | |

For hourly output, a daily file should contain output for 0 UTC, 1 UTC, ... , 23 UTC, where the time corresponds to the instantaneous model fields (or center of an averaging interval). Output at 15 minute resolution should be provided in an analogous way for 00 UTC, 00:15 UTC, 00:30 UTC etc.

The vertical model domain should at least cover altitudes up to 2400 m above sea level. The atmospheric boundary layer height was about 1800 m on 23 May 2018.

4. Observations

Aircraft measurements include in situ and remote sensing observations. In situ measurements include CO₂ and other trace gases as well as meteorological parameters. Remote sensing observations include CO₂ column anomalies from the MAMAP spectrometer and CO₂ column mixing ratios from the CHARM-F Lidar. In both cases, the measurements are representative for the CO₂ columns below the aircraft.

Interpolation to aircraft measurements for model evaluation will be done centrally by Empa.

5. Logistics

Input

Inputs are available from the CoCO2 ftp server

ftp [coco2@ftp.ecmwf.int](ftp://coco2@ftp.ecmwf.int)

in the following subdirectories:

/WP4/Plume_Simulations/Jaenschwalde: Inputs specific for Janschwalde case (including protocol)

/WP4/TNO_Emissions: 1 km emission data set from TNO covering parts of Europe

Output

Output should be uploaded to [tbd].

Please submit your results by 17 December 2021.

Protocol for CoCO₂ Power Plant Plume Simulations

Author: Maarten Krol (based on Dominik Brunner, Erik Koene)

Version: v1.0, 28 March 2022

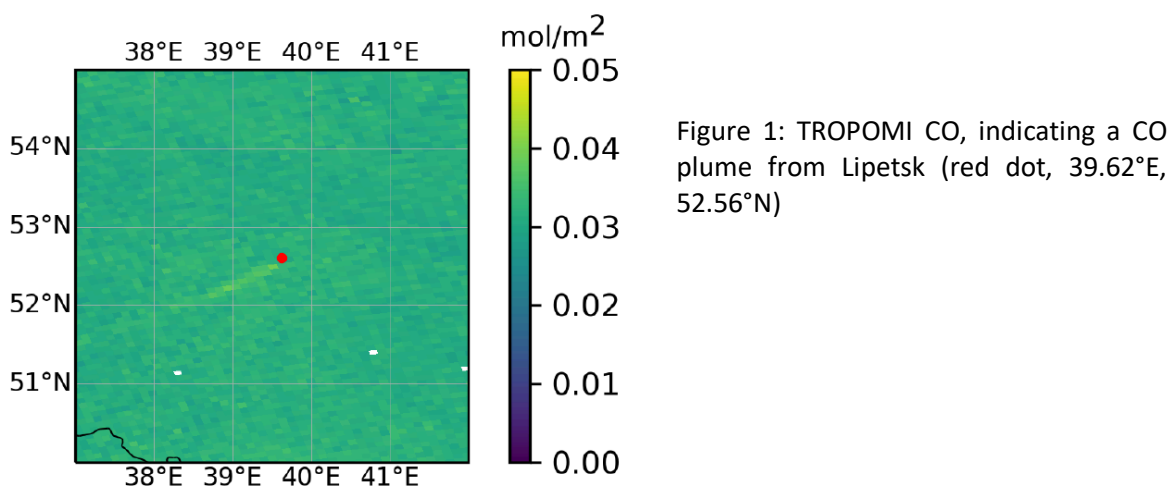
Table of Contents

| | |
|--|---|
| Protocol for CoCO ₂ Power Plant Plume Simulations | 1 |
| 1. Simulations | 2 |
| 2. Input Data | 3 |
| 2.1. Meteorology | 3 |
| 2.2 Emissions | 3 |
| 2.3 Background fields | 5 |
| 2.4 Other anthropogenic emissions in the modelling domain | 5 |
| 2.5 Photosynthesis and biospheric fluxes | 5 |
| 2.6 Possible outputs | 6 |
| 3. Output | 6 |
| 4. Observations | 8 |
| 5. Logistics | 8 |

1. Simulations

Since the protocol should be applicable to a wide range of models with different resolutions and associated computational costs, the protocol defines a set of minimal requirements plus a set of options.

Table 1 describes the minimum domain and time period that has to be covered by the simulations. The main day of interest is **13 June 2019**, a day on which clear CO and NO₂ plumes were observed from the TROPOMI instrument (Figure 1).



The simulation's time period includes 1 day of spin-up, but modellers may choose a longer spin-up period if required to obtain robust results not affected by the initialization.

Table 1. Simulations

| ID | Steel plant | Domain lon range | lat range | Time period (time in UTC, dates in 2019) |
|-----|-------------|---------------------|-------------|---|
| LIP | Lipetsk | 39.0–39.9°E | 52.0–52.8°N | 12/06 00:00 – 14/06 00:00 |

The model domain can be larger than the minimum domain specified in Table 1. Simulations should be performed at a typical resolution of the model and on the model's specific projection. Output needs to be generated on, or projected to, a regular latitude-longitude grid (see section 3).

Each simulation needs to include at least three CO₂ tracers representing three different release altitudes and optionally tracers for CO, NO₂ and NO (or NO_x, for models that do not consider a non-linear chemistry) for the reference release altitude:

Table 2. Power plant emission tracers included in each simulation

| High release case | Middle release case (reference) | Low release case (at the surface) | Mandatory |
|-------------------|------------------------------------|--------------------------------------|-----------|
| CO2_PP_H | CO2_PP_M | CO2_PP_L | Yes |
| | CO_PP_M | | No |
| | NO2_PP_M | | No |
| | NO_PP_M (Or NOX_PP_M) | | No |

Additional optional tracers for CO₂, CO and NO and NO₂ (or NO_x, for models without non-linear chemistry) representing background concentrations and other fluxes within the model domain are denoted as follows:

Table 3. Optional tracers relating to background fields, anthropogenic emissions and biospheric fluxes

| Background fields transported from outside the domain ¹ | Other anthropogenic emissions in the modelling domain (except those from Lipetsk) ² | Biospheric fluxes (photosynthesis and respiration) ³ | Total anthropogenic emissions (background fields + other anthropogenic emissions + Lipetsk emissions) |
|--|--|---|---|
| CO2_BG | CO2_ANTH | CO2_BIO | CO2_TOT_ANTH |
| CO_BG | CO_ANTH | | CO_TOT_ANTH |
| NO2_BG | NO2_ANTH | | NO2_TOT_ANTH |
| NO_BG | NO_ANTH | NOX_ANTH | NOX_TOT_ANTH |

These tracers are optional but recommended to produce realistic concentration fields in the surroundings of the power plant.

Simulations with full chemistry should only provide CO_TOT_ANTH, NO2_TOT_ANTH and NO_TOT_ANTH, rather than the individual components in the other columns of the table. Models with no or idealized chemistry (e.g. constant NO_x lifetime) should provide the individual components. For CO₂, the three tracers CO2_BG, CO2_ANTH and CO2_BIO should be provided separately whenever possible.

High-resolution models may include additional tracers representing emissions from individual stacks (see section 2.2).

2. Input Data

2.1. Meteorology

The changing meteorological conditions during the simulation period should be captured as accurately as possible. Models should, therefore, be driven or constrained by meteorological (re-)analysis fields from ECMWF, either from the operational stream or from ERA5.

Online models should use ECMWF meteorological fields as initial and boundary conditions. In case of multiple nested domains, ECMWF fields should constrain the outermost domain. It is also recommended to turn on standard meteorological data assimilation/nudging, in order to keep the simulated meteorology as close to observed meteorology as possible.

2.2 Emissions

The Lipetsk steel plant (Novolipetsk Steel) has a number of furnaces and cooling towers, and little information is available on where CO₂/NO_x/CO are emitted. For a photographic impression: https://www.123rf.com/photo_82299759_lipetsk-russia-july-11-2017-metallurgical-plant-nlmk-group-general-view-from-height.html.

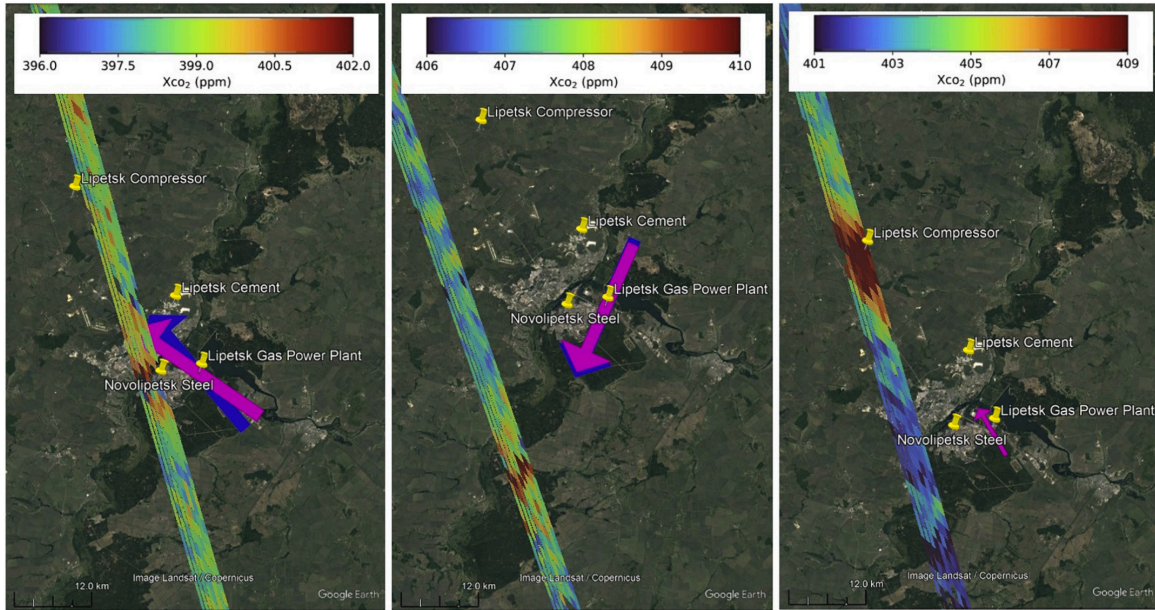
On checking the TNO inventory, some point sources around Lipetsk are reported, but not at the magnitude in we found in industry reports. On top of that, Lipetsk also houses a gas-power plant, a cement plant, and a compressor station. See figure 1, from Nassar et al. (2021). For this

¹ See section 2.3

² See section 2.4

³ See section 2.5

intercomparison, we will test whether reported emissions of the steel plant are sufficient to explain the observations of TROPOMI CO/NO2.



All models need to include the tracers representing the total emissions from the steel plant as a single source (denoted as "single" in Table 4).

Table 4. Source locations and strengths

| Steel plant | Stack/tower | Coordinate longitude, latitude | Emission rate | | | NO _x tracer [NO ₂ mass equivalent/s] | |
|-------------|-------------|-----------------------------------|-------------------------|-----------|-------------------------|--|-------|
| | | | [kg CO ₂ /s] | [kg CO/s] | [kg NO ₂ /s] | | |
| Lipetsk | Single | 39.6296°E, 52.5574°N | 906.93 | 7.46 | 0.0415 | 0.515 | 0.831 |

The locations and the suggested emission strengths are listed in Table 4. Note that the coordinates are taken from a report (not verified). The source strengths correspond to the values reported in the same report (NLMK, 2020 Annual report). VOC emissions are reported as 0.0888 kg/s.

For models that do not consider any (non-linear) chemistry, it is fine to submit NO_x tracers rather than the separate NO₂ and NO components. To convert between NO₂, NO, and NO_x we use the relation $NO = 0.95 \cdot NO_x \cdot (30/46)$ and $NO_2 = 0.05 \cdot NO_x$, where 30 and 46 are the molar masses of NO and NO₂ respectively, and NO_x is given in NO₂ mass equivalent units (as, e.g., in the TNO dataset). Again, the CO/NO/NO₂/NO_x tracers are not mandatory.

Vertical emission profiles

To study the impact of the vertical distribution of the emissions, we will use the TNO CAMS recommendations for the Industry and Public Power sectors. The rationale is that it will be difficult to separate the steel plant (Industry) from the gas power plant (Public Power).

Table 5 lists the vertical profiles recommended by TNO CAMS V4.2 (and surface emissions).

Table 5. Parameters for emission heights.

| Sector | 0-20m | 20-92m | 92-184m | 184-324m | 324-522m | 522-781m | 781-1106m |
|---------------|-------|--------|---------|----------|----------|----------|-----------|
| A_PublicPower | 0 | 0 | 0.0025 | 0.51 | 0.453 | 0.0325 | 0 |
| B_Industry | 0.06 | 0.16 | 0.75 | 0.03 | 0 | 0 | 0 |
| Surface | 1 | 0 | 0 | 0 | 0 | 0 | 0 |

All models need to simulate tracers with fixed vertical emission profiles representing a high, middle and a low (i.e., surface) release case (tracers *_PP_H, *_PP_M and *_PP_L as described in section 1). The middle release case corresponds to the B_Industry profile, whereas the high case represents A_PublicPower profile. *_PP_L represent emissions at the surface.

Models which simulate additional tracers for individual stacks should use the B_industry profile for these tracers, since we investigate emissions from a steel plant.

Temporal emission profiles

For these simulations, we will not assume a temporal evolution, i.e., constant emissions over time.

2.3 Background fields

For the modelling of optional background tracers, corresponding to the fields transported from outside the model domain into the model, we *recommend* using the CAMS reanalysis dataset (at a horizontal resolution of 80 km), which is available both for greenhouse gases like CO₂ and for reactive gases (CO, NO_x). The CAMS global GHG reanalysis (EGG4) as well as the CAMS global atmospheric composition reanalysis (EAC4) can be obtained from the Copernicus Atmosphere Data Store (ADS) on fixed pressure levels or on the model levels, and at 0.75°x0.75° horizontal and 3-hourly temporal resolution. For details see

<https://ads.atmosphere.copernicus.eu/cdsapp#!/dataset/cams-global-ghg-reanalysis-egg4>

<https://ads.atmosphere.copernicus.eu/cdsapp#!/dataset/cams-global-reanalysis-eac4>

2.4 Other anthropogenic emissions in the modelling domain

For the optional modelling of anthropogenic emissions in the modelling domain (except for the power plant itself, which is modelled with its separate tracer), we provide the CAMS_REG_v4 gridded emissions (resolution 0.1 degree longitude, 0.05 degree latitude) on the coco2 ftp (see below). Note that the units for NO_x emissions are given in kg NO₂. Please emit 5% as NO₂, and 95% as NO as described above. Since emissions from the steel plant could not be found in the TNO inventory, we do not remove these from the domain. On the ftp-site, you will find python routines (in Notebook form (.ipynb)) to read in the CAMS background emissions (TNO_GHGco_v4_0_year2018.nc) for CO₂, NO_x, CO, and NMVOC, and to convert to kg/m²/s. Figure 3 plots the large point sources in the vicinity of Lipetsk according to the TNO inventory.

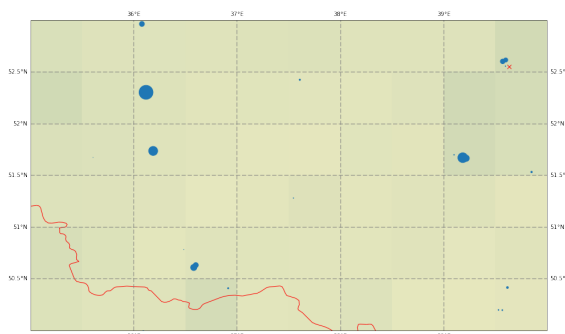


Figure 2: Location of the CO₂-ff point sources in the TNO inventory (the larger the size, the more emissions). The red cross indicates the location of the Lipetsk Steel Plant.

2.5 Photosynthesis and biospheric fluxes

For the optional modelling of biospheric fluxes in the modelling domain, each group should use its standard approach.

2.6 Possible outputs

To summarize, table 6 lists all possible tracers that may be computed.

Table 6. List of all possible tracers for which output may be computed. NO_x fields can be supplied in place of separate NO₂ and NO tracers, if no (non-linear) chemistry is considered.

| | |
|--------------|--------------|
| CO2_PP_H | |
| CO2_PP_M | |
| CO2_PP_L | |
| CO_PP_M | |
| NO2_PP_M | NOX_PP_M |
| NO_PP_M | |
| CO2_BG | |
| CO_BG | |
| NO2_BG | NOX_BG |
| NO_BG | |
| CO2_ANTH | |
| CO_ANTH | |
| NO2_ANTH | NOX_ANTH |
| NO_ANTH | |
| CO2_BIO | |
| CO2_TOT_ANTH | |
| CO_TOT_ANTH | |
| NO2_TOT_ANTH | NOX_TOT_ANTH |
| NO_TOT_ANTH | |
| CO2_PP_M_E | |
| CO2_PP_M_W | |
| CO_PP_M_E | |
| CO_PP_M_W | |
| NO2_PP_M_E | NOX_PP_M_E |
| NO_PP_M_E | |
| NO2_PP_M_W | NOX_PP_M_W |
| NO_PP_M_W | |

3. Output

To facilitate the processing and inter-comparison of the simulations, please follow the following guidelines for the file content and formats as closely as possible. Only gridded output is requested. Interpolation to the measurements will be done centrally in a unified way. Output should be generated on the native vertical grid of the model but horizontally interpolated to a regular latitude-longitude grid (using the WGS84 geodetic reference). Output frequency should be at least hourly. Output every 15 minutes is recommended.

To account for the different resolutions and domain sizes, output should be provided for two different domains. The smaller inner domain fully encompasses the aircraft measurements and targets the near-field of the plumes. The larger outer domain extends about 100 km on all sides of the power plant.

Table 6. Output grids (all coordinates denote grid cell centers) and output frequency.

| Power plant | Domain | Longitude range | Latitude range | resolution dlon x dlat | Size nx x ny | Freq. hr |
|-------------|--------|-----------------|----------------|---------------------------|-----------------|-------------|
|-------------|--------|-----------------|----------------|---------------------------|-----------------|-------------|

| | | | | | | |
|---------|-------|---------------|-----------------|-----------------|-----------|-------------------|
| Lipetsk | SMALL | 39 – 39.9°E | 52.00 – 52.80°N | 0.003° x 0.002° | 300 x 400 | 0.25 ⁴ |
| Lipetsk | LARGE | 37.9 – 40.0°E | 51.50 – 53.00°N | 0.015° x 0.01° | 140 x 150 | 1.00 |

We ask you to provide output in netCDF format with **one file per day** containing the following dimensions and variables:⁵

File name format: **LIP_[Domain]_[yyyymmdd]_[group]_[model].nc**

Where domain is either SMALL or LARGE. Group can be e.g. LSCE, model e.g. CHIMERE. Please use capital letters. In case of multiple simulations, please include the simulation version in the model name, e.g. CHIMERE-SIM1.

Dimensions:

| | |
|------------|---|
| latitude: | Number of grid points in zonal direction |
| longitude: | Number of grid points in meridional direction |
| level: | Number of full (cell center) vertical levels |
| levelh: | Number of half (cell edge) vertical levels |
| time: | Number of time steps |

⁴ ARTM can only provide hourly output

⁵ See also the deliverable D4.1, section 5, and an example for the Jänschwalde output placed at <https://confluence.ecmwf.int/display/CoCO2/Overview+of+simulations+and+model+systems>

Variables:

| VARIABLE | DESCRIPTION | UNITS | DIMENSIONS | COMMENTS |
|----------------|---|-----------------------|-----------------------------------|--|
| time | Time | UTC | time | Hours since 12 June 2019 00:00 (UTC) |
| longitude | Zonal location | degrees | latitude, longitude | |
| latitude | Meridional location | degrees | latitude, longitude | |
| p | Air pressure at cell center | Pa | time, level, latitude, longitude | |
| z | Height above surface at cell center | m | time, level, latitude, longitude | Even for models that do not have a time-varying grid |
| ph | Air pressure at cell edge | Pa | time, levelh, latitude, longitude | |
| zh | Height above surface at cell edge | m | time, levelh, latitude, longitude | |
| ta | Air temperature | K | time, level, latitude, longitude | |
| hus | Specific humidity | kg kg ⁻¹ | time, level, latitude, longitude | |
| ua | Eastward wind | m s ⁻¹ | time, level, latitude, longitude | |
| va | Northward wind | m s ⁻¹ | time, level, latitude, longitude | |
| wa | Vertical wind | m s ⁻¹ | time, level, latitude, longitude | |
| ps | Surface pressure | Pa | time, latitude, longitude | |
| zsurf | Surface elevation | m | time, latitude, longitude | |
| CO2_PP_H | CO ₂ tracer mole fraction high release | mol mol ⁻¹ | time, level, latitude, longitude | |
| CO_PP_H | CO tracer mole fraction high release | mol mol ⁻¹ | time, level, latitude, longitude | |
| ...Etcetera... | | | | |

For hourly output, a daily file should contain output for 0 UTC, 1 UTC, ... , 23 UTC, where the time corresponds to the instantaneous model fields (or center of an averaging interval). Output at 15 minute resolution should be provided in an analogous way for 00 UTC, 00:15 UTC, 00:30 UTC etc.

The vertical model domain should at least cover altitudes up to 2400 m above sea level. The atmospheric boundary layer height was about 1800 m on 07 June 2018.

4. Observations

Observations are available from TROPOMI CO/NO₂. Relevant tracks will be uploaded to the ICOS notebook server.

5. Logistics

Input

Inputs are available from the CoCO₂ ftp server

ftp [coco2@ftp.ecmwf.int](ftp:coco2@ftp.ecmwf.int)

in the following subdirectories:

/WP4/Plume_Simulations/Lipetsk: Inputs specific for Lipetsk case (including protocol)

Output

Output should be uploaded to the [ICOS Fileshare](#).

Please submit your results by [31 March 2021](#).

References:

Nassar, R., Mastrogiacomo, J. P., Bateman-Hemphill, W., McCracken, C., MacDonald, C. G., Hill, T., O'Dell, C. W., Kiel, M., & Crisp, D. (2021). Advances in quantifying power plant CO₂ emissions with OCO-2. *Remote Sensing of Environment*, 264. <https://doi.org/10.1016/j.rse.2021.112579>

Protocol for CoCO₂ Power Plant Plume Simulations (Case study for Matimba power station in South Africa)

Author: Janne Hakkarainen, Dominik Brunner, Erik Koene

Version: v1.2, 29 April 2022

Table of Contents

| | |
|---|---|
| Protocol for CoCO ₂ Power Plant Plume Simulations (Case study for Matimba power station in South Africa) | 1 |
| 1. Simulations | 2 |
| 2. Input Data | 3 |
| 2.1. Meteorology | 3 |
| 2.2 Emissions | 4 |
| 2.3 Background fields | 5 |
| 2.4 Other anthropogenic emissions in the modelling domain | 5 |
| 2.5 Photosynthesis and biospheric fluxes | 5 |
| 2.6 Possible outputs | 5 |
| 3. Output | 6 |
| 4. Observations | 7 |
| 5. Logistics | 7 |

1. Simulations

Since the protocol should be applicable to a wide range of models with different resolutions and associated computational costs, the protocol defines a set of minimal requirements plus a set of options.

Table 1 describes the minimum domain and time period that has to be covered by the simulations. The main day of interest is 25 July 2020, when the plume was observed with S5p/TROPOMI and OCO-2 around noon, see Figure 1. Thirteen other potential cases with both TROPOMI and OCO-2 observations available are discussed by Hakkarainen et al., 2021¹. The simulation's time period thus includes 1 day of spin-up, but modellers may choose a longer spin-up period if required to obtain robust results not affected by the initialization.

Table 1. Simulations

| ID | Power plant | Domain lon range | lat range | Time period (time in UTC, dates in 2020) |
|-----|-------------|---------------------|-------------|---|
| MAT | Matimba | 25.5–29°E | 25.5–22.5°S | 24/07 00:00 – 26/07 00:00 |

The model domain can be larger than the minimum domain specified in Table 1. Especially if other days are considered the modelling domain should be enlarged to the entire area specified in Figure 1. The domain now includes only the visible TROPOMI NO₂ plume. Simulations should be performed at a typical resolution of the model and on the model's specific projection. Output needs to be generated on, or projected to, a regular latitude-longitude grid (see section 3).

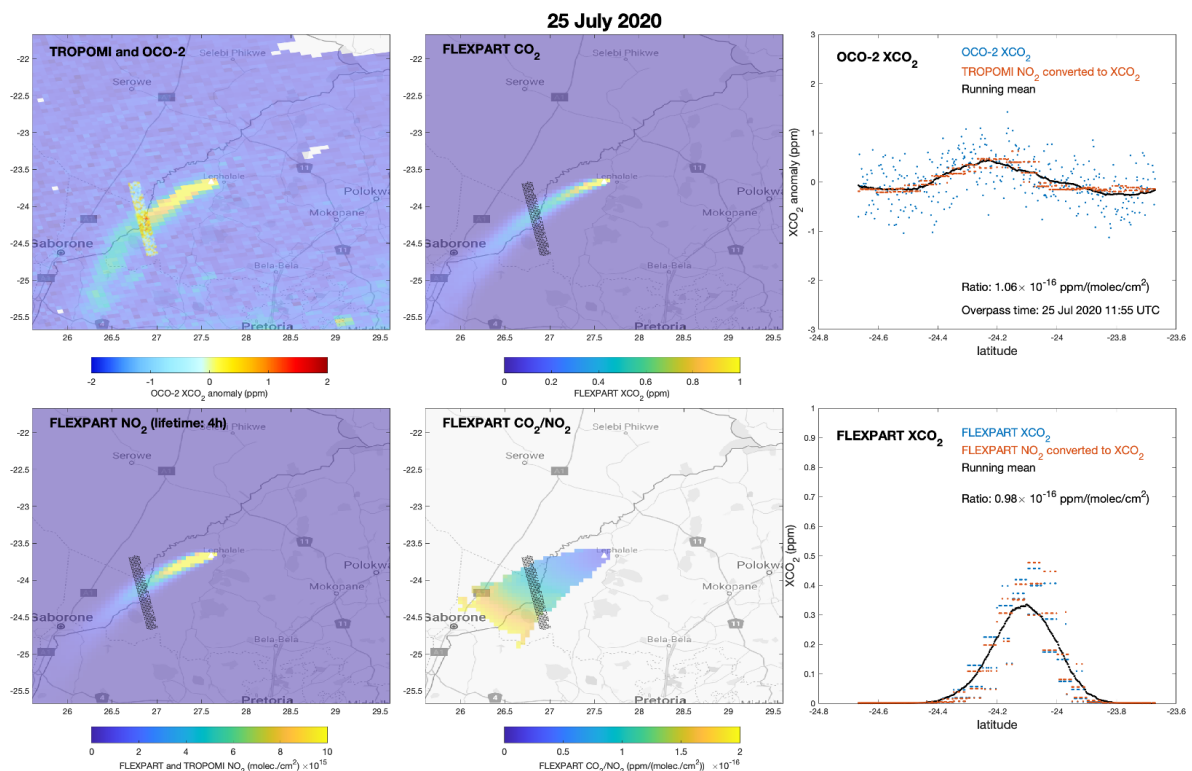


Figure 1 OCO-2 and TROPOMI observations on 25 July 2020 with FLEXPART model simulations.

¹ Available online at <https://doi.org/10.1016/j.aeaoa.2021.100110>.

Each simulation needs to include at least three CO₂ tracers representing three different release altitudes and optionally tracers for CO, NO₂ and NO (or NO_x, for models that do not consider a non-linear chemistry) for the reference release altitude:

Table 2. Power plant emission tracers included in each simulation

| High release case | Middle release case (reference) | Low release case (at the surface) | Mandatory |
|-------------------|---------------------------------|-----------------------------------|-----------|
| CO2_PP_H | CO2_PP_M | CO2_PP_L | Yes |
| | CO_PP_M | | No |
| | NO2_PP_M | (Or NOX_PP_M) | No |
| | NO_PP_M | | No |

Additional optional tracers for CO₂, CO and NO and NO₂ (or NO_x, for models without non-linear chemistry) representing background concentrations and other fluxes within the model domain are denoted as follows:

Table 3. Optional tracers relating to background fields, anthropogenic emissions and biospheric fluxes

| Background fields transported from outside the domain ² | Other anthropogenic emissions in the modelling domain (except those from Matimba) ³ | Biospheric fluxes (photosynthesis and respiration) ⁴ | Total anthropogenic emissions (background fields + other anthropogenic emissions + Matimba emissions) |
|--|--|---|---|
| CO2_BG | CO2_ANTH | CO2_BIO | CO2_TOT_ANTH |
| CO_BG | CO_ANTH | | CO_TOT_ANTH |
| NO2_BG | NO2_ANTH | | NO2_TOT_ANTH |
| NO_BG | NO_ANTH | NOX_ANTH | NO_TOT_ANTH |
| | NOX_BG | | NOX_TOT_ANTH |

These tracers are optional but recommended to produce realistic concentration fields in the surroundings of the power plant.

Simulations with full chemistry should only provide CO_TOT_ANTH, NO2_TOT_ANTH and NO_TOT_ANTH, rather than the individual components in the other columns of the table. Models with no or idealized chemistry (e.g. constant NO_x lifetime) should provide the individual components. For CO₂, the three tracers CO2_BG, CO2_ANTH and CO2_BIO should be provided separately whenever possible.

2. Input Data

2.1. Meteorology

The changing meteorological conditions during the simulation period should be captured as accurately as possible. Models should, therefore, be driven or constrained by meteorological (re-)analysis fields from ECMWF, either from the operational stream or from ERA5.

Online models should use ECMWF meteorological fields as initial and boundary conditions. In case of multiple nested domains, ECMWF fields should constrain the outermost domain. It is also recommended to turn on standard meteorological data assimilation/nudging, in order to keep the simulated meteorology as close to observed meteorology as possible.

² See section 2.3

³ See section 2.4

⁴ See section 2.5

2.2 Emissions

The power plant Matimba releases emissions from several stacks, but we do not have the exact location of the stacks.

All models need to include the tracers representing the total emissions from the power plant as a single source (denoted as "single" in Table 4). These tracers should be named according to Table 2.

Table 4. Source locations and strengths

| Power plant | Stack/tower | Coordinate longitude, latitude | Emission rate | | | | NO _x tracer [NO ₂ mass equivalent/s] |
|-------------|-------------|-----------------------------------|-------------------------|-----------|-------------------------|-----------|--|
| | | | [kg CO ₂ /s] | [kg CO/s] | [kg NO ₂ /s] | [kg NO/s] | |
| Matimba | Single | 27.610556°E, 23.668333°S | 794.0972 | 0.0636 | 0.0984 | 1.2191 | 1.9676 |

The locations and the suggested emission strengths are listed in Table 4. The source strengths correspond to the Community Emissions Data System (NO_x) and ODIAC (CO₂) values for the year 2014 and are the same values used by Hakkarainen et al., 2021. We note that Matimba is a missing source in EDGAR emission inventory. The report for the month of February by the ESKOM, the company operating Matimba power station, indicates the total emission of 1969837 tonnes (CO₂) and 4895 tonnes (NO_x). This would indicate the emission rates 814 kg/s (CO₂) and 2.0 kg/s (NO_x). We did not find emission estimates for CO. Instead, we calculated from EDGAR v3 HTAP dataset. (https://edgar.jrc.ec.europa.eu/dataset_htap_v3) a typical CO-to-NO_x emission ratio for energy sector in South African Highveld region, CO:NO_x=0.0323. For Matimba power station, we did not see any visual CO enhancements in TROPOMI data.

For models that do not consider any (non-linear) chemistry, it is fine to submit NO_x tracers rather than the separate NO₂ and NO components. To convert between NO₂, NO, and NO_x we use the relation $NO = 0.95 \cdot NO_x \cdot (30/46)$ and $NO_2 = 0.05 \cdot NO_x$, where 30 and 46 are the molar masses of NO and NO₂ respectively, and NO_x is given in NO₂ mass equivalent units (as, e.g., in the TNO dataset). Again, the CO/NO/NO₂/NO_x tracers are not mandatory. **Note:** For Matimba power station 4 h is a good estimate for NO_x lifetime and should be used in the simulations that do not consider chemistry (Beirle et al, 2019; Hakkarainen et al., 2021).

Vertical emission profiles

Emissions from the power plants undergo plume rise due to the momentum and buoyancy of the flue gas. Plume rise depends on stack and effluent parameters as well as on meteorological conditions (wind speed, stability). Matimba is located at high altitude with elevation of 921 m with stack height of 250 m.

To study the impact of the vertical distribution of the emissions, we have modified the TNO CAMS recommendations for the Public Power sectors as presented for the Lipetsk steel plant protocol.

Table 5 lists the vertical profiles.

Table 5. Parameters for emission heights (above ground).

| Sector | 0-150m | 150-250m | 250-350m | 350-500m | 500-800m | 800-1000m |
|--------|--------|----------|----------|----------|----------|-----------|
| High | 0 | 0 | 0.0025 | 0.51 | 0.453 | 0.0325 |
| Middle | 0 | 0.0025 | 0.51 | 0.453 | 0.0325 | 0 |
| Low | 1 | 0 | 0 | 0 | 0 | 0 |

All models need to simulate tracers with fixed vertical emission profiles representing a high, middle and a low (i.e., surface) release case (tracers *_PP_H, *_PP_M and *_PP_L as described in section 1).

Temporal emission profiles

For these simulations, we will not assume a temporal evolution, i.e., constant emissions over time.

2.3 Background fields

For the modelling of optional background tracers, corresponding to the fields transported from outside the model domain into the model, we *recommend* using the CAMS reanalysis dataset (at a horizontal resolution of 80 km), which is available both for greenhouse gases like CO₂ and for reactive gases (CO, NO_x). The CAMS global GHG reanalysis (EGG4) as well as the CAMS global atmospheric composition reanalysis (EAC4) can be obtained from the Copernicus Atmosphere Data Store (ADS) on fixed pressure levels or on the model levels, and at 0.75°x0.75° horizontal and 3-hourly temporal resolution. For details see

<https://ads.atmosphere.copernicus.eu/cdsapp#!/dataset/cams-global-ghg-reanalysis-egg4>

<https://ads.atmosphere.copernicus.eu/cdsapp#!/dataset/cams-global-reanalysis-eac4>

We note that Matimba is a missing emission source in EDGAR, and it is not available in CAMS simulations.

2.4 Other anthropogenic emissions in the modelling domain

For the optional modelling of anthropogenic emissions in the modelling domain (except for the power plant itself, which is modelled with its separate tracer), one can use the EDGAR emissions available at https://edgar.jrc.ec.europa.eu/emissions_data_and_maps

We note that Matimba is a missing emission source in EDGAR.

2.5 Photosynthesis and biospheric fluxes

For the optional modelling of biospheric fluxes in the modelling domain, each group should use its standard approach.

2.6 Possible outputs

To summarize, table 6 lists all possible tracers that may be computed.

Table 6. List of all possible tracers for which output may be computed. NO_x fields can be supplied in place of separate NO₂ and NO tracers, if no (non-linear) chemistry is considered.

| | |
|--------------|----------|
| CO2_PP_H | |
| CO2_PP_M | |
| CO2_PP_L | |
| CO_PP_M | |
| NO2_PP_M | NOX_PP_M |
| NO_PP_M | |
| CO2_BG | |
| CO_BG | |
| NO2_BG | NOX_BG |
| NO_BG | |
| CO2_ANTH | |
| CO_ANTH | |
| NO2_ANTH | NOX_ANTH |
| NO_ANTH | |
| CO2_BIO | |
| CO2_TOT_ANTH | |

| | |
|--------------|--------------|
| CO_TOT_ANTH | |
| NO2_TOT_ANTH | NOX_TOT_ANTH |
| NO_TOT_ANTH | |
| CO2_PP_M_E | |
| CO2_PP_M_W | |
| CO_PP_M_E | |
| CO_PP_M_W | |
| NO2_PP_M_E | NOX_PP_M_E |
| NO_PP_M_E | |
| NO2_PP_M_W | NOX_PP_M_W |
| NO_PP_M_W | |

3. Output

To facilitate the processing and inter-comparison of the simulations, please follow the following guidelines for the file content and formats as closely as possible. Only gridded output is requested. Interpolation to the observations can be done centrally in a unified way. Output should be generated on the native vertical grid of the model but horizontally interpolated to a regular latitude-longitude grid (using the WGS84 geodetic reference). Output frequency should be at least hourly. Output every 15 minutes is recommended.

Table 6. Output grids (all coordinates denote grid cell centers) and output frequency.

| Power plant | Domain | Longitude range | Latitude range | resolution dlon x dlat | Size nx x ny | Freq. hr |
|-------------|--------|-----------------|----------------|---------------------------|-----------------|-------------|
| Matimba | LARGE | 25.5–29°E | 25.5–22.5°S | 0.01° x 0.01° | 351 x 301 | 1.00 |
| Matimba | SMALL | 26.5-28°E | 25–23.5°S | 0.003° x 0.002° | 501 x 751 | 0.25 |

We ask you to provide output in netCDF format with **one file per day** containing the following dimensions and variables:⁵

File name format: **MAT_[Domain]_[yyyymmdd]_[group]_[model].nc**

Where domain is either SMALL or LARGE. Group can be e.g. LSCE, model e.g. CHIMERE. Please use capital letters. In case of multiple simulations, please include the simulation version in the model name, e.g. CHIMERE-SIM1.

Dimensions:

- latitude: Number of grid points in zonal direction
- longitude: Number of grid points in meridional direction
- level: Number of full (cell center) vertical levels
- levelh: Number of half (cell edge) vertical levels
- time: Number of time steps

⁵ See also the deliverable D4.1, section 5, and an example for the Jänschwalde output placed at <https://confluence.ecmwf.int/display/CoCO2/Overview+of+simulations+and+model+systems>

Variables:

| VARIABLE | DESCRIPTION | UNITS | DIMENSIONS | COMMENTS |
|----------------|---|-----------------------|-----------------------------------|--|
| time | Time | UTC | time | Hours since 24 July 2020 00:00 (UTC) |
| longitude | Zonal location | degrees | latitude, longitude | |
| latitude | Meridional location | degrees | latitude, longitude | |
| p | Air pressure at cell center | Pa | time, level, latitude, longitude | |
| z | Height above surface at cell center | m | time, level, latitude, longitude | Even for models that do not have a time-varying grid |
| ph | Air pressure at cell edge | Pa | time, levelh, latitude, longitude | |
| zh | Height above surface at cell edge | m | time, levelh, latitude, longitude | |
| ta | Air temperature | K | time, level, latitude, longitude | |
| hus | Specific humidity | kg kg ⁻¹ | time, level, latitude, longitude | |
| ua | Eastward wind | m s ⁻¹ | time, level, latitude, longitude | |
| va | Northward wind | m s ⁻¹ | time, level, latitude, longitude | |
| wa | Vertical wind | m s ⁻¹ | time, level, latitude, longitude | |
| ps | Surface pressure | Pa | time, latitude, longitude | |
| zsurf | Surface elevation | m | time, latitude, longitude | |
| CO2_PP_H | CO ₂ tracer mole fraction high release | mol mol ⁻¹ | time, level, latitude, longitude | |
| CO_PP_H | CO tracer mole fraction high release | mol mol ⁻¹ | time, level, latitude, longitude | |
| ...Etcetera... | | | | |

For hourly output, a daily file should contain output for 0 UTC, 1 UTC, ... , 23 UTC, where the time corresponds to the instantaneous model fields (or center of an averaging interval). Output at 15 minute resolution should be provided in an analogous way for 00 UTC, 00:15 UTC, 00:30 UTC etc.

Matimba is located at high altitude with elevation 921 m, stacks 250 m. The vertical model domain should at least cover altitudes up to 3000 m above sea level.

4. Observations

The day include satellite observations of both NO₂ and CO₂ by S5p/TROPOMI and OCO-2, respectively. Satellite products will be provided to the ICOS server by FMI.

Interpolation to satellite observations for model evaluation can be done centrally by FMI or separately by each modelling team.

5. Logistics

Input

Not applicable

Output

Output should be uploaded to the ICOS Fileshare.

Please submit your results by the end of June 2022.

Protocol for CoCO2 Berlin City Simulations

Authors: Erik Koene, Dominik Brunner

Version: v2.0, 22 April 2022

Table of Contents

| | |
|---|---|
| Protocol for CoCO2 Berlin City Simulations | 1 |
| 1. Simulations | 2 |
| 2. Input Data | 3 |
| 2.1. Meteorology | 3 |
| 2.2 Emissions | 3 |
| 2.3 Background fields | 4 |
| 2.4 Other anthropogenic emissions in the modelling domain | 4 |
| 2.5 Photosynthesis and biospheric fluxes | 4 |
| 2.6 Possible outputs | 4 |
| 3. Output | 5 |
| 4. Observations | 6 |
| 5. Logistics | 6 |

1. Simulations

Since the protocol should be applicable to a wide range of models with different resolutions and associated computational costs, the protocol defines a set of minimal requirements plus a set of options.

Table 1 describes the minimum domain and time period that has to be covered by the simulations. The main day of interest is 20 July, when the plume of the city of Berlin was observed from the DLR Cessna 208B Grand Caravan (Klausner et al., 2020, <https://doi.org/10.1525/elementa.411>) and the TROPOMI satellite around noon. The aircraft observations provide measurements of NO₂, CH₄ and CO₂ (and other gases), while TROPOMI provides only measurements of NO₂ and CH₄ but not of CO₂. In order to capture also other days with good TROPOMI observations under clear-sky conditions before and after 20 July, the model simulation should cover at least the days from 18-26 July.

Table 1. Simulations

| ID | City | Domain | | Time period (time in UTC, dates in 2018) |
|-----|--------|---------------|-------------|---|
| | | lon range | lat range | |
| BER | Berlin | 11.25–15.75°E | 51.0–54.0°N | 18/07 00:00 – 27/07 00:00 |

The model domain can be larger than the minimum specified in Table 1. Simulations should be performed at a typical resolution of the model and on the model's specific projection. Output needs to be generated on, or projected to, a regular latitude-longitude grid (see section 3).

Each simulation needs to include one passive CO₂ tracer representing the entire city of Berlin (CO₂_CITY) and either one tracer for NO_x (NO_x_CITY) with a 4-hour exponential decay time, or separate tracers for NO₂ and NO for models that consider chemistry with a similar naming scheme, i.e., NO₂_CITY, and NO_CITY. Modelling of CO is optional, but when performed must be denoted as CO_CITY.

Additional tracers for CO₂, CO and NO and NO₂ (or NO_x, for models without non-linear chemistry) representing background concentrations and other fluxes within the model domain are denoted as follows, and are also required to be modelled:

Table 2. Optional tracers relating to background fields, anthropogenic emissions and biospheric fluxes

| Background fields transported from outside the domain ¹ | | Other anthropogenic emissions in the modelling domain (except those from Berlin) ² | | Biospheric fluxes (photosynthesis and respiration) ³ | Total anthropogenic emissions (background fields + other anthropogenic emissions + Berlin emissions) | |
|--|---------------------|---|-----------------------|---|--|---------------------------|
| CO ₂ _BG | | CO ₂ _ANTH | | CO ₂ _BIO | CO ₂ _TOT_ANTH | |
| CO_BG | | CO_ANTH | | | CO_TOT_ANTH | |
| NO ₂ _BG | NO _x _BG | NO ₂ _ANTH | NO _x _ANTH | | NO ₂ _TOT_ANTH | NO _x _TOT_ANTH |
| NO_BG | | NO_ANTH | | NO_TOT_ANTH | | |

¹ See section 2.3

² See section 2.4

³ See section 2.5

2. Input Data

2.1. Meteorology

The changing meteorological conditions during the simulation period should be captured as accurately as possible. Models should, therefore, be driven or constrained by meteorological (re-)analysis fields from ECMWF, either from the operational stream or from ERA5.

Online models should use ECMWF meteorological fields as initial and boundary conditions. In case of multiple nested domains, ECMWF fields should constrain the outermost domain. It is also recommended to turn on standard meteorological data assimilation/nudging, in order to keep the simulated meteorology as close to observed meteorology as possible.

2.2 Emissions

The city Berlin is a large urban emitting region with estimated emissions of about 33 Mt CO₂ per year. In a study from Klausner et al. (2020, <https://doi.org/10.1525/elementa.411>), the CO₂ emissions reported by inventories were found to match observations well. We will thus follow the suggested emission strengths from the TNO inventory developed for the VERIFY project, extrapolated from 2017 to 2018. We provide a separate emission dataset on the CoCO2 FTP site containing only emissions that lie on or within the city boundaries of Berlin (no correction has been made to account for fractional coverage of the city at the boundaries with the TNO inventory): */WP4/Plume_simulations/Berlin/TNO_emissions__Berlin_only_compressed.nc*.

For models that do not consider any interactive chemistry, it is fine to submit NO_x tracers rather than the separate NO₂ and NO components. To convert between NO₂, NO, and NO_x we use the relation $NO = 0.95 \cdot NO_x \cdot (30/46)$ and $NO_2 = 0.05 \cdot NO_x$, where 30 and 46 are the molar masses of NO and NO₂ respectively, and NO_x is given in NO₂ mass equivalent units (as, e.g., in the TNO dataset). Note that the NO_x tracers are to be simulated with a 1/e decay time of 4 hours.

Vertical emission profiles

We will use the standard vertical profiles for the TNO CAMS (GHG_cov4_0) inventory corresponding to the different emission categories.

Table 3. Vertical emission profiles for the different GNFR-categories of the inventory

| GNFR_CATEGORY_NAME | 0 - 20M | 20 - 92M | 92 - 184M | 184 - 324M | 324 - 522M | 522 - 781M | 781 - 1106M |
|----------------------------------|---------|----------|-----------|------------|------------|------------|-------------|
| A_PUBLICPOWER | 0 | 0 | 0.0025 | 0.51 | 0.453 | 0.0325 | 0.002 |
| B_INDUSTRY | 0.06 | 0.16 | 0.75 | 0.03 | 0 | 0 | 0 |
| C_OTHERSTATIONARYCOMB | 1 | 0 | 0 | 0 | 0 | 0 | 0 |
| D_FUGITIVES | 0.02 | 0.08 | 0.6 | 0.3 | 0 | 0 | 0 |
| E_SOLVENTS | 1 | 0 | 0 | 0 | 0 | 0 | 0 |
| F_ROADTRANSPORT_EXHAUST_GASOLINE | 1 | 0 | 0 | 0 | 0 | 0 | 0 |
| F_ROADTRANSPORT_EXHAUST_DIESEL | 1 | 0 | 0 | 0 | 0 | 0 | 0 |
| F_ROADTRANSPORT_EXHAUST_LPG_GAS | 1 | 0 | 0 | 0 | 0 | 0 | 0 |
| F_ROADTRANSPORT_NON-EXHAUST | 1 | 0 | 0 | 0 | 0 | 0 | 0 |
| G_SHIPPING | 0.2 | 0.8 | 0 | 0 | 0 | 0 | 0 |
| H_AVIATION | 0.25 | 0.25 | 0.1 | 0.1 | 0.1 | 0.1 | 0.1 |

| | | | | | | | |
|-----------------|---|---|------|------|------|---|---|
| I_OFFROAD | 1 | 0 | 0 | 0 | 0 | 0 | 0 |
| J_WASTE | 0 | 0 | 0.41 | 0.57 | 0.02 | 0 | 0 |
| K_AGRILIVESTOCK | 1 | 0 | 0 | 0 | 0 | 0 | 0 |
| L_AGRIOOTHER | 1 | 0 | 0 | 0 | 0 | 0 | 0 |

Temporal emission profiles

For these simulations, we will assume source-specific temporal profiles, corresponding to those provided by TNO for the various GNFR categories, also found on the FTP as */WP4/Plume_simulations/Berlin/timeprofiles*.csv* .

2.3 Background fields

For the modelling of background tracers, corresponding to the fields transported from outside the model domain into the model, the CAMS reanalysis dataset should be used, which is available both for greenhouse gases like CO₂ and for reactive gases (CO, NO_x) at a horizontal resolution of 80 km. The CAMS global GHG reanalysis (EGG4) as well as the CAMS global atmospheric composition reanalysis (EAC4) can be obtained from the Copernicus Atmosphere Data Store (ADS) on fixed pressure levels or on the model levels, and at 0.75°x0.75° horizontal and 3-hourly temporal resolution. For details see

<https://ads.atmosphere.copernicus.eu/cdsapp#!/dataset/cams-global-ghg-reanalysis-egg4>

<https://ads.atmosphere.copernicus.eu/cdsapp#!/dataset/cams-global-reanalysis-eac4>

2.4 Other anthropogenic emissions in the modelling domain

For the modelling of anthropogenic emissions outside of Berlin we prescribe the high-resolution (1 km x 1 km) emissions dataset from TNO extrapolated for the year 2018 (see Section 5 for access to the data set). We provide an emission dataset on the CoCO2 FTP site containing only emissions that lie outside the city boundaries of Berlin (no correction has been made to account for fractional coverage of the city at the boundaries with the TNO inventory): */WP4/Plume_simulations/Berlin/TNO_emissions_without_Berlin_compressed.nc*. Here we, equally, do assume a temporal evolution of the emissions.

2.5 Photosynthesis and biospheric fluxes

For the modelling of biospheric CO₂ fluxes in the modelling domain, each group should use its standard approach.

2.6 Possible outputs

To summarize, table 4 lists all possible tracers that may be computed.

Table 4. List of all possible tracers for which output may be computed. NO_x fields can be supplied in place of separate NO₂ and NO tracers, if no (non-linear) chemistry is considered.

| | |
|----------|----------|
| CO2_CITY | |
| CO_CITY | |
| NO2_CITY | NOX_CITY |
| NO_CITY | |

| | |
|--------------|--------------|
| CO2_BG | |
| CO_BG | |
| NO2_BG | NOX_BG |
| NO_BG | |
| CO2_ANTH | |
| CO_ANTH | |
| NO2_ANTH | NOX_ANTH |
| NO_ANTH | |
| CO2_BIO | |
| CO2_TOT_ANTH | |
| CO_TOT_ANTH | |
| NO2_TOT_ANTH | NOX_TOT_ANTH |
| NO_TOT_ANTH | |

3. Output

To facilitate the processing and inter-comparison of the simulations, please follow the following guidelines for the file content and formats as closely as possible. Only gridded output is requested. Interpolation to the measurements will be done centrally in a unified way. Output should be generated on the native vertical grid of the model but horizontally interpolated to a regular latitude-longitude grid (using the WGS84 geodetic reference). Output frequency is hourly. The output domain extends about 150 km on all sides of Berlin. For consistency with other simulations for the power plants, where two separate output domains are requested, the domain is called LARGE.

Table 5. Output grids (all coordinates denote grid cell centers) and output frequency.

| City | Domain | Longitude range | Latitude range | resolution dlon x dlat | Size nx x ny | Freq. hr |
|--------|--------|-----------------|-----------------|---------------------------|-----------------|-------------|
| Berlin | LARGE | 11.25 – 15.75°E | 51.00 – 54.00°N | 0.015° x 0.01° | 301 x 301 | 1.00 |

We ask you to provide output in netCDF format with **one file per day** containing the following dimensions and variables:⁴

File name format: **BER_LARGE_[yyyymmdd]_[group]_[model].nc**

Group can be e.g. LSCE, model e.g. CHIMERE. Please use capital letters. In case of multiple simulations, please include the simulation version in the model name, e.g. CHIMERE-SIM1.

Dimensions:

- latitude: Number of grid points in zonal direction
- longitude: Number of grid points in meridional direction
- level: Number of full (cell center) vertical levels
- levelh: Number of half (cell edge) vertical levels
- time: Number of time steps

⁴ See also the deliverable D4.1, section 5, and an example for the Jänschwalde output placed at <https://confluence.ecmwf.int/display/CoCO2/Overview+of+simulations+and+model+systems>

Variables:

| VARIABLE | DESCRIPTION | UNITS | DIMENSIONS | COMMENTS |
|----------------|--|-----------------------|-----------------------------------|--|
| time | Time | UTC | time | Hours since 18 July 2018 00:00 (UTC) |
| longitude | Zonal location | degrees | latitude, longitude | |
| latitude | Meridional location | degrees | latitude, longitude | |
| p | Air pressure at cell center | Pa | time, level, latitude, longitude | |
| z | Height above surface at cell center | m | time, level, latitude, longitude | Even for models that do not have a time-varying grid |
| ph | Air pressure at cell edge | Pa | time, levelh, latitude, longitude | |
| zh | Height above surface at cell edge | m | time, levelh, latitude, longitude | |
| ta | Air temperature | K | time, level, latitude, longitude | |
| hus | Specific humidity | kg kg ⁻¹ | time, level, latitude, longitude | |
| ua | Eastward wind | m s ⁻¹ | time, level, latitude, longitude | |
| va | Northward wind | m s ⁻¹ | time, level, latitude, longitude | |
| wa | Vertical wind | m s ⁻¹ | time, level, latitude, longitude | |
| ps | Surface pressure | Pa | time, latitude, longitude | |
| zsurf | Surface elevation | m | time, latitude, longitude | |
| CO2_CITY | CO ₂ tracer mole fraction of the city | mol mol ⁻¹ | time, level, latitude, longitude | |
| CO_CITY | CO tracer mole fraction of the city | mol mol ⁻¹ | time, level, latitude, longitude | |
| ...Etcetera... | | | | |

A daily file should contain output for 0 UTC, 1 UTC, ... , 23 UTC, where the time corresponds to the instantaneous model fields (or center of an averaging interval).

The vertical model domain should at least cover altitudes up to 3000 m above sea level since the atmospheric boundary layer height was about 2700 m on 20 July 2018.

4. Observations

Aircraft measurements include in situ and remote sensing observations. In situ measurements include CO₂ and other trace gases as well as meteorological parameters. Remote sensing observations include an NO₂ column from TROPOMI.

Interpolation to aircraft measurements for model evaluation will be done centrally by Empa.

5. Logistics

Input

Inputs are available from the CoCO₂ ftp server

<ftp://coco2@ftp.ecmwf.int>

in the following subdirectories:

/WP4/Plume_Simulations/Berlin: Inputs specific for Berlin case (including protocol)

Output

Output should be uploaded to the ICOS Fileshare.

Please submit your results by the end of June 2022.

Protocol for CoCO2 Paris City Simulations

Authors: Jinghui Lian, Michel Ramonet, Grégoire Broquet

Version: v1.0, 13 June 2022

Table of Contents

| | |
|---|---|
| Protocol for CoCO2 Paris City Simulations | 1 |
| 1. Simulations | 2 |
| 2. Input Data | 3 |
| 2.1 Meteorology | 3 |
| 2.2 Emissions | 3 |
| 2.3 Background fields | 4 |
| 2.4 Other anthropogenic emissions in the modelling domain | 4 |
| 2.5 Photosynthesis and biospheric fluxes | 5 |
| 2.6 Possible outputs | 5 |
| 3. Output | 5 |
| 4. Observations | 7 |
| 5. Logistics | 7 |

1. Simulations

Since the protocol should be applicable to a wide range of models with different resolutions and associated computational costs, the protocol defines a set of minimal requirements plus a set of options.

Table 1 describes the minimum domain and time period that has to be covered by the simulations. The main week of interest is the first of August 2018 (01/08 to 08/08) with the availability of 1) in situ measurements from both Paris urban stations of that time (JUS and CDS) in addition to the in situ measurement of the peri-urban stations (all stations from LSCE / ICOS-Fr network; see Lian et al. 2022, <https://pubs.acs.org/doi/10.1021/acs.est.1c04973>) 2) XCO₂ data from the TCCON JUS in Paris (operated by LERMA; see e.g. <https://acp.copernicus.org/preprints/acp-2020-114/acp-2020-114.pdf>; <https://tcccon-wiki.caltech.edu/Main/TCCONSites>) 3) full clear sky images of NO₂ plumes from Paris (and within the minimum modelling domain) by TROPOMI (the plume from Paris is much more difficult to detect in the CO images from current TROPOMI images during all periods). The model simulation should cover at least the days from 1-8 August. We recommend a few days (typically 5-day) spin-up if the models covering few of the last days of July, especially for multiple nested domains.

Table 1. Simulations

| ID | City | Domain | | Time period (time in UTC, dates in 2018) |
|-----|-------|--------------|-----------|---|
| | | lon range | lat range | |
| PAR | Paris | 1.1°E–3.8°E, | 48–49.4°N | 01/08 00:00 – 09/08 00:00 |

The model domain can be larger than the minimum specified in Table 1. For multiple nested domains, the innermost domain should cover the minimum domain. Simulations should be performed at a typical resolution of the model and on the model's specific projection. Output needs to be generated on, or projected to, a regular latitude-longitude grid (see section 3).

Each simulation needs to include one passive CO₂ tracer representing the entire urban area of Paris (so-called "Grand Paris", defined based on the CORINE land cover map) (CO₂_CITY). As an option, they can also include either one tracer for NO_x (NO_x_CITY) with a 4-hour exponential decay time, or separate tracers for NO₂ and NO for models that consider chemistry with a similar naming scheme, i.e., NO₂_CITY, and NO_CITY. Modelling of CO is also optional, and when performed must be denoted as CO_CITY.

Additional tracers for CO₂, CO and NO and NO₂ (or NO_x, for models without non-linear chemistry) representing background concentrations and other fluxes within the model domain are denoted as follows. The additional tracers for CO₂ are the only ones which are required to be modelled. In case of multiple nested domains, all those fields should correspond to the innermost domain i.e. the background concentrations should correspond to the boundary conditions of the innermost domain and the fluxes should be fluxes within the innermost domain.

Table 2. Required and optional tracers relating to background fields, anthropogenic emissions and biospheric fluxes

| Background fields transported from outside the | Other anthropogenic emissions in the modelling domain | Biospheric fluxes (photosynth | Total anthropogenic emissions (background fields + other anthropogenic emissions + Paris emissions) |
|--|---|-------------------------------|---|
|--|---|-------------------------------|---|

| (innermost) domain ¹ | | (except those from the Paris urban area) ² | | esis and respiration) ³ | |
|---------------------------------|--------|---|----------|------------------------------------|--------------|
| CO2_BG | | CO2_ANTH | | CO2_BIO | CO2_TOT_ANTH |
| CO_BG | | CO_ANTH | | | CO_TOT_ANTH |
| NO2_BG | NOX_BG | NO2_ANTH | NOX_ANTH | | NO2_TOT_ANTH |
| NO_BG | | NO_ANTH | | | NO_TOT_ANTH |
| | | | | | NOX_TOT_ANTH |

2. Input Data

2.1 Meteorology

The changing meteorological conditions during the simulation period should be captured as accurately as possible. Models should, therefore, be driven or constrained by meteorological (re-)analysis fields from ECMWF, either from the operational stream or from ERA5.

Online models should use ECMWF meteorological fields as initial and boundary conditions. In case of multiple nested domains, ECMWF fields should constrain the outermost domain. It is also recommended to turn on standard meteorological data assimilation/nudging, in order to keep the simulated meteorology as close to observed meteorology as possible.

2.2 Emissions

The "Grand Paris" is a large urban emitting region with estimated emissions exceeding 17 Mt CO₂ per year. We will use CO₂ emissions from the high resolution (1km) TNO inventory developed for the VERIFY project, extrapolated from 2017 to 2018 (TNO_GHGco_1x1km_2018_2019_v1_0), found on ftp as */WP4/Plume_simulations/Paris/TNO_GHGco_1x1km_2018_2019_v1_0*. We also recommend a sensitivity test (optional, not required) with an additional simulation where the CO₂ emissions are taken from the high resolution (1km) TNO inventory for 2018 recently developed for the CoCO₂ project (TNO_GHGco_1x1km_v4_0_year2018), found on ftp as */WP4/Plume_simulations/Paris/TNO_GHGco_1x1km_v4_0_year2018*. We provide a shapefile corresponding to the boundaries of the Grand Paris on the CoCO₂ FTP site for the simulation of CITY and ANTH tracers (the boundaries of this area are slightly approximative since the "Grand Paris" discussed here corresponds to the core urban area centred on Paris and they are defined based on the CORINE landcover dataset rather than to an administrative entity): */WP4/Plume_simulations/Paris/Boundaries_Paris.shp*.

Vertical emission profiles

We will use the standard vertical profiles for the TNO inventory corresponding to the different emission categories (Table 3), also found on the FTP as */WP4/Plume_simulations/Paris/TNO_height-distribution_GNFR.csv*.

Table 3. Vertical emission profiles for the different GNFR-categories of the inventory

| GNFR_CATEGORY_NAME | 0 - 20M | 20 - 92M | 92 - 184M | 184 - 324M | 324 - 522M | 522 - 781M | 781 - 1106M |
|-----------------------|---------|----------|-----------|------------|------------|------------|-------------|
| A_PUBLICPOWER | 0 | 0 | 0.0025 | 0.51 | 0.453 | 0.0325 | 0.002 |
| B_INDUSTRY | 0.06 | 0.16 | 0.75 | 0.03 | 0 | 0 | 0 |
| C_OTHERSTATIONARYCOMB | 1 | 0 | 0 | 0 | 0 | 0 | 0 |
| D_FUGITIVES | 0.02 | 0.08 | 0.6 | 0.3 | 0 | 0 | 0 |

¹ See section 2.3; for multiple nested domains, the background corresponds to the boundaries of the innermost domain

² See section 2.4

³ See section 2.5

| | | | | | | | |
|----------------------------------|------|------|------|------|------|-----|-----|
| E_SOLVENTS | 1 | 0 | 0 | 0 | 0 | 0 | 0 |
| F_ROADTRANSPORT_EXHAUST_GASOLINE | 1 | 0 | 0 | 0 | 0 | 0 | 0 |
| F_ROADTRANSPORT_EXHAUST_DIESEL | 1 | 0 | 0 | 0 | 0 | 0 | 0 |
| F_ROADTRANSPORT_EXHAUST_LPG_GAS | 1 | 0 | 0 | 0 | 0 | 0 | 0 |
| F_ROADTRANSPORT_NON-EXHAUST | 1 | 0 | 0 | 0 | 0 | 0 | 0 |
| G_SHIPPING | 0.2 | 0.8 | 0 | 0 | 0 | 0 | 0 |
| H_AVIATION | 0.25 | 0.25 | 0.1 | 0.1 | 0.1 | 0.1 | 0.1 |
| I_OFFROAD | 1 | 0 | 0 | 0 | 0 | 0 | 0 |
| J_WASTE | 0 | 0 | 0.41 | 0.57 | 0.02 | 0 | 0 |
| K_AGRILIVESTOCK | 1 | 0 | 0 | 0 | 0 | 0 | 0 |
| L_AGRIOOTHER | 1 | 0 | 0 | 0 | 0 | 0 | 0 |

Temporal emission profiles

For these simulations, we will assume source-specific temporal profiles, corresponding to those provided by TNO for the various GNFR categories, also found on the FTP as */WP4/Plume_simulations/Paris/timeprofiles*.csv* .

2.3 Boundary conditions

For the initial and lateral boundary conditions for CO₂, the CAMS global CO₂ atmospheric inversion product (version v18r1), with a horizontal resolution of 3.75°×1.90° (longitude × latitude) and 39 vertical levels between the surface and the tropopause, should be used. For the initial and lateral boundary conditions for NO_x and CO, the CAMS reanalysis dataset at a horizontal resolution of 80 km (0.75°×0.75°) should be used. The CAMS global inversion as well as the CAMS global atmospheric composition reanalysis (EAC4) can be obtained from the Copernicus Atmosphere Data Store (ADS) at 3-hourly temporal resolution.

For details see:

<https://ads.atmosphere.copernicus.eu/cdsapp#!/dataset/cams-global-greenhouse-gas-inversion?tab=form>

https://atmosphere.copernicus.eu/sites/default/files/2020-06/CAMS73_2018SC2_%20D5.2.1-2020_202004_%20CO2%20inversion%20production%20chain_v1.pdf

<https://ads.atmosphere.copernicus.eu/cdsapp#!/dataset/cams-global-reanalysis-eac4>

In case of multiple nested domains, these fields should constrain the outermost domain.

2.4 Other anthropogenic emissions in the modelling domain

For the modelling of anthropogenic emissions outside of Grand Paris we prescribe the high-resolution (1 km x 1 km) emissions dataset from TNO extrapolated for the year 2018 (see Section 5 for access to the data set), and, for the optional sensitivity test, the high-resolution (1 km x 1 km) emissions dataset from TNO recently developed for the year 2018. Here we, equally, do assume a temporal evolution and vertical distribution of the emissions. See section 2.2 regarding the two products, the mask corresponding to the Grand Paris area and the temporal and vertical profiles for the emissions.

2.5 Photosynthesis and biospheric fluxes

For the modelling of biospheric CO₂ fluxes in the modelling domain, each group should use its standard approach.

2.6 Possible outputs

To summarize, Table 4 lists all possible tracers that may be computed.

Table 4. List of all possible tracers for which output may be computed (mandatory ones are in black). NO_x fields can be supplied in place of separate NO₂ and NO tracers, if no (non-linear) chemistry is considered.

| | |
|--------------|--------------|
| CO2_CITY | |
| CO_CITY | |
| NO2_CITY | NOX_CITY |
| NO_CITY | |
| CO2_BG | |
| CO_BG | |
| NO2_BG | NOX_BG |
| NO_BG | |
| CO2_ANTH | |
| CO_ANTH | |
| NO2_ANTH | NOX_ANTH |
| NO_ANTH | |
| CO2_BIO | |
| CO2_TOT_ANTH | |
| CO_TOT_ANTH | |
| NO2_TOT_ANTH | NOX_TOT_ANTH |
| NO_TOT_ANTH | |

3. Output

To facilitate the processing and inter-comparison of the simulations, please follow the following guidelines for the file content and formats as closely as possible. Only gridded output is requested. Interpolation to the measurements will be done centrally in a unified way. Output should be generated on the native vertical grid of the model but horizontally interpolated to a regular latitude-longitude grid (using the WGS84 geodetic reference). Output frequency is hourly. The output domain is the same as the minimum simulation domain.

Table 5. Output grids (all coordinates denote grid cell centers) and output frequency.

| City | Domain | Longitude range | Latitude range | resolution dlon x dlat | Size nx x ny | Freq. hr |
|-------|--------|-----------------|----------------|---------------------------|-----------------|-------------|
| Paris | MIN | 1.1°E–3.8°E | 48–49.4°N | 0.015° x 0.01° | 180 x 140 | 1.00 |

We ask you to provide output in netCDF format with **one file per day** containing the following dimensions and variables:⁴

File name format: **PAR_MIN_[yyyymmdd]_[group]_[model].nc**

⁴ See also the deliverable D4.1, section 5, and an example for the Jänschwalde output placed at <https://confluence.ecmwf.int/display/CoCO2/Overview+of+simulations+and+model+systems>

Group can be e.g. LSCE, model e.g. WRFCHM. Please use capital letters. In case of multiple simulations, please include the simulation version in the model name, e.g. WRFCHM-SIM1.

Dimensions:

- latitude: Number of grid points in zonal direction
- longitude: Number of grid points in meridional direction
- level: Number of full (cell center) vertical levels
- levelh: Number of half (cell edge) vertical levels
- time: Number of time steps

Variables:

| VARIABLE | DESCRIPTION | UNITS | DIMENSIONS | COMMENTS |
|----------------|--|-----------------------|-----------------------------------|--|
| time | Time | UTC | time | Hours since 1 August 2018 00:00 (UTC) |
| longitude | Zonal location | degrees | latitude, longitude | |
| latitude | Meridional location | degrees | latitude, longitude | |
| p | Air pressure at cell center | Pa | time, level, latitude, longitude | |
| z | Height above surface at cell center | m | time, level, latitude, longitude | Even for models that do not have a time-varying grid |
| ph | Air pressure at cell edge | Pa | time, levelh, latitude, longitude | |
| zh | Height above surface at cell edge | m | time, levelh, latitude, longitude | |
| ta | Air temperature | K | time, level, latitude, longitude | |
| hus | Specific humidity | kg kg ⁻¹ | time, level, latitude, longitude | |
| ua | Eastward wind | m s ⁻¹ | time, level, latitude, longitude | |
| va | Northward wind | m s ⁻¹ | time, level, latitude, longitude | |
| wa | Vertical wind | m s ⁻¹ | time, level, latitude, longitude | |
| ps | Surface pressure | Pa | time, latitude, longitude | |
| zsurf | Surface elevation | m | time, latitude, longitude | |
| CO2_CITY | CO ₂ tracer mole fraction of the city | mol mol ⁻¹ | time, level, latitude, longitude | |
| CO2_BG | CO tracer mole fraction of the city | mol mol ⁻¹ | time, level, latitude, longitude | |
| ...Etcetera... | | | | |

A daily file should contain output for 0 UTC, 1 UTC, ... , 23 UTC, where the time corresponds to the instantaneous model fields (or center of an averaging interval).

The vertical model domain should at least cover altitudes up to 4000 m above sea level since the atmospheric boundary layer height reached a maximum of ~3000 m in July/August 2018 (according to measurements made at the SIRTA station in the Paris area).

4. Observations

In summer 2018, the CO₂ measurement network in the Paris region consisted of seven measurement stations, all of which measured CO₂, CO and CH₄. Among these stations is the ICOS tower in Saclay, which takes measurements at three levels: 15, 60 and 100m above the ground. In addition to GHG measurements, meteorological information (wind speed, and direction, temperature, relative humidity and pressure) is also available at the 3 sampling levels. One other station (OVS) is located at about 20km in the South West of Paris, two (JUS, CDS) are located in the center of Paris, whereas 3 (AND, COU, GNS) are located in the North East in order to cover the CO₂ gradients in the direction of the dominant wind fields. NO_x measurements (10 m agl) are also available near the Saclay tower (2 km), as part of SIRTACTRIS, in addition to the AIRPARIF network. Finally, we also provide total column measurements of CO₂ from the Paris TCCON station located at Jussieu in the center of Paris.

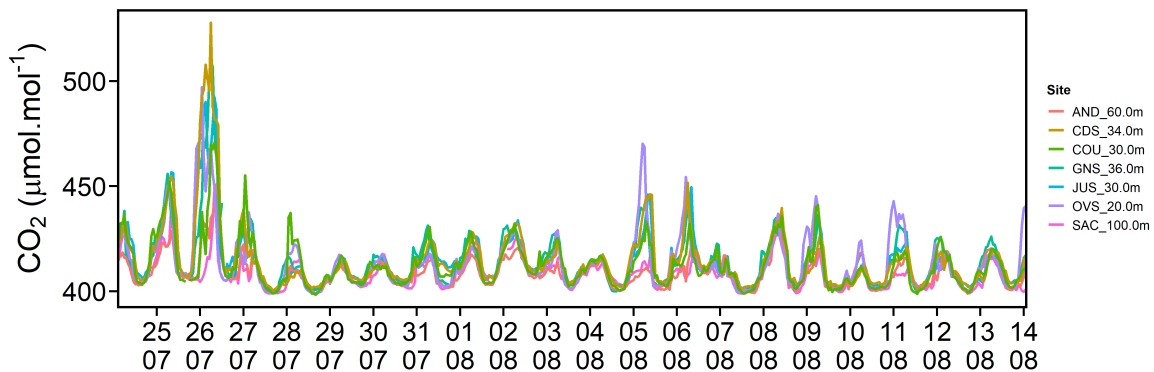


Figure: CO₂ measurements in July/August 2018 in the Parisian monitoring network

5. Logistics

Input

Inputs are available from the CoCO₂ ftp server

ftp [coco2@ftp.ecmwf.int](ftp://coco2@ftp.ecmwf.int)

in the following subdirectories:

/WP4/Plume_Simulations/Paris: Inputs specific for Paris case (including protocol)

Output

Output should be uploaded to the ICOS Fileshare.

Please submit your results by the end of June 2022.

Protocol for CoCO2 NL Randstad Simulations

Authors: Teresa Steinke, Arjo Segers

Version: v2.0, 8 August 2022

Table of Contents

| | |
|--|---|
| Protocol for CoCO2 NL Randstad Simulations..... | 1 |
| 1. Simulations..... | 2 |
| 2. Input Data | 3 |
| 2.1. Meteorology..... | 3 |
| 2.2 Emissions..... | 3 |
| 2.3 Background fields..... | 4 |
| 2.4 Other anthropogenic emissions in the modelling domain..... | 4 |
| 2.5 Photosynthesis and biospheric fluxes | 4 |
| 2.6 Possible outputs..... | 4 |
| 3. Output..... | 5 |
| 4. Observations | 6 |
| 5. Logistics..... | 6 |

1. Simulations

Currently, only TNO – LOTOS-EUROS team is planning to submit simulations of the Randstad (NL) area. In case, further modelling groups are interested in submitting a Randstad simulation, this protocol defines a set of minimal requirements plus a set of options and should be used as a common base. It is based on the previous modelling protocol (by EMPA) for the city of Berlin. Please let the modelling group of TNO know (teresa.steinke@tno.nl) in case you are interested to submit a simulation nevertheless.

The plumes of the Randstad area in the Netherlands during a time span in winter (NL_W) and a time span in summer (NL_S) shall be simulated. The two different time spans allow to evaluate for different emission and meteorological conditions. Table 1 describes the minimum domain and time period that has to be covered by the simulations. The main days of interest are chosen based on the wind profile (towards the inland), such that insitu observations (CO₂) of Dutch stations and TROPOMI observations (NO₂) capture the Randstad emissions.

Table 1. Simulations

| ID | City | Domain | | Time period (time in UTC, dates in 2018) |
|------|----------|----------------|-----------------|---|
| | | lon range | lat range | |
| NL_S | Randstad | 2.20 – 9.70°E | 50.00 – 54.00°N | 16/06 00:00 – 24/06 00:00 |
| NL_W | Randstad | 2.20 – 9.70 °E | 50.00 – 54.00°N | 16/12 00:00 – 24/12 00:00 |

The model domain can be larger than the minimum specified in Table 1. Simulations should be performed at a typical resolution of the model and on the model's specific projection. Output needs to be generated on, or projected to, a regular latitude-longitude grid (see section 3).

Each simulation needs to include one passive CO₂ tracer representing the entire Randstad of the Netherlands (CO_{2_RS}) and either one tracer for NO_x (NO_{x_RS}) with a 4-hour exponential decay time, or separate tracers for NO₂ and NO for models that consider chemistry with a similar naming scheme, i.e., NO_{2_RS}, and NO_RS. Modelling of CO is optional, but when performed must be denoted as CO_RS.

Additional tracers for CO₂, CO and NO and NO₂ (or NO_x, for models without non-linear chemistry) representing background concentrations and other fluxes within the model domain are denoted as follows, and are also required to be modelled:

Table 2. Optional tracers relating to background fields, anthropogenic emissions and biospheric fluxes

| Background fields transported from outside the domain ¹ | | Other anthropogenic emissions in the modelling domain (except those from the Randstad area) ² | | Biospheric fluxes (photosynthesis and respiration) ³ | Total anthropogenic emissions (background fields + other anthropogenic emissions + Randstad emissions) | |
|--|--------------------|--|----------------------|---|--|--------------------------|
| CO _{2_BG} | | CO _{2_ANTH} | | CO _{2_BIO} | CO _{2_TOT_ANTH} | |
| CO_BG | | CO_ANTH | | | CO_TOT_ANTH | |
| NO _{2_BG} | NO _{x_BG} | NO _{2_ANTH} | NO _{x_ANTH} | | NO _{2_TOT_ANTH} | NO _{x_TOT_ANTH} |
| NO_BG | | NO_ANTH | | NO_TOT_ANTH | | |

¹ See section 2.3

² See section 2.4

³ See section 2.5

2. Input Data

2.1. Meteorology

The changing meteorological conditions during the simulation period should be captured as accurately as possible. Models should, therefore, be driven or constrained by meteorological (re-)analysis fields from ECMWF, either from the operational stream or from ERA5.

Online models should use ECMWF meteorological fields as initial and boundary conditions. In case of multiple nested domains, ECMWF fields should constrain the outermost domain. It is also recommended to turn on standard meteorological data assimilation/nudging, in order to keep the simulated meteorology as close to observed meteorology as possible.

2.2 Emissions

Randstad is a large urban emitting region in the Netherlands with estimated emissions of more than 70 Mt CO₂ per year. We will thus follow the suggested emission strengths from the TNO inventory developed for the VERIFY project, extrapolated from 2017 to 2018. We use a separate emission dataset containing only emissions that lie in the **Randstad area covering the area 4.00 – 5.20°E and 51.70 – 52.50°N**. For models that do not consider any interactive chemistry, it is fine to submit NO_x tracers rather than the separate NO₂ and NO components. To convert between NO₂, NO, and NO_x we use the relation $NO = 0.95 \cdot NO_x \cdot (30/46)$ and $NO_2 = 0.05 \cdot NO_x$, where 30 and 46 are the molar masses of NO and NO₂ respectively, and NO_x is given in NO₂ mass equivalent units (as, e.g., in the TNO dataset). Note that the NO_x tracers are to be simulated with a 1/e decay time of 4 hours.

Vertical emission profiles

We will use the standard vertical profiles for the TNO CAMS (GHG_cov4_0) inventory corresponding to the different emission categories.

Table 3. Vertical emission profiles for the different GNFR-categories of the inventory

| GNFR_CATEGORY_NAME | 0 - 20M | 20 - 92M | 92 - 184M | 184 - 324M | 324 - 522M | 522 - 781M | 781 - 1106M |
|----------------------------------|---------|----------|-----------|------------|------------|------------|-------------|
| A_PUBLICPOWER | 0 | 0 | 0.0025 | 0.51 | 0.453 | 0.0325 | 0.002 |
| B_INDUSTRY | 0.06 | 0.16 | 0.75 | 0.03 | 0 | 0 | 0 |
| C_OTHERSTATIONARYCOMB | 1 | 0 | 0 | 0 | 0 | 0 | 0 |
| D_FUGITIVES | 0.02 | 0.08 | 0.6 | 0.3 | 0 | 0 | 0 |
| E_SOLVENTS | 1 | 0 | 0 | 0 | 0 | 0 | 0 |
| F_ROADTRANSPORT_EXHAUST_GASOLINE | 1 | 0 | 0 | 0 | 0 | 0 | 0 |
| F_ROADTRANSPORT_EXHAUST_DIESEL | 1 | 0 | 0 | 0 | 0 | 0 | 0 |
| F_ROADTRANSPORT_EXHAUST_LPG_GAS | 1 | 0 | 0 | 0 | 0 | 0 | 0 |
| F_ROADTRANSPORT_NON-EXHAUST | 1 | 0 | 0 | 0 | 0 | 0 | 0 |
| G_SHIPPING | 0.2 | 0.8 | 0 | 0 | 0 | 0 | 0 |
| H_AVIATION | 0.25 | 0.25 | 0.1 | 0.1 | 0.1 | 0.1 | 0.1 |
| I_OFFROAD | 1 | 0 | 0 | 0 | 0 | 0 | 0 |
| J_WASTE | 0 | 0 | 0.41 | 0.57 | 0.02 | 0 | 0 |
| K_AGRILIVESTOCK | 1 | 0 | 0 | 0 | 0 | 0 | 0 |
| L_AGRIOOTHER | 1 | 0 | 0 | 0 | 0 | 0 | 0 |

Temporal emission profiles

For these simulations, we will assume source-specific temporal profiles, corresponding to those provided by TNO for the various GNFR categories.

2.3 Background fields

For the modelling of background tracers, corresponding to the fields transported from outside the model domain into the model, the CAMS reanalysis dataset should be used, which is available both for greenhouse gases like CO₂ and for reactive gases (CO, NO_x) at a horizontal resolution of 80 km. The CAMS global GHG reanalysis (EGG4) as well as the CAMS global atmospheric composition reanalysis (EAC4) can be obtained from the Copernicus Atmosphere Data Store (ADS) on fixed pressure levels or on the model levels, and at 0.75°x0.75° horizontal and 3-hourly temporal resolution. For details see

<https://ads.atmosphere.copernicus.eu/cdsapp#!/dataset/cams-global-ghg-reanalysis-egg4>

<https://ads.atmosphere.copernicus.eu/cdsapp#!/dataset/cams-global-reanalysis-eac4>

2.4 Other anthropogenic emissions in the modelling domain

For the modelling of anthropogenic emissions outside of Berlin we prescribe the high-resolution (1 km x 1 km) emissions dataset from TNO extrapolated for the year 2018 (see Section 5 for access to the data set). We use an emission dataset containing only emissions that lie outside the Randstad area **covering the area 4.00 – 5.20°E and 51.70 – 52.50°N.**

2.5 Photosynthesis and biospheric fluxes

For the modelling of biospheric CO₂ fluxes in the modelling domain, each group should use its standard approach. We use recently updated VPRM fluxes (https://swiftbrowser.dkrz.de/public/dkrz_713c5812-40a6-4d9c-a938-50cfce20c44f/CoCO2_VPRM_fluxes_2021/)

2.6 Possible outputs

To summarize, table 4 lists all possible tracers that may be computed.

Table 4. List of all possible tracers for which output may be computed. NO_x fields can be supplied in place of separate NO₂ and NO tracers, if no (non-linear) chemistry is considered.

| | |
|----------|----------|
| CO2_RS | |
| CO_RS | |
| NO2_RS | NOX_RS |
| NO_RS | |
| CO2_BG | |
| CO_BG | |
| NO2_BG | NOX_BG |
| NO_BG | |
| CO2_ANTH | |
| CO_ANTH | |
| NO2_ANTH | NOX_ANTH |

| | |
|--------------|--------------|
| NO_ANTH | |
| CO2_BIO | |
| CO2_TOT_ANTH | |
| CO_TOT_ANTH | |
| NO2_TOT_ANTH | NOX_TOT_ANTH |
| NO_TOT_ANTH | |

3. Output

To facilitate the processing and inter-comparison of the simulations, please follow the following guidelines for the file content and formats as closely as possible. Only gridded output is requested. Interpolation to the measurements will be done centrally in a unified way. Output should be generated on the native vertical grid of the model but horizontally interpolated to a regular latitude-longitude grid (using the WGS84 geodetic reference). Output frequency is hourly. The output domain extends approx. 1.5° in all sides from the Randstad area. The requested domain is called SMALL.

Table 5. Output grids (all coordinates denote grid cell centers) and output frequency.

| City | Domain | Longitude range | Latitude range | resolution dlon x dlat | Size nx x ny | Freq. hr |
|----------|--------|-----------------|-----------------|---------------------------|-----------------|-------------|
| Randstad | SMALL | 2.20 – 9.70 °E | 49.50 – 54.50°N | 0.03° x 0.02° | 251 x 251 | 1.00 |

We ask you to provide output in netCDF format with **one file per day** containing the following dimensions and variables:⁴

File name format: **NL_[S/W]_SMALL_[yyyymmdd]_[group]_[model].nc**

Group can be e.g. LSCE, model e.g. CHIMERE. Please use capital letters. In case of multiple simulations, please include the simulation version in the model name, e.g. CHIMERE-SIM1.

Dimensions:

- latitude: Number of grid points in zonal direction
- longitude: Number of grid points in meridional direction
- level: Number of full (cell center) vertical levels
- levelh: Number of half (cell edge) vertical levels
- time: Number of time steps

⁴ See also the deliverable D4.1, section 5, and an example for the Jänschwalde output placed at <https://confluence.ecmwf.int/display/CoCO2/Overview+of+simulations+and+model+systems>

Variables:

| VARIABLE | DESCRIPTION | UNITS | DIMENSIONS | COMMENTS |
|----------------|--|-----------------------|-----------------------------------|--|
| time | Time | UTC | time | Hours since 18 July 2018 00:00 (UTC) |
| longitude | Zonal location | degrees | latitude, longitude | |
| latitude | Meridional location | degrees | latitude, longitude | |
| p | Air pressure at cell center | Pa | time, level, latitude, longitude | |
| z | Height above surface at cell center | m | time, level, latitude, longitude | Even for models that do not have a time-varying grid |
| ph | Air pressure at cell edge | Pa | time, levelh, latitude, longitude | |
| zh | Height above surface at cell edge | m | time, levelh, latitude, longitude | |
| ta | Air temperature | K | time, level, latitude, longitude | |
| hus | Specific humidity | kg kg ⁻¹ | time, level, latitude, longitude | |
| ua | Eastward wind | m s ⁻¹ | time, level, latitude, longitude | |
| va | Northward wind | m s ⁻¹ | time, level, latitude, longitude | |
| wa | Vertical wind | m s ⁻¹ | time, level, latitude, longitude | |
| ps | Surface pressure | Pa | time, latitude, longitude | |
| zsurf | Surface elevation | m | time, latitude, longitude | |
| CO2_RS | CO ₂ tracer mole fraction of the city | mol mol ⁻¹ | time, level, latitude, longitude | |
| CO_RS | CO tracer mole fraction of the city | mol mol ⁻¹ | time, level, latitude, longitude | |
| ...Etcetera... | | | | |

A daily file should contain output for 0 UTC, 1 UTC, ... , 23 UTC, where the time corresponds to the instantaneous model fields (or center of an averaging interval).

The vertical model domain should at least cover altitudes up to 3000 m above sea level.

4. Observations

At this point, we do not know of any available aircraft measurements for the given time span, area and species. In situ measurements including CO₂ and other species are available. The usability of remote sensing observations (NO₂ column from TROPOMI) for the given time span needs to be checked.

5. Logistics

Input

The TNO data set is available at ftp [CoCO2@ftp0015.web-ftp81@web-ftp81.tno.nl](ftp://CoCO2@ftp0015.web-ftp81@web-ftp81.tno.nl), under /WP2/CoCO2_inventory_2018_v1_0: 1 km emission data set from TNO Europe

Emission sets “only-Randstad” and “without-Randstad” of the TNO data set (compiled as described in Section 2.2 and 2.4 of this protocol) can be made available on request (teresa.steinke@tno.nl).

Output

Please let LOTOS-EUROS modelling team (TNO) know (teresa.steinke@tno.nl) if you are interested to submit a simulation.

Output should be uploaded to the ICOS Fileshare. Aiming for end of August.